DISSERTATION

SYNTHESIS, PROPERTIES AND APPLICATIONS OF SINGLE-COMPONENT ANION-EXCHANGE MATERIALS

Submitted by

Samira Caamaño

Department of Chemistry

In partial fulfillment of the requirements

For the Degree of Doctor of Philosophy

Colorado State University

Fort Collins, Colorado

Summer 2009

COLORADO STATE UNIVERSITY

June 18th, 2009

WE HEREBY RECOMMEND THAT THE THESIS PREPARED UNDER OUR SUPERVISION BY SAMIRA CAAMAÑO ENTITLED *SYNTHESIS, PROPERTIES AND APPLICATIONS OF SINGLE-COMPONENT ANION-EXCHANGE MATERIALS* BE ACCEPTED AS FULFILLING IN PART REQUIREMENTS FOR THE DEGREE OF DOCTOR OF PHILOSOPHY.

Committee on Graduate work

_____

Thomas Meersmann

_____

Dawn Rickey

_____

C. Michael Elliott

_____

Sally Sutton

_____

Advisor Steven H. Strauss

_____

Department Head Anthony K. Rappé

ABSTRACT OF DISSERTATION

SYNTHESIS, PROPERTIES AND APPLICATIONS

OF SINGLE-COMPONENT ANION-EXCHANGE MATERIALS

Several tetraalkylated ferrocenium salts and neutral modified ferrocenes, both new and previously synthesized, were studied in detail. Some of these salts have been used in the past as anion-exchange extractants for attenuated total reflectance-Fourier transform infrared (ATR-FTIR) spectroscopy. Different crystallographic, electrochemical and spectroscopic parameters were analyzed to study properties like cation size and its effect in selectivity, morphology of thin films made from these salts, both in the surface and in the bulk of the film, and film changes with time. It was found that when relative cation sizes are compared for different cations in these salts, the size increases in one dimension, which affects ion-exchange selectivity depending on what the non-aqueous phase containing the extractant is (either a water-immiscible solvent, a three-dimensional thin film or a monolayer self-assembled on an electrode surface). The effect of C–H...O hydrogen bonding in the cation–anion interactions was investigated. A model was proposed for the structure of thin films of a particular type of the ferrocenium salts, which was based on atom distances from the crystallographic data. Atomic force microscopy was used to study the morphology of surfaces of thin films, which had never been done before; the results were consistent with the hypothesis that there is a clear difference in the way that organic solutions of ferrocenium$^{+}NO_3^{-}$ and ferrocenium$^{+}ClO_4^{-}$ arrange molecularly as solvent evaporates, forming very different thin films.

The use of an ATR-FTIR technique previously developed for the detection and quantification of anionic pollutants was investigated and optimized for new sample volumes, film thicknesses and analytes. Multiple-anion detection in aqueous media was

examined. Among the new analytes studied was dodecylsulfate, (DDS^-), the anion in the detergent sodium dodecylsulfate (SDS). These studies constituted a novel application of the ATR-FTIR spectroscopy technique in heart-valve research, which uses the detergent to decellularize tissue samples with the objective of preparing biological scaffolds free of cytotoxicity.

A new ferrocene salt containing a nitrogen atom, which bears the positive charge of the cation, was successfully synthesized. This compound displayed better stability in biological solutions than other ferrocenium salts used previously. The use of this compound aided in answering the question of whether SDS leaches out of SDS-treated tissues after a soaking regime has been implemented: SDS does leach from treated tissues in potentially cytotoxic concentrations which are dependent on the initial treatment. It was also discovered that SDS leaches both as a free anion and, in initial stages of the soaking regime, complexed to other species.

A new method was developed to detect and quantify anions in aqueous samples. This method also mitigated instability issues present in the use of certain ferrocenium salts and opened doors for conventional FTIR quantification of species using this kind of extractant.

The synthesis of [^{35}S]SDS was evaluated by successfully synthesizing SDS in the Strauss Research Group laboratories, using standard starting materials, one of which (H_2SO_4) can be obtained in its radioactively labeled form. A long term objective of this synthesis was to eventually quantify [^{35}S]SDS directly in [^{35}S]SDS-treated tissue samples, after a soaking regime, using beta scintillation counting.

Samira Caamaño
Chemistry Department
Colorado State University
Fort Collins, CO 80523
Summer 2009

Table of Contents

List of Tables

List of Figures

Chapter 1

Introduction

I. About This Work.

Analytical chemistry has been around for as long as chemistry has existed as a science, as there has always been a need to analyze and understand the matter around us. It did not exist as a discipline from the beginning, however, and only in the last 150 years has it included instrumental analysis. Since then, and as technology expanded, the field has grown tremendously, focusing nowadays on exploration of the latest advances in measurements and the best new ways to increase accuracy, selectivity, sensitivity, and reproducibility, as well as significant applications.

The analytical work presented here was aimed to investigate details and applications of an infrared spectroscopic technique: attenuated total reflectance Fourier-transform infrared (ATR-FTIR) spectroscopy. Also, the optimization of an existing anion-exchange quantification method and the development of a new method to detect and quantify anions in different aqueous media were explored. The synthesis of new compounds and the characterization of old ones developed in the Strauss Research Group by previous group members, which are used as extracting salts to quantify anions in aqueous solutions, completes this investigation.

In this first chapter, the author introduces the principles of anion exchange thermodynamics, necessary to understand how extracting materials work and behave. These materials are crucial to the low limits of detection (LODs) achieved and to the application of FTIR spectroscopy to aqueous samples, as will be described later. The

infrared technique and the ATR instrument and principles of operation are described here.

Chapter two focuses on the nature of the cation-anion interactions in certain single-crystal ferrocenium salts. The salts were used to coat ATR crystals to extract, detect, and quantify anions in aqueous media, greatly enhancing the sensitivity of the method. The chapter also offers an explanation for some of the behavioral details observed when comparing the exchanging abilities of these salts.

Chapter three describes the author's use of a method developed by former members of the Strauss Research Group for anion quantification using ATR-FTIR spectroscopy: the time- dependent exchange method. In this method, an aqueous solution of the analyte is placed in contact with the ATR probe, which has previously been coated with a thin film of the ferrocenium salts. The anion in the salt undergoes exchange with the anionic analyte, which preconcentrates the analyte within the film and hence allows for LODs as low as ppb. The author introduced modifications to the time-dependent exchange method and explored the use of new extractants, which expanded the method's application to new anions, allowed the use of smaller sample volume for analysis and permitted for thinner films for detection purposes.

Chapter four describes applications and a new method developed by the author for quantification of anions: the equilibrium liquid-liquid exchange method. In this method, two heterogeneous solutions, an aqueous one containing the analyte and an organic one containing excess amounts of one of the extracting ferrocenium salts is placed in a scintillation vial, and the vial is shaken to allow temporary mixing of the two phases. During this mixing, the exchange takes place. A portion of the organic phase is then extracted and used to make a film on the ATR crystal, which is subsequently analyzed. This chapter also discusses how to quantify an anionic detergent in aqueous biological samples using the equilibrium liquid-liquid exchange method: a protocol is presented to carefully wash bovine tissue samples which had been submitted to a decellularization

treatment with the detergent, and subsequently, quantitative results are obtained by applying the equilibrium liquid-liquid exchange method to the aqueous samples used for the washes. This constitutes the first quantitative, systematic study of sodium dodecylsulfate (SDS, the detergent) leaching out of tissue samples.

II. An ATR-FTIR-Based Analytical Technique. Attenuated total reflectance (ATR) infrared spectroscopy is a versatile technique that allows for the analysis of solid (surface analysis technique) and liquid IR active compounds. When coupled with Fourier transform infrared (FTIR) spectroscopy, it constitutes a sensitive, selective analytical technique. This methodology can be used to detect ppb concentrations of anions in aqueous samples when an extractant is coated on the ATR crystal. In previous years, Fourier transform infrared spectroscopy has not been viewed as a useful method for the detection of trace amounts of analytes in aqueous matrixes due to the intense ν(OH) and δ(OH) bands which extend over large regions of the IR spectrum[1]. With the development of ATR-FTIR spectroscopy and the use of thin film coatings this problem has been overcome.

II.1. The Instrument and Detection Principles. Figure 1.1 shows the instrument used for the ATR-FTIR experiments presented in this work. In this technique, the sample is placed on a crystal with a high refractive index through which a beam of infrared radiation is transmitted. The beam enters the crystal through a bisected end with an angle such that it bounces within the crystal many times: it is internally, totally reflected. For this to occur the angle of incidence needs to be $\geq \theta_c$, the critical angle; otherwise on every bounce on the crystal edge, the beam is partially reflected and partially refracted, moving from the more dense crystal to the less dense sample. The refractive indexes of the materials at the interface are related to θ_c by Equation 1.1, where η_1 and η_2 are the refractive indexes of the ATR crystal and the sample, respectively.[2]

Figure 1.1. Instrument and ATR Probes used for ATR-FTIR Spectroscopy. **Top.** ReactIR-1000, ATR-FTIR spectrometer from Mettler-Toledo, connected to a computer and the ATR probes. **Bottom, left.** Top view of the Diamond probe, showing the Di crystal in the center of the stainless steel enclosure. **Bottom, center.** Silicon probe detail showing a $DEC^{+}NO_3^{-}$ film on the Si crystal and 1 mL of water used for equilibration. **Bottom, right.** Silicon probe, shown on the side, with a custom glass container attached.

$$\sin\theta_c = \frac{\eta_2}{\eta_1} \qquad 1.1$$

The sensing takes place at the crystal/sample interface, where the incident and reflected radiation interact to form a wave, generally referred to as the evanescent wave. This wave penetrates into the adjoining medium, which is less dense (i.e., has a smaller index of refraction, η) than the crystal, and decays away following an exponential curve (Figure 1.2), as described in Equation 1.2, where E is energy, E_0 is the initial energy of the electromagnetic wave at the surface interface, z is the distance in the z-axis direction away from the surface, and d_p is the penetration depth of the evanescent wave.[2] This penetration depth, important for sensing, is given by Equation 1.3, where ν is the wavenumber of the radiation, and all other parameters are as defined previously.[3]

$$E = E_0 e^{-z/dp} \qquad 1.2$$

$$d_p = \frac{1}{2\pi\nu\sqrt{\eta_1^2 \sin\theta - \eta_2^2}} \qquad 1.3$$

If an IR active species is present in the area adjacent to the crystal, it absorbs part of the radiation and it is detected, as long as it is in the narrow region probed by the evanescent wave. The short d_p that results from commonly used wavenumbers and materials reduces the amount of IR radiation absorbed by water, compared to transmission IR; therefore the detection of aqueous analytes at millimolar concentrations is possible.

Two commercially available crystals were used in the experiments presented in this work: a silicon crystal (Si), which allows for 30 beam bounces, and a diamond crystal (Di), which permits 18. The gains used were 1 for the Si probe and 2 for the Di probe. Although both probes have a low end wavenumber cutoff at approximately 600 cm^{-1}, the

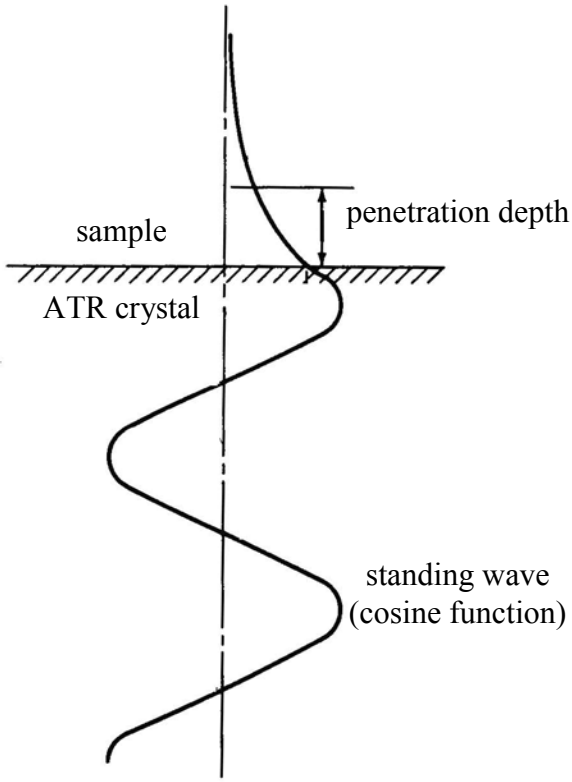

Figure 1.2. The evanescent wave within the ATR crystal that decays exponentially in the less dense sample medium.

Di probe also has an essentially zero-throughput region between 1950 and 2150 cm^{-1}. Also, a better sensitivity below 1000 cm^{-1} has been observed for the Di probe by previous members of the Strauss group,[4] which can be explained by the fact that the IR throughput of the Si ATR crystal decreases more significantly below 1000 cm^{-1} than the throughput of the Di crystal. Other minor factors might also contribute to this phenomenon, like the difference in evanescent wave penetration depths (which will vary because diamond and silicon have different ηs) and the possibility of different film morphologies on the different ATR crystals. Nevertheless, the result is an increase in noise below 1000 cm^{-1} for the Si probe, which is contrary to what could be expected if only the number of internal reflections in each crystal were considered.

The system was purged with nitrogen gas, non-IR active, in order to stop any possible beam attenuation on its way from the source to the detector.

II.2. ATR-FTIR and Transmission FTIR Spectroscopies. Peak intensity in ATR-FTIR spectroscopy cannot be directly correlated to peak intensity in transmission FTIR spectroscopy for the same molecule at the same aqueous concentration. This is due to the molar absorptivity, which is characteristic of each molecule and is related to the amount of radiation it can absorb per mole. For traditional FTIR, this property is wavenumber dependent and it is directly related to absorbance through Beer's Law.[5] However, when using ATR-FTIR spectroscopy, the relative absorbance intensity is not equal to that in FTIR spectroscopy at all wavenumbers.[2,3] Compared to transmission spectra, bands are relatively more intense at smaller wavenumbers in ATR spectra. However, no significant shift in the wavenumber of the bands is observed. Because of this difference in the absorbance spectrum, ATR-FTIR spectra are often converted from percent transmission into absorbance units, using the Kramers-Kronig relationship, which minimizes these differences.[3] Due to software limitations this algorithm was not used for the experiments described and the spectra presented as part of this work.

II.3. The Extractants. The use of thin film coatings on the ATR probe allows the IR technique to be used to study aqueous samples containing *ppb* concentrations of polyatomic anions. These coatings serve two purposes: they exclude the water from the area probed by the IR beam and they serve as a preconcentrator, as the anion in the extractant film exchanges with the analyte in the sample. The Strauss Group has developed a series of modified ferrocenium salts for this purpose, with the general structure shown in Figure 1.3. These salts have shown exceptional properties as anion-exchange extractants.[4,6] Salts of one of these modified ferroceniums, in particular 1,1′,3,3′-tetrakis(2-methyl-2-nonyl)ferrocenium (DEC^+), have been used for the efficient extraction and recovery of weakly hydrated anions from water.[4] The nature and characteristics of these ferrocenium salts are discussed in Chapter 2.

II.4. The Ion Exchange Thermodynamics. The factor that controls a hypothetical anion exchange between the aqueous and the organic phases is known as the difference in standard Gibbs free energy of transfer, $\Delta\Delta G°_{tr}$, which refers to the process of transferring an ion from water into the gas phase, and resolvating it in another solvent containing a cation. Three factors contribute to $\Delta\Delta G°_{tr}$: the differences in hydration energy ($\Delta\Delta G°_{hyd}$) and solvation energy ($\Delta\Delta G°_{solv}$) of the two anions, and the difference in the ion-pair energies ($\Delta\Delta G°_{ion\text{-}pair}$) for the pairs formed between the anions with the extractant cation in the non-aqueous solvent (in this model, it is assumed that ion pairing in the aqueous phase is negligible).

$$\Delta\Delta G°_{tr} \approx \Delta\Delta G°_{hyd} + \Delta\Delta G°_{solv} + \Delta\Delta G°_{ion\text{-}pair} \qquad 1.2$$

These three entities can be related to the three main processes that play a part in ion exchange, as shown in the following example for NO_3^- in a film and ClO_4^- in water:

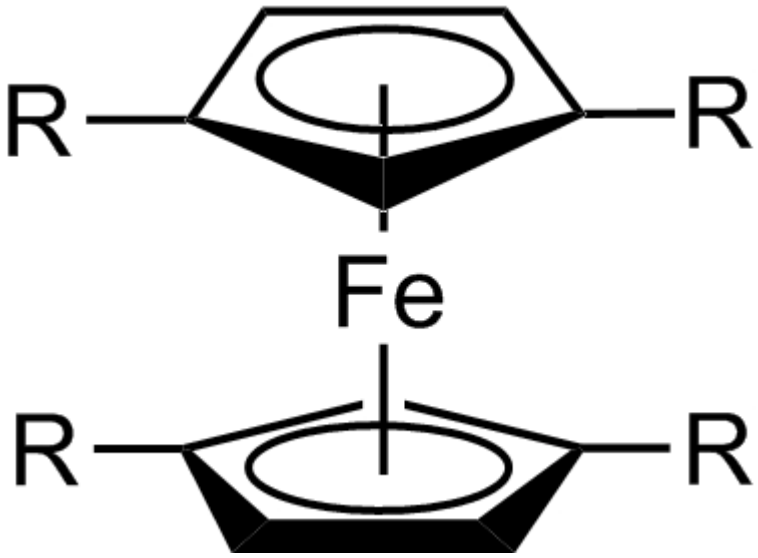

Figure 1.3. General structure for the modified ferrocenium salts used in this work. R = 2-methyl-2-nonyl in DEC; R = 2-methyl-2-hexyl in HEP; R = t-butyl in BUT.

$$DEC^{+}NO_3^{-}\,(org) \rightleftharpoons DEC^{+}\,(org) + NO_3^{-}\,(org) \qquad -\Delta G^{\circ}_{ion\text{-}pair}\,(NO_3^{-})$$

$$NO_3^{-}\,(org) \rightleftharpoons NO_3^{-}\,(g) \qquad -\Delta G^{\circ}_{solv}\,(NO_3^{-})$$

$$NO_3^{-}\,(g) \rightleftharpoons NO_3^{-}\,(aq) \qquad \Delta G^{\circ}_{hyd}\,(NO_3^{-})$$

$$ClO_4^{-}\,(aq) \rightleftharpoons ClO_4^{-}\,(g) \qquad -\Delta G^{\circ}_{hyd}\,(ClO_4^{-})$$

$$ClO_4^{-}\,(g) \rightleftharpoons ClO_4^{-}\,(org) \qquad \Delta G^{\circ}_{solv}\,(ClO_4^{-})$$

$$DEC^{+}\,(org) + ClO_4^{-}\,(org) \rightleftharpoons DEC^{+}ClO_4^{-}\,(org) \qquad \Delta G^{\circ}_{ion\text{-}pair}\,(ClO_4^{-})$$

Since the hydration energies of ClO_4^- and NO_3^- are –259 and –314 kcal mol^{-1},[7] respectively, the overall difference in hydration energies ($\Delta\Delta G^{\circ}_{hyd}$) is –55 kcal mol^{-1}, which indicates a favorable process. The $\Delta\Delta G^{\circ}_{solv}$ term can be minimized by using a solvent with a low dielectric constant. The $\Delta\Delta G^{\circ}_{ion\text{-}pair}$ term can be minimized by (i) using a large cationic extractant or (ii) using an organic solvent with a high dielectric constant. The former factor is achieved by the choice of $DEC^{+}NO_3^{-}$, while the latter is in conflict with the low dielectric constant required to minimize $\Delta\Delta G^{\circ}_{solv}$. Since both $\Delta\Delta G^{\circ}_{solv}$ and $\Delta\Delta G^{\circ}_{ion\text{-}pair}$ are dependent on the dielectric constant of the organic solvent, a compromise is necessary. These factors can be summarized in a modified Born model, based on Coulomb's law,[8] for $\Delta\Delta G^{\circ}_{tr}$ as shown:

$$\Delta\Delta G^{\circ}_{tr}(\text{kJ/mol}) = B\left\{\frac{1}{\varepsilon_S}\left[\left(\frac{1}{r_X}-\frac{1}{r_Y}\right)+2\left(\frac{1}{r_Y+r_R}-\frac{1}{r_X+r_R}\right)\right]+\frac{1}{\varepsilon_W}\left(\frac{1}{r_Y}-\frac{1}{r_X}\right)\right\} \qquad 1.3$$

where B is a temperature independent constant equal to −69.47 kJ nm mol^{-1} r_Y and r_X are the size of the respective anions, r_R is the radius of the cationic extractant, ε_W is the dielectric constant of water, and ε_S is the dielectric constant of the solvent. If r_R is made infinite, then the term containing the size of the cationic extractant is reduced to zero. This results in an inverse relation between $\Delta\Delta G^{\circ}_{tr}$ and both the dielectric constant of the solvent and the anionic radii. Note that the anionic radii also have an inverse relation with $\Delta\Delta G^{\circ}_{hyd}$. In this case, a lower dielectric solvent can be used without compromising

relation with $\Delta\Delta G°_{hyd}$. In this case, a lower dielectric solvent can be used without compromising selectivity, being now evident the usefulness of the larger size of the $DEC^{+}NO_3^{-}$ extractant compared to others containing shorter alkyl chains.

III. References

(1) Griffiths, P. R.; de Haseth, J. A. *Fourier Transform Infrared Spectrometry*; John Wiley & Sons: New York, 1986.

(2) Harrick, N. J. *Internal Reflection Spectroscopy*; Interscience: New York, 1967.

(3) Urban, M. W. *Attenuated Total Reflectance Spectroscopy of Polymers. Theory and Practice*; American Chemical Society: Washington DC, 1996.

(4) Hebert, G. N.; Odom, M. A.; Bowman, S. C.; Strauss, S. H. *Analytical Chemistry* **2004**, *76*, 781-787.

(5) Skoog, D. A.; Leary, J. J. *Principles of Instrumental Analysis*, 4th ed.; Saunders College Publishing: New York, 1992.

(6) Clark, J. F.; Clark, D. L.; Whitener, G. D.; Schroeder, N. C.; Strauss, S. H. *Environ. Sci. Technol.* **1996**, *30*, 3124-3127.

(7) Moyer, B. A.; Bonnesen, P. V. *Supramolecular Chemistry of Anions*; VCH Publishers: New York, 1997.

(8) Moyer, B. A.; Bonnesen, P. V. In *Supramolecular Chemistry of Anions*; Bianchi, A., Bowman-James, K., Garcia Espana, E., Eds.; VCH Publishers: New York, 1997, pp 1–44.

Chapter 2

Cation-Anion Interactions in Ferrocenium Salt Thin Films and Single Crystals

I. Introduction

I.1. Why Study Extracting Materials in Detail? The analytical chemistry that will be presented in Chapter 3 is based on the determination of concentrations of polyatomic aqueous monoanions (generically EX_n^-) in the parts-per-billion to parts-per-million range. This is done by allowing the anion to undergo ion exchange into a thin film of a water-insoluble ferrocenium salt deposited on an ATR-FTIR crystal, in contact with the aqueous sample, and monitoring the absorbance of one or more infrared-active ν(EX) as a function of time. The analyses are based on sets of time-dependent ATR-FTIR spectra of thin films in contact with aqueous media (each set can contain up to 60 or 120 individual spectra). Detailed descriptions of the instrumentation, materials, and methodology used were presented in Chapter 1, along with some of the fundamentals of ATR-FTIR spectroscopy that are relevant to this work.

In addition to providing the information needed to determine the aqueous concentrations of the anions studied, the spectroscopic results also revealed interesting information about the nature of the cation–anion interactions in the thin films. The interpretation of these results requires a detailed understanding of these interactions, and for this reason an analysis of the crystal structures of relevant ferrocenium salts, determined by single-crystal X-ray diffraction, will be presented in this chapter. (Many of the crystals were grown by other co-workers, some were grown by the author specifically for this analysis, and none of the X-ray structures has yet been published.) Finally, the current working model in the Strauss Research Group for the structures of the thin films,

which is based on the crystal-structure analysis and on additional spectroscopic experiments, will also be presented in this chapter. This model accounts for the selectivity of the films for large, weakly-hydrated anions and for the relatively rapid rate of anion exchange.

I.1.1. The Advantage of Using Thin Films of Ion-Exchange Materials. Although FTIR spectroscopy has not traditionally been regarded as a suitable choice for detecting low concentrations of analytes in aqueous solution (primarily because of the strong interference of the intense ν(OH) and δ(OH) IR bands of water[1]), previous members of the Strauss Research Group have developed an ATR-FTIR method to detect ppb concentrations of polyatomic anions in aqueous samples.[2-4] This is possible for two reasons. First, the evanescent wave only penetrates ca. 1 μm into the sample (depending on the IR wavelength and the η values of the sample and the ATR crystal) and therefore does not have to pass through a macroscopic amount of water (typical IR solution-cell pathlengths are ca. 0.1 or 0.05 mm). Second, the ATR method involves the preconcentration of the analyte in the thin film of ion-exchange material (i.e., in the evanescent-wave region) *in real time during the analysis*. As discussed later, the preconcentration factor can be up to five or six orders of magnitude when complete ion-exchange has occurred. The net result is that signals from bulk water are minimized (although not eliminated) and the detection limit is orders of magnitude lower than it would be if a thin film would not be used (for an equivalent amount of time per analysis).[2]

I.1.2. Time-Dependent ATR-FTIR Spectra of Thin Films during Ion Exchange. Figure 2.1 shows the ATR-FTIR spectra over time of a $DEC^+NO_3^-$ thin film in contact with a 5 μM aqueous solution of $KClO_4$. These spectra will serve to define the scientific questions that led to the structural analysis described in this chapter. The intense ν(NO) band of the NO_3^- anion decreases over time, and ν(ClO) bands of the

ClO_4^- anion increase over time, as the ion-exchange reaction shown in Equation 2.1 proceeds.

$$DEC^+NO_3^-(s,\ thin\ film) + ClO_4^-(aq) \rightarrow DEC^+ClO_4^-(s,\ thin\ film) + NO_3^-(aq) \qquad \textbf{2.1}$$

It is apparent that these two spectral changes are occurring at the same rate, which is consistent with the reaction in Equation 2.1 that presumably describes the process that produces the spectral changes. Any model of the structure of the thin film (i.e., the packing of anions and cations) must account for the fact that the ion exchange occurs relatively rapidly under these conditions. Furthermore, in the early stages of the ion exchange, only one ν(ClO) band is discernable, whereas at longer times multiple ν(ClO) bands grow in (this will be discussed in more detail below), and the thin-film structure model must also account for that apparent change in the site symmetry of the ClO_4^- anion. Finally, it can be seen that the most intense ν(ClO) band is prominent even after only a few minutes (i.e., in spectra 2–5), which is significant because the concentration of aqueous ClO_4^- that produced these spectral changes is *more than 100 times lower* than the 0.8 mM lower-limit concentration that can be detected in 10 minutes with the same instrument *in the absence* of the organometallic thin film (the 10-minute limit-of-detection of ClO_4^- *in the presence* of this particular thin film is 0.04 μM, which is 20,000 times lower than 0.8 mM).[2]

II. Results and Discussion

II.1. Analysis of Ferrocenium Salt Single-Crystal X-ray Structures. The series of tetraalkylferrocenes used in this study are shown schematically in Figure 2.2, along with their abbreviations. The compounds BUT and PENT were reported by Leigh in 1964.[5] The compound BUT2 was reported by Hughes et al. in 1994.[6] The compounds HEX,[7] HEP,[8] and DEC[9] were first prepared by previous members of the Strauss group. Salts of

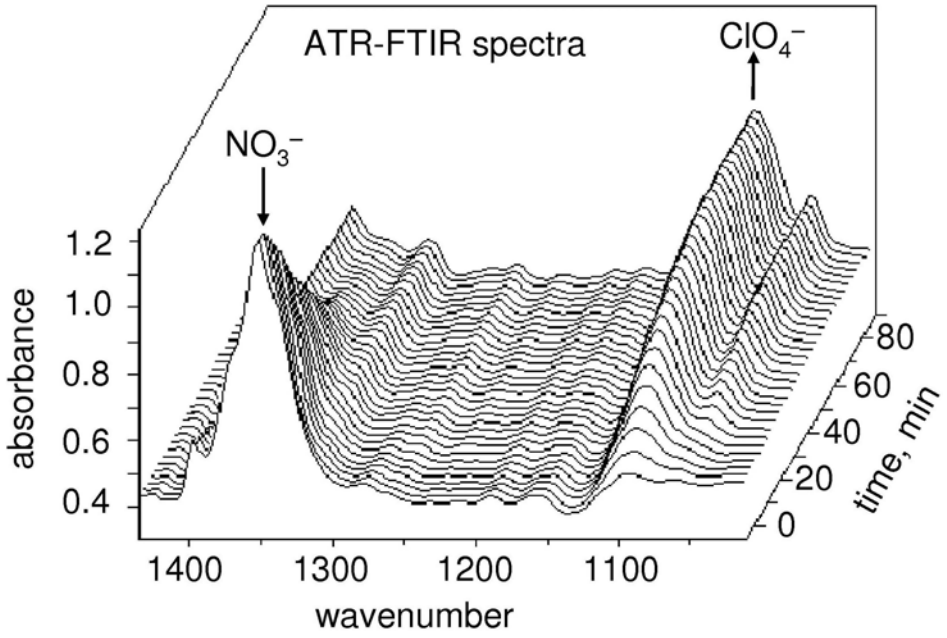

Figure 2.1. Time-dependent ATR-FTIR spectra of a ca. 1 μm thin film of $DEC^+NO_3^-$ in contact with a 5 μM aqueous solution of $KClO_4$ (30-bounce silicon ATR window, 4 cm^{-1} resolution; DEC^+ = 1,1',3,3'-tetra(2-methyl-2-nonyl)ferrocenium cation). This figure was adapted from a similar figure in the 2004 Colorado State University Ph.D. dissertation of Gretchen Hebert (data collected by Gretchen Hebert).

these compounds were typically prepared by treating a dichloromethane solution of the ferrocene with the silver(I) salt of the appropriate anion, either nitrate, perchlorate, or perrhenate. Filtration of the reaction mixture to remove metallic silver and slow evaporation of the filtrate resulted in diffraction quality single crystals of the ferrocenium salts listed in Table 2.1. The two crystalline salts prepared by the author of this dissertation are $BUT^+ClO_4^-\cdot CHCl_3$ and $BUT^+ClO_4^-\cdot CH_2Cl_2$.

Both BUT2 and the $BUT2^+$ cation have a 1,2 substitution pattern on each cyclopentadienyl (Cp) ring and therefore the highest symmetry possible for either molecular species is C_{2h}. All of the other ferrocenes and ferrocenium salts referred to in this dissertation have a 1,3 substitution pattern on each ring and, because the Cp rings are not co-planar, can have C_2 symmetry at best and are therefore chiral cations. In fact, the DEC^+ cations in the X-ray structures of $DEC^+NO_3^-$, $DEC^+ClO_4^-$, and $DEC^+ReO_4^-$ all have crystallographic C_2 symmetry.

II.1.1. Determination of X-ray Structures. Table 2.1 lists the ferrocenes and ferrocenium salts that have been structurally characterized at CSU by single-crystal X-ray diffraction and that will be discussed in this chapter. Many of them were prepared by previous members of the Strauss group. Their structures were determined by S. M. Miller and Prof. O. P. Anderson in the X-ray Laboratory in the CSU Department of Chemistry.

II.1.2. Crystal and Molecular Structures of the Ferrocenes and Ferrocenium Salts. Thermal ellipsoid plots of BUT^+, HEP^+, and DEC^+ (from the structures of $BUT^+NO_3^-\cdot CHCl_3$, $HEP^+NO_3^-$, and $DEC^+NO_3^-$, respectively) are shown in Figure 2.3. The footprint or cross-sectional area of each molecular cation (and neutral molecule) were previously estimated by Brady Clapsaddle by drawing a rectangle around the molecular species and including the van der Waals radii of the H atoms (1.2 Å[10]). These footprints are 120 $Å^2$ for BUT^+, 180 $Å^2$ for HEP^+, and 290 $Å^2$ for DEC^+.[9]

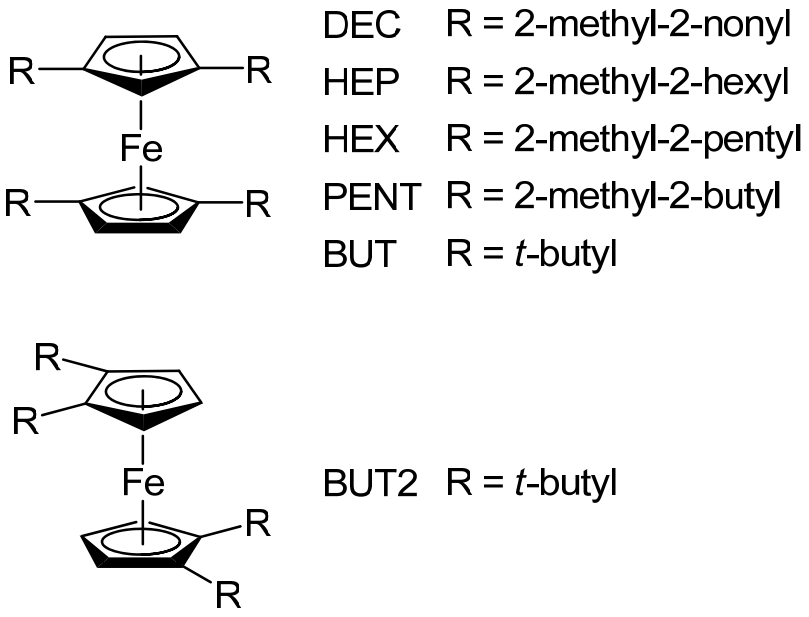

Figure 2.2. Schematic drawings of the ferrocenes used in this work and the abbreviations used for them in this dissertation. Each of these compounds can be converted to the corresponding ferrocenium salt with NO_3^-, ClO_4^-, or ReO_4^- counterions by treating the ferrocene with $AgNO_3$, $AgClO_4$, or $AgReO_4$, respectively, in dichloromethane. The oxidation states of iron atoms are 2+ and 3+ in the neutral ferrocenes and monocationic ferrocenium ions, respectively.

Table 2.1. Crystal data and structure refinement parameters for ferrocenium salts[a]

compd abbreviation		$BUT^+NO_3^-\cdot CHCl_3$	$BUT^+ClO_4^-\cdot CHCl_3$	$BUT^+ClO_4^-\cdot CH_2Cl_2$
crystals grown by		Michael Bayless	Samira Caamaño	Samira Caamaño
formula, formula weight (g mol^{-1})		$C_{27}H_{43}Cl_3FeNO_3$, 591.84	$C_{27}H_{43}Cl_4FeO_4$, 629.26	$C_{27}H_{44}Cl_3FeO_4$, 660.66
crystal system, space group, Z		mono., Cc, 4	ortho., $Pna2_1$, 4	ortho., $P2_12_12_1$, 4
color of crystal		green	green	green
unit cell dimensions	a, Å	12.818(3)	21.175(5)	9.7666(4)
	b, Å	26.102(5)	14.926(4)	15.0359(7)
	c, Å	10.573(2)	9.718(2)	19.9772(9)
	α, deg	90	90	90
	β, deg	121.44(1)	90	90
	γ, deg	90	90	90
temperature, °C		–173(2)	–173(2)	–173(2)
final R indices [$I > 2\sigma(I)$]		R_1 = 0.0524,	R_1 = 0.0681,	R_1 = 0.0342,
		wR_2 = 0.1241	wR_2 = 0.1261	wR_2 = 0.0863
goodness-of-fit on F^2		1.027	0.961	1.010

[a] mono. = monoclinic; ortho. = orthorhombic; tri. = triclinic; BUT = 1,1',3,3'-tetra-*t*-butylferrocene; BUT2 = 1,1',2,2'-tetra-*t*-butylferrocene; HEP = 1,1',3,3'-tetra-(2-methyl-2-hexyl)ferrocene; DEC = 1,1',3,3'-tetra-(2-methyl-2-nonyl)ferrocene.

Table 2.1. Crystal data and structure refinement parameters for ferrocenium salts[a] (continued)

compd abbreviation		HEP	$HEP^+NO_3^-$	$BUT2^+ReO_4^-$
crystals grown by		Brady Clapsaddle	Dustin Clark	Kristina Rohal
formula, formula weight (g mol^{-1})		$C_{38}H_{66}Fe$, 578.76	$C_{38}H_{66}FeNO_3$, 640.77	$C_{26}H_{42}FeO_4Re$, 660.66
crystal system, space group, Z		ortho., $Fdd2$, 8	tri., $P\bar{1}$, 2	mono., $P2_1/c$, 8
color of crystal		orange	green	green
unit cell dimensions	a, Å	18.833(12)	10.7055(7)	16.3501(1)
	b, Å	43.00(2)	14.3445(9)	16.7310(2)
	c, Å	8.849(5)	25.815(2)	20.9034(4)
	α, deg	90	76.265(2)	90
	β, deg	90	83.174(2)	106.785(1)
	γ, deg	90	77.547(2)	90
temperature, °C		–103(2)	–110(2)	–109(2)
final R indices [$I > 2\sigma(I)$]		R_1 = 0.0726,	R_1 = 0.0750,	R_1 = 0.0783,
		wR_2 = 0.1602	wR_2 = 0.1309	wR_2 = 0.1024
goodness-of-fit on F^2		0.756	0.878	1.085

[a] mono. = monoclinic; ortho. = orthorhombic; tri. = triclinic; BUT = 1,1',3,3'-tetra-*t*-butylferrocene; BUT2 = 1,1',2,2'-tetra-*t*-butylferrocene; HEP = 1,1',3,3'-tetra-(2-methyl-2-hexyl)ferrocene; DEC = 1,1',3,3'-tetra-(2-methyl-2-nonyl)ferrocene.

Table 2.1. Crystal data and structure refinement parameters for ferrocenium salts[a] (continued)

compd abbreviation		DEC	$DEC^+NO_3^-$	$DEC^+ClO_4^-$	$DEC^+ReO_4^-$
crystals grown by		Brady Clapsaddle	Yoshi Kobayashi	Brady Clapsaddle	Brady Clapsaddle
formula, formula weight (g mol^{-1})		$C_{50}H_{90}Fe$, 747.07	$C_{50}H_{90}FeNO_3$, 809.08	$C_{50}H_{90}ClFeO_4$, 846.52	$C_{50}H_{90}FeO_4Re$, 997.27
crystal system, space group, *Z*		mono., *C*2/*c*, 4	mono., *P*2/*n*, 2	mono., *P*2/*n*, 2	mono., *P*2/*n*, 2
color of crystal		orange	green	green	green
unit cell dimensions	*a*, Å	18.7606(8)	9.3913(14)	10.2152(10)	10.458(2)
	b, Å	8.7418(4)	8.6868(13)	8.7223(8)	8.8509(17)
	c, Å	28.808(1)	29.695(5)	27.602(3)	27.359(6)
	α, deg	90	90	90	90
	β, deg	101.736(1)	93.691(4)	99.074(2)	99.311(4)
	γ, deg	90	90	90	90
temperature, °C		–103(2)	–100(2)	–100(2)	–100(2)
final *R* indices [$I > 2\sigma(I)$]		$R_1 = 0.0675$,	$R_1 = 0.0484$,	$R_1 = 0.0542$,	$R_1 = 0.0421$,
		$wR_2 = 0.1385$	$wR_2 = 0.1180$	$wR_2 = 0.1290$	$wR_2 = 0.0887$
goodness-of-fit on F^2		0.865	1.023	1.033	0.996

[a] mono. = monoclinic; ortho. = orthorhombic; tri. = triclinic; BUT = 1,1',3,3'-tetra-*t*-butylferrocene; BUT2 = 1,1',2,2'-tetra-*t*-butylferrocene; HEP = 1,1',3,3'-tetra-(2-methyl-2-hexyl)ferrocene; DEC = 1,1',3,3'-tetra-(2-methyl-2-nonyl)ferrocene.

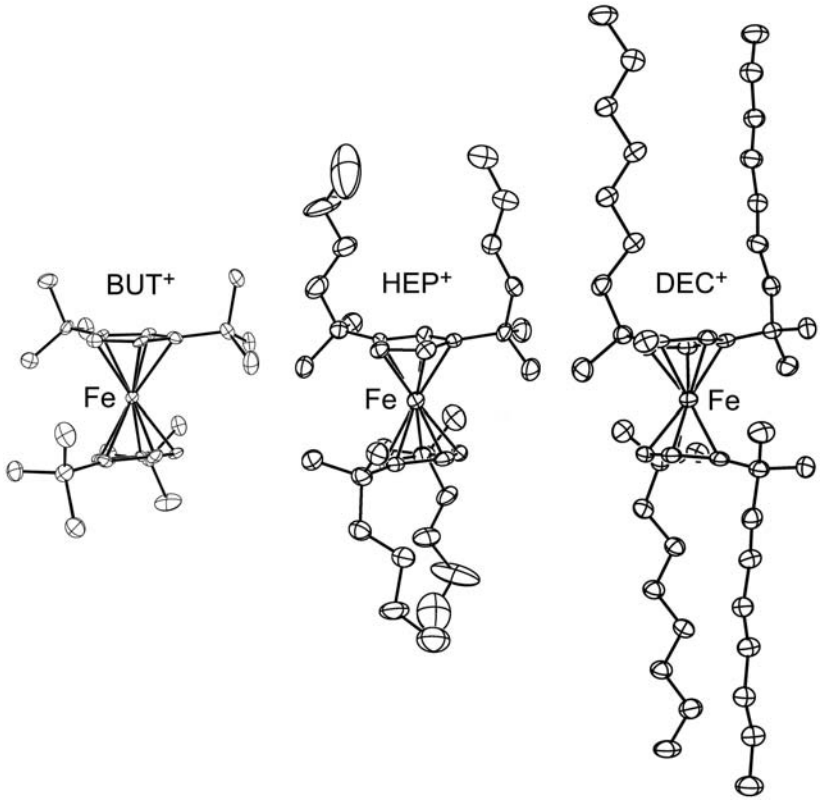

Figure 2.3. Drawings of the BUT^+, HEP^+, and DEC^+ cations from the X-ray structures of $BUT^+NO_3^-\cdot CHCl_3$, $HEP^+NO_3^-$, and $DEC^+NO_3^-$, respectively (50% probability ellipsoids).

In the structures of neutral HEP and DEC, layers of these molecules are arranged so that the Fe atoms are co-planar with the alkyl substituents, extending above and below the plane of the Fe atoms. The Fe atoms form a distorted hexagonal array in both structures, as shown in Figure 2.4. The Fe atoms in the structure of neutral BUT, which was reported by Boese et al. in 1993, also form layers that approximate a hexagonal array.[11] The spacings between the approximately hexagonal layers of Fe atoms are 6.06 Å in BUT,[11] 10.75 Å in HEP, and 14.10 Å in DEC. There is another kind of layering in the structure of DEC that is relevant to the thin-film packing of DEC^+ salts, and that is the layering shown in Figure 2.5. Layers of DEC molecules with their 2-methyl-2-nonyl alkyl chains interdigitated are stacked upon similar layers with a van der Waals gap of 8.53 Å (this is the distance between the layers of co-planar Fe atoms in consecutive interdigitated layers). The layers that are 14.10 Å apart are tilted 65.4° with respect to the interdigitated layers. The interdigitation of the alkyl chains in DEC, shown in Figure 2.6, is very similar to the interdigitation of polyethylene molecules in crystalline polyethylene.[12]

The anions are located in the van der Waals gaps between nearly-congruent interdigitated layers of DEC^+ cations, according to the the X-ray structures of $DEC^+NO_3^-$, $DEC^+ClO_4^-$, and $DEC^+ReO_4^-$, as shown in Figure 2.7. Remarkably, even though the average N–O, Cl–O, and Re–O distances are all greater than 1.23 Å, and the van der Waals radius of an O atom is 1.52 Å,[10] the interdigitated layers in these three salts, at 9.11, 9.01, and 9.16 Å, respectively, are only ca. 0.5–0.6 Å farther apart than in neutral DEC (8.53 Å). (The ranges of N–O and Cl–O distances in $DEC^+NO_3^-$ and $DEC^+ClO_4^-$ are 1.237(2)–1.261(4) Å and 1.443(2)–1.261(4) Å, respectively; the Re–O distances in $DEC^+ReO_4^-$ are not reliable because of the disorder in the ReO_4^- ion, but it is probably the same as the Re–O distance in $KReO_4$, which is 1.736(2) Å.[13])

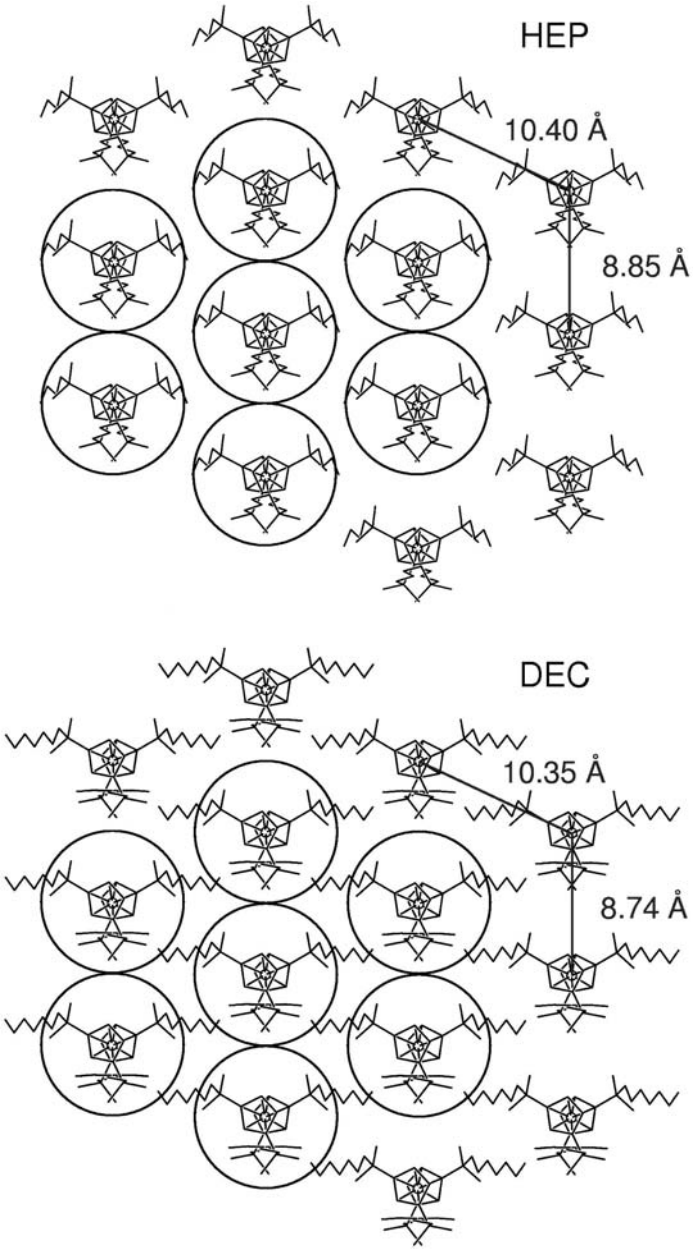

Figure 2.4. The approximately hexagonal array of neutral tetraalkylferrocene molecules in the X-ray structures of HEP and DEC.

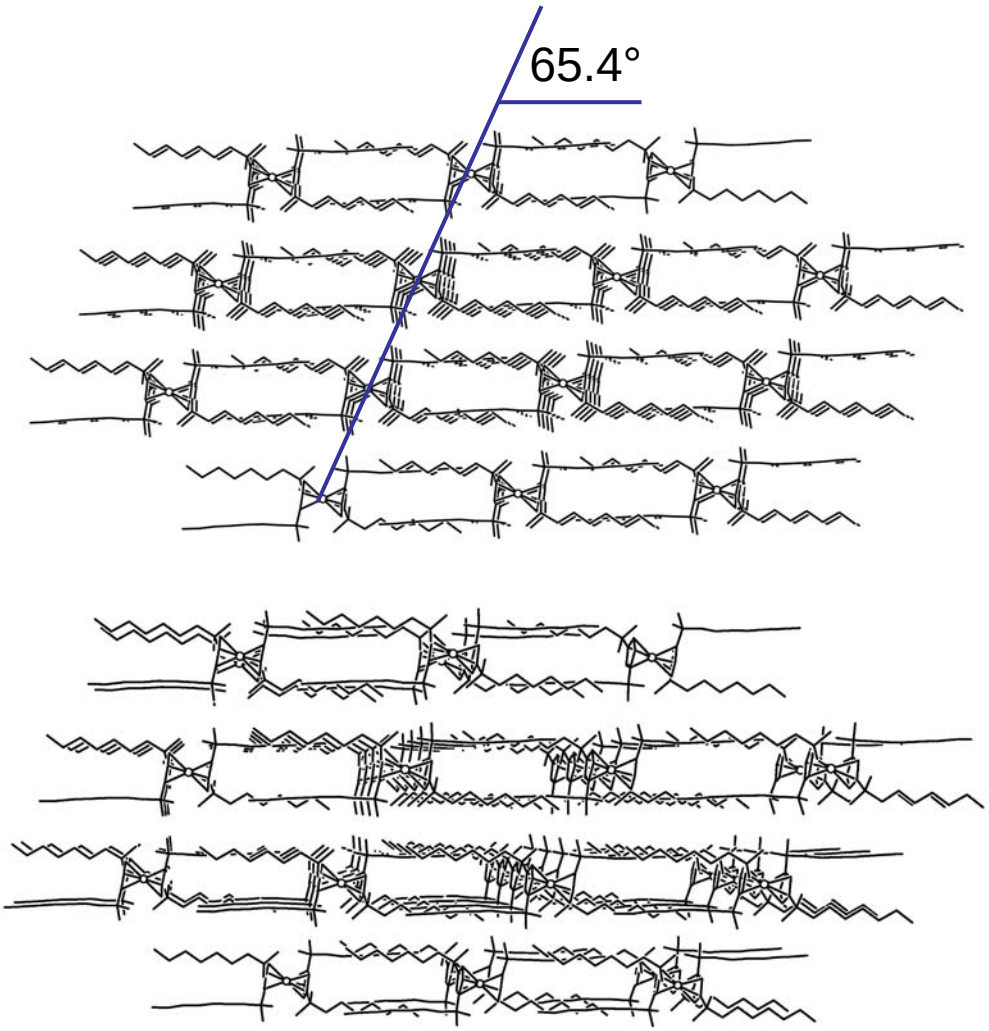

Figure 2.5. Drawings of two orientations of the stacking of interdigitated layers of DEC molecules in the X-ray structure of DEC. The perpendicular distance between the rigorously co-planar layers of Fe atoms in consecutive interdigitated layers (i.e., the van der Waals gap) is 8.53 Å. The rigorously co-planar layers of Fe atoms in the diagonal direction, which correspond to the approximately hexagonal layers of DEC molecules shown in Figure 2.4, are 14.10 Å apart. These layers are tilted 65.4° with respect to the interdigitated-layer stacking direction.

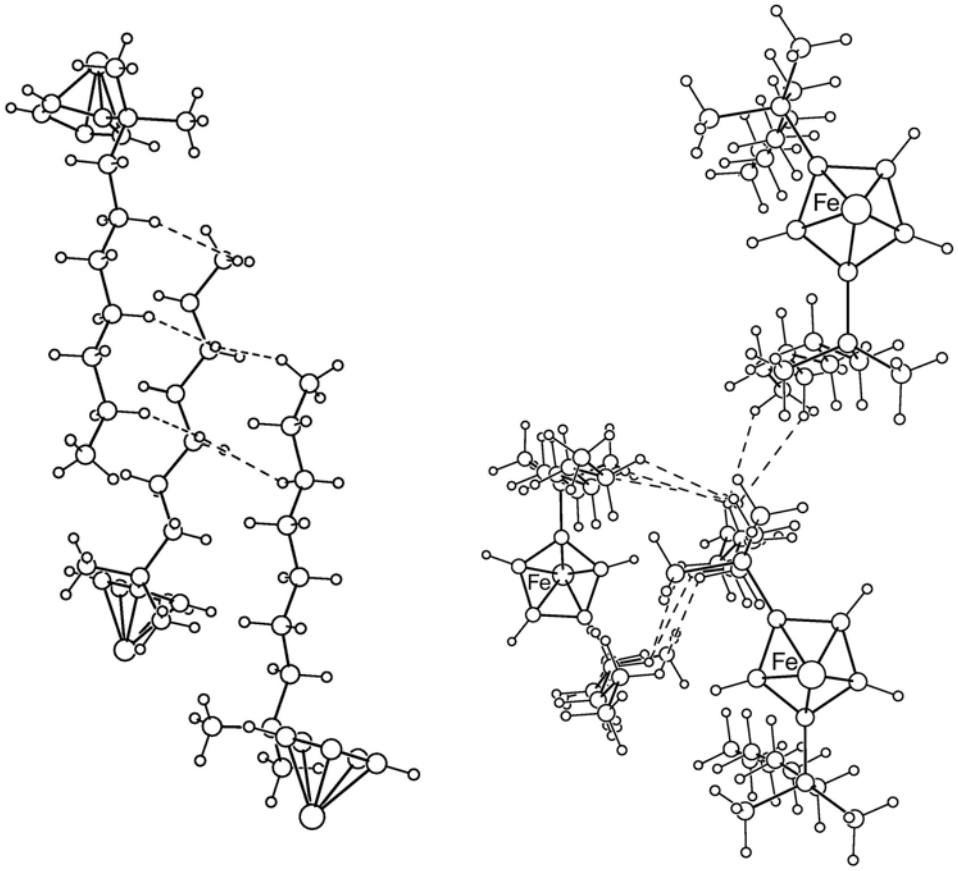

Figure 2.6. Two fragments of the X-ray structure of DEC showing the interdigitation of the alkyl substituents on the cyclopentadienyl ring. Only one dialkylcyclopentadienyl ring per Fe atom is shown for clarity. In the drawing on the left, only one 2-methyl-2-nonyl substituent per ring is shown. The H···H non-bonded contacts that are shown range from 2.48–3.06 Å (the van der Waals radius of an H atom is 1.20 Å).

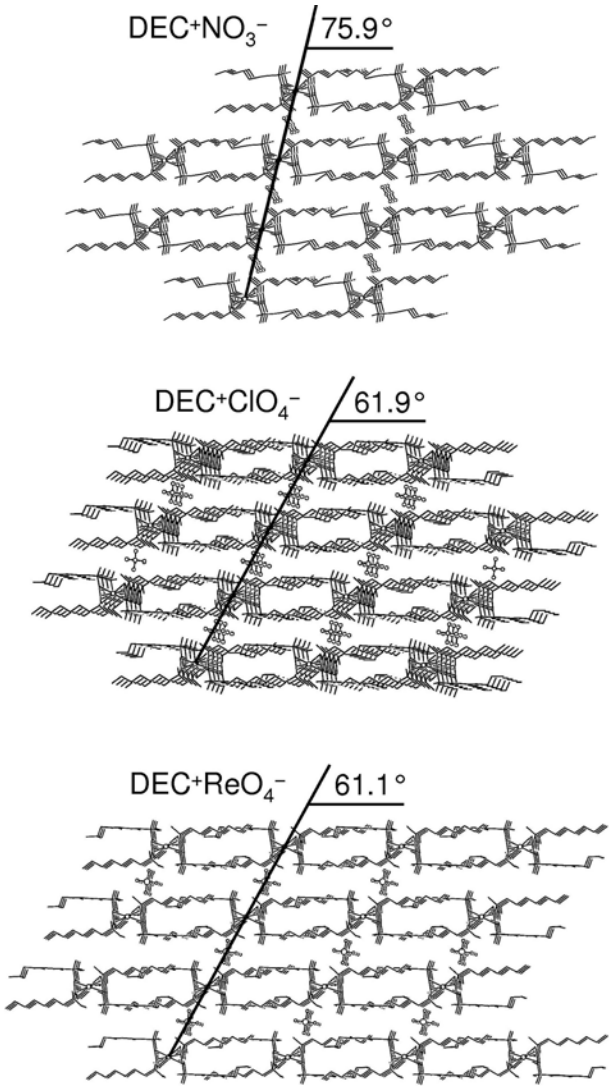

Figure 2.7. Drawings of the stacking of interdigitated layers of DEC^+ cations in the X-ray structures of $DEC^+NO_3^-$, $DEC^+ClO_4^-$, and $DEC^+ReO_4^-$. The counteranions are located in the van der Waals gaps between each interdigitated layer of cations. The perpendicular distances between the rigorously co-planar layers Fe atoms in consecutive interdigitated layers are 9.11 Å for $DEC^+NO_3^-$, 9.01 Å for $DEC^+ClO_4^-$, and 9.16 Å for $DEC^+ReO_4^-$. The layers of Fe atoms in the diagonal direction are 14.82, 13.63, and 13.50 Å apart for $DEC^+NO_3^-$, $DEC^+ClO_4^-$, and $DEC^+ReO_4^-$, respectively. The Fe and anion central atoms in these layers are rigorously co-planar.

The isomorphous structures of $DEC^+NO_3^-$, $DEC^+ClO_4^-$, and $DEC^+ReO_4^-$ can be thought of as alternating diagonal domains of (i) cations and anions and (ii) polyethylene-like hydrocarbon stacked left-to-right in Figure 2.7. Within the ionic domains, the Fe atoms and the central atoms of the anions (or, in the case of $DEC^+ReO_4^-$, the average position of the disordered Re atoms) are co-planar with the Fe atoms. The DEC^+ cations are not packed in a hexagonal array as are the DEC molecules in the X-ray structure of DEC. Instead, they are arranged in rectangular arrays, with interpenetrating rectangular arrays of anions, as shown in Figure 2.8. This results in each cation being surrounded by four anions, two at a shorter distance and two at a much longer distance (the interionic distances referred to here are Fe···N, Fe···Cl, and Fe···Re distances). These sets of distances ([short, long]) are [5.262(2), 7.864(2) Å], [5.560(2), 8.288(2) Å], and [5.65(8), 8.51(8) Å] for $DEC^+NO_3^-$, $DEC^+ClO_4^-$, and $DEC^+ReO_4^-$, respectively. This arrangement of anions and cations, with only two "short" (≤ 6.1 Å in these cases) center-to-center cation-anion distances, is unusual for ionic compounds, which generally have four or more nearest-neighbor ions around each ion of opposite charge. For example, in the X-ray structure of $HEP^+NO_3^-$ there are *three* short Fe···N distances of 5.131(2)–5.619(2) Å (the next longest distance is ca. 10.6 Å), and in the X-ray structure of $BUT2^+ReO_4^-$ there are *four* short Fe···Re distances of 5.8–6.1 Å and one longer distance of ca. 8.6 Å.

Even though the cations are arranged in rectangular arrays in the DEC^+ salts instead of hexagonal arrays, as in the structure of DEC, the interdigitation of the alkyl chains in the DEC^+ salts is similar to that in neutral DEC. This is shown for the cations in $DEC^+ReO_4^-$ in Figure 2.9.

II.1.3. The Relevant Relative Sizes of DEC^+, HEP^+, and BUT^+. As discussed in Chapter 1, the size of an extractant cation in part determines the ion-exchange selectivity of salts of that cation for weakly-hydrated anions. The larger the cation, the higher the selectivity, because ion-pairing in the non-aqueous phase is minimized for larger cations,

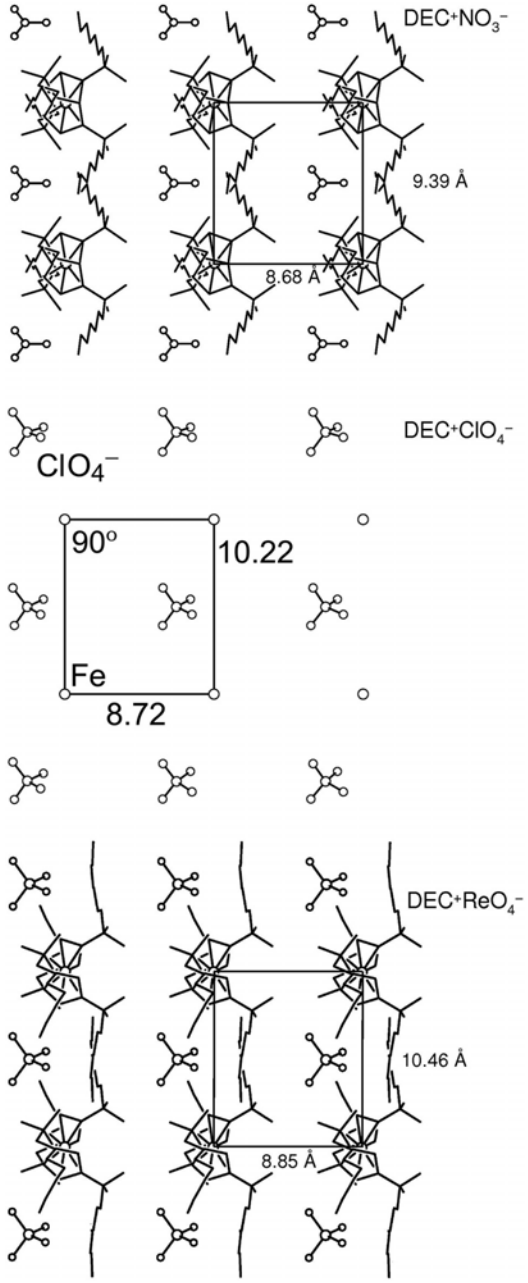

Figure 2.8. Arrangement of cations and anions in the ionic domains in the X-ray structures of $DEC^{+}NO_3^{-}$, $DEC^{+}ClO_4^{-}$, and $DEC^{+}ReO_4^{-}$. Only the average positions of the disordered Re and O atoms in $DEC^{+}ReO_4^{-}$ are shown. Distances shown in the middle drawing are also in Angstroms (Å).

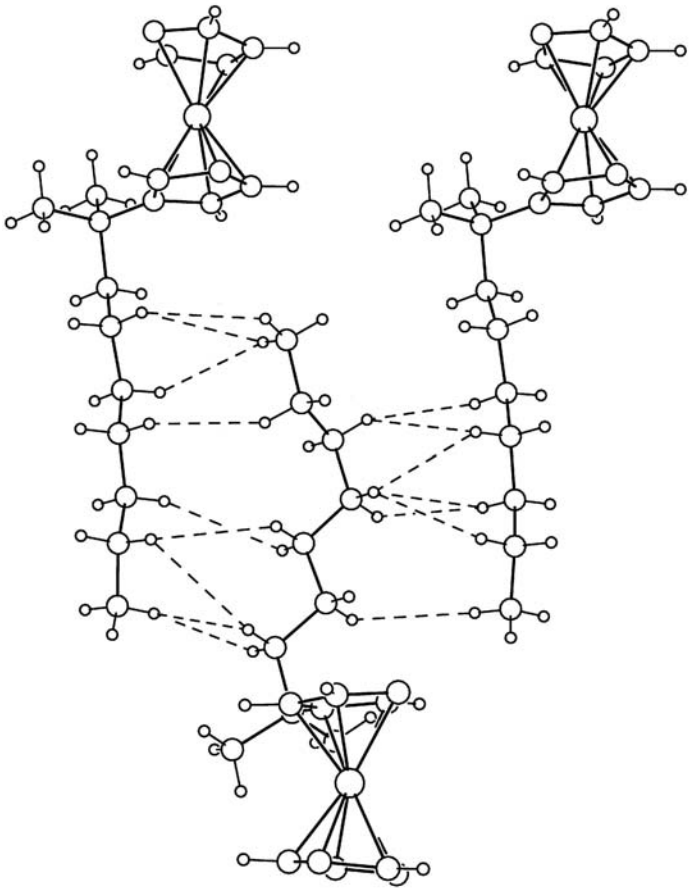

Figure 2.9. Fragment of the X-ray structure of $DEC^{+}ReO_4^{-}$ showing the interdigitation of the alkyl substituents on the cyclopentadienyl rings. Only one 2-methyl-2-nonyl alkyl group per DEC molecule is shown for clarity. The 15 H···H non-bonded interactions shown range from 2.45–3.04 Å (the van der Waals radius of an H atom is 1.20 Å). Compare this figure to the drawing on the left in Figure 2.6.

and the minimization of the *difference* in ion-pairing free energies between the target anion and the extractant anion leads to a larger ion-exchange equilibrium constant (note that the non-aqueous phase can be a liquid or a solid thin film on an inert support). The drawings in Figure 2.3 show that the footprints of BUT, HEP, and DEC vary significantly. The sizes of the neutral molecules and the corresponding cations are virtually the same because the Fe–C distances do not vary significantly. Accordingly, the size of the DEC^+ cation is significantly greater than the size of the BUT^+ cation. Or is it?

In the Ph.D. dissertation research of former Strauss group member Matthew Odom, it was shown that, K_d*, an ion-exchange figure of merit, increased by a factor of three over the range of ferrocenium nitrates with BUT^+, $PENT^+$, HEX^+, HEP^+, and DEC^+ cations, as shown in Figure 2.10.[14] In this case, the non-aqueous phase was a thin film of the ferrocenium salt physisorbed to Amberlite XAD-7 acrylic ester beads.[14] Similar results were reported by former Strauss group member Brady Clapsaddle based on ion-exchange selectivities measured by electrochemical methods, as also shown in Figure 2.10.[9] In this case, the non-aqueous phase was a monolayer of the modified ferrocenium salt self-assembled on a gold electrode (the modified ferrocenium cation had an additional ω-SH-undecanyl group on one of the cyclopentadienyl rings).[9] At the time, these results were attributed to the difference in size of the cations:[9,14] the "larger" cation, DEC^+, forms a weaker ion pair with the counteranion than the "smaller" HEP^+ cation, which forms a weaker ion pair with the anion than the HEX^+ cation, and so on. However, these results were in conflict with liquid-liquid ion-exchange figures of merit determined by former Strauss group member Professor C. Kevin Chambliss and co-workers at Baylor University, which show *negligible* differences in $D(ClO_4^-)$ or $D(ReO_4^-)$ values for the series of extractant salts $PENT^+NO_3^-$, $HEX^+NO_3^-$, $HEP^+NO_3^-$, and $DEC^+NO_3^-$ dissolved in chlorobenzene.

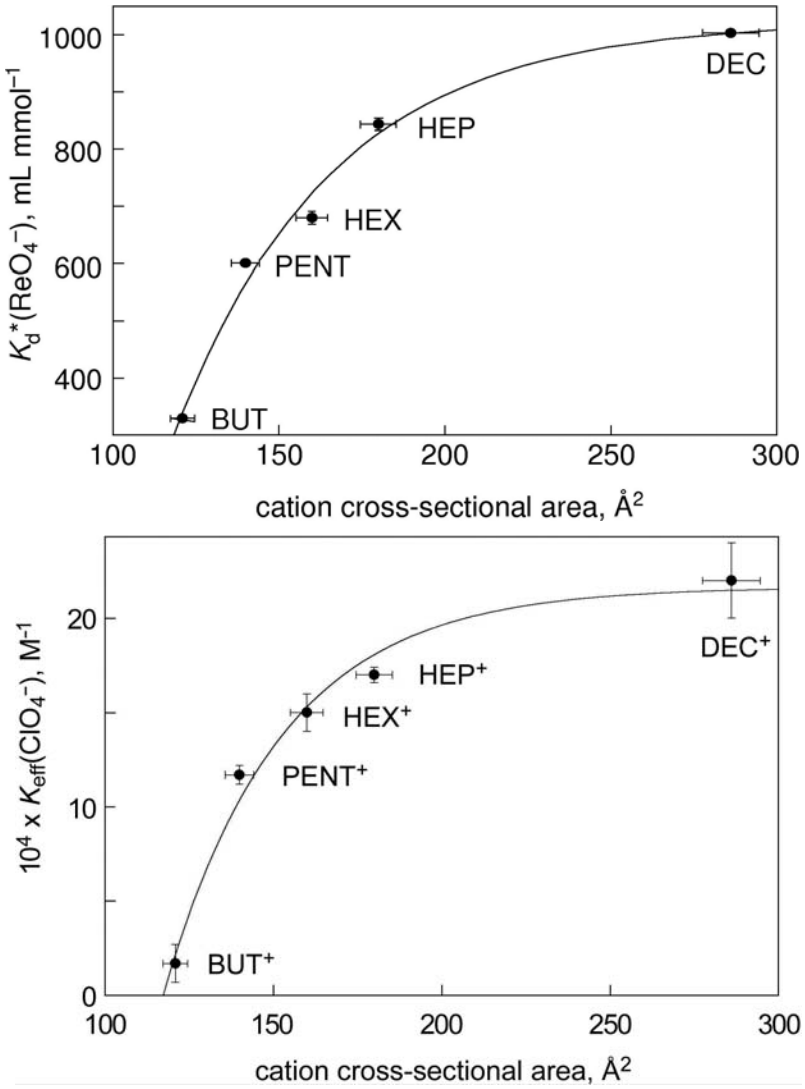

Figure 2.10. Top. The selectivity of thin films of $Fe(Cp')_2^+NO_3^-$ physisorbed on Amberlite XAD-7 polymer beads for aqueous ReO_4^- in the presence of 0.1 M aqueous $NaNO_3$. The ion-exchange figure of merit $K_d^*(ReO_4^-)$ is proportional to the change in concentration of ReO_4^- in the aqueous phase divided by the final concentration of ReO_4^- in the aqueous phase. **Bottom.** Similar selectivity plot for ClO_4^- in the presence of 0.1 M H_2SO_4 based on electrochemical measurements. These figures were adapted from similar figures in the Ph.D. dissertations of Matthew Odom (top)[14] and Brady Clapsaddle (bottom).[9]

These results are shown in Figure 2.11. So, are these ferrocenium cations different in size in the way that matters for ion-exchange or not, and why does the answer to this question depend on whether the non-aqueous phase is a solution of the extractant salt or a solid thin film or monolayer of the extractant salt? The analysis of the X-ray structures in Table 2.1 described in this chapter has finally provided plausible answers to these questions.

Figure 2.12 is a plot of the formula-unit volumes vs. the shortest Fe···N or Fe···Re distance in $BUT^+NO_3^-{\cdot}CHCl_3$, $HEP^+NO_3^-$, $DEC^+NO_3^-$, $BUT2^+ReO_4^-$, and $DEC^+NO_3^-$ (an estimate of the formula-unit volume of $CHCl_3$ was substracted from the formula-unit volume for $BUT^+NO_3^-$ shown in the plot). Also shown in Figure 2.12 is a plot of formula-unit volume vs. M···Cl distance for $LiClO_4$,[15] $NaClO_4$,[16] $KClO_4$,[17] $RbClO_4$,[18] and $CsClO_4$.[18] Note that the limits on the left and right *y* axes in this figure are proportional to one another. For the alkali metal perchlorates, the formula unit volume increases by 58% and the interionic distance increases by 37% from the Li^+ salt to the Cs^+ salt. It is clear that Cs^+ is a larger cation than Li^+, but more importantly, Cs^+ is *isotropically* larger than Li^+. In other words, not only are the six Cs···Cl distances in crystalline $CsClO_4$ ca. 37% longer than the six Li···Cl distances in crystalline $LiClO_4$ (all of the alkali metal perchlorates exhibit a NaCl-like structure), but, hypothetically, in a non-aqueous phase a $Cs^+ClO_4^-$ ion pair would have a Cs···Cl distance ca. 37% longer than the Li···Cl distance in the corresponding $Li^+ClO_4^-$ ion pair.

The situation is quite different for the five ferrocenium cations, because their size difference is anisotropic: it is confined to one dimension, not all three (see Figure 2.3). For the ferrocenium nitrate and perrhenate salts shown in Figure 2.12, the formula unit volume increases by ca. 70% on going from the BUT^+ salt to the DEC^+ salt but the *shortest* solid-state interionic distances are essentially the same. This means that there should be no significant difference in the *ion-pairing* energies of BUT^+X^- and DEC^+X^-

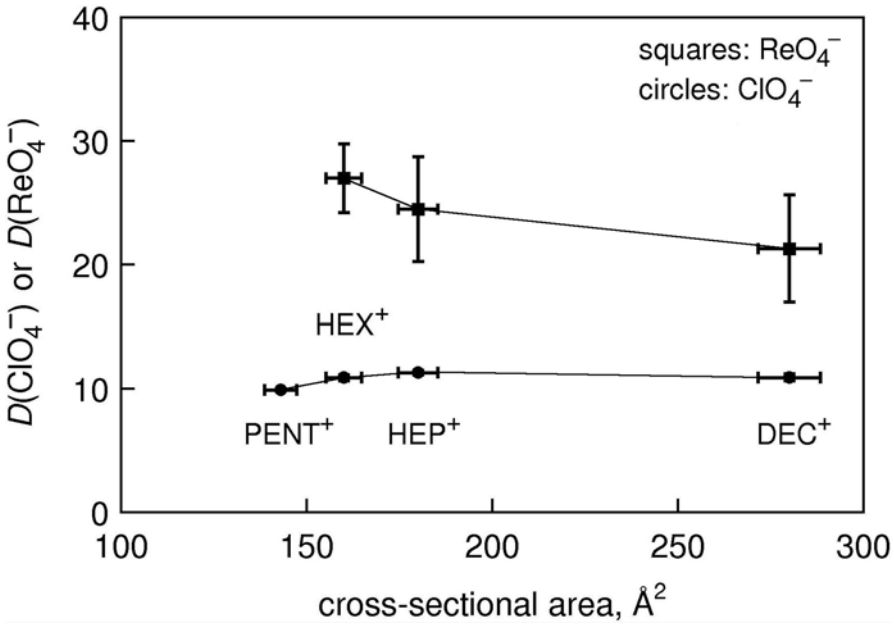

Figure 2.11. Plot of $D(ClO_4^-)$ or $D(ReO_4^-)$ values determined by ion chromatography for 2 mM chlorobenzene solutions of the nitrate salts of $PENT^+$, HEX^+, HEP^+, and DEC^+. The ion-exchange figure of merit $D(X^-)$ is the ratio of the equilibrium concentration of anion in the non-aqueous phase to the concentration of the anion in the aqueous phase. In these experiments, the initial phase contained 0.2 mM $KClO_4$ or $KReO_4$ and 0.2 M KNO_3. The errors shown for the D values are $\pm 1\sigma$ (the y-axis error bars are smaller than the data points for the $D(ClO_4^-)$ values). The errors shown for the footprints are arbitrarily set at ±3%. These data are unpublished results from the laboratory of Professor C. Kevin Chambliss at Baylor University (Chambliss, Strauss, et al., manuscript in preparation).

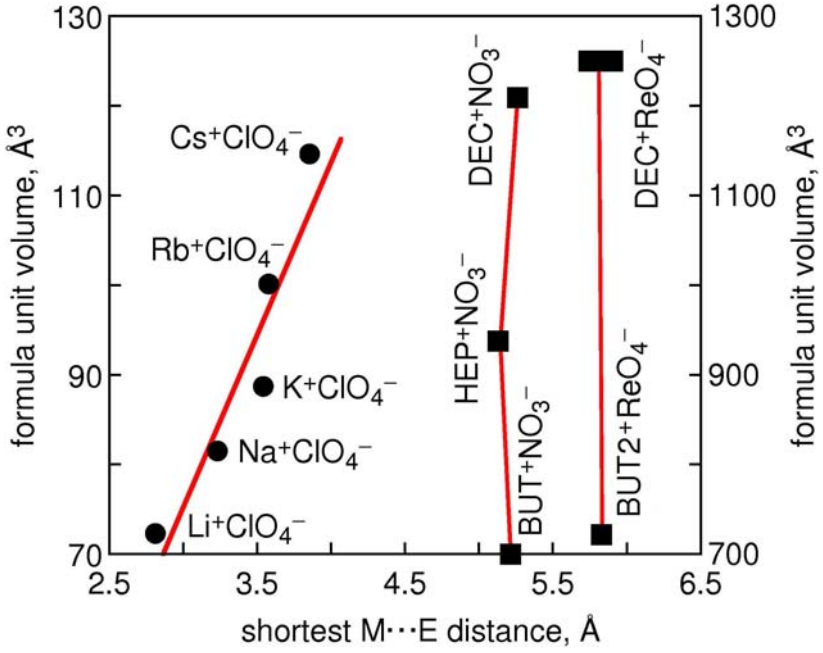

Figure 2.12. Plots of formula unit volumes vs. the shortest M···E distance in the X-ray structures of alkali metal perchlorates and several ferrocenium salts (E = N, Cl, or Re).

salts in a *liquid* non-aqueous phase for a given anion X^-, and this conclusion is in harmony with the constant $D(ClO_4^-)$ and $D(ReO_4^-)$ values shown in Figure 2.11. However, to the extent that the cation–anion packing in thin films of the ferrocenium salts resemble the crystal structures determined by X-ray diffraction, the *number* of cations that can surround the anion at a relatively short distance of ca. 6 Å or less (this is equal to the number of anions that can surround any given cation) varies from BUT^+ (four short distances) to HEP^+ (three short distances) to DEC^+ (two short distances). For this reason, the ion-clustering energy for thin films of the extractants should be largest for BUT^+ salts and smallest for DEC^+ salts, and this conclusion is consistent with the $K_d^*(ReO_4^-)$ values shown in the top plot in Figure 2.10. As the alkyl substituent changes from 2-methyl-2-propyl (i.e., *t*-butyl) in BUT^+ to 2-methyl-2-hexyl in HEP^+ to 2-methyl-2-nonyl in DEC^+, the hydrocarbon domain in the ferrocenium salts increases in size, restricting the "short-distance coordination number" of the ions. In a simple "electrostatic only" model based on the interionic distances, the four Fe···Re distances of ca. 5.95 Å and one longer distance of ca. 8.6 Å in $BUT2^+ReO_4^-$ would give an ion-clustering-energy figure of merit of ca. 0.8 (i.e., 4/5.95 Å + 1/8.6 Å = 0.79 $Å^{-1}$), whereas the corresponding figure of merit for $BUT2^+ReO_4^-$ would be ca. 0.6 (i.e., 2/5.65 + 2/8.51 = 0.59 $Å^{-1}$), about 25% smaller.

A short digression is necessary here. We are *not* arguing that the total cohesive energy (i.e., the "lattice energy") of a thin film of BUT^+X^- is necessarily larger than that of the corresponding DEC^+ salt. The interdigitated, polyethylene-like hydrocarbon domains of DEC^+ salts undoubtedly contributes to the lattice energy in a way that is not possible for BUT^+ salts. The discussion above is focused exclusively on the ionic component of the lattice energy, because the arrangement of the cations around the anions, and the inverse sum of the anion–cation center-to-center distances, are the relevant terms to consider as far as the ion-clustering term in the ion-exchange equilibrium equation (see Equation 1.2) is concerned.

Finally, the increasing $K_{eff}(ClO_4^-)$ values with increasing alkyl chain length for *monolayers* of the five extractant salts self-assembled on a gold electrode, which are shown in the bottom plot in Figure 2.10, requires yet a different explanation. This is because the packing of anions and cations in the monolayer should be nearly the same for all five extractant salts, since the cations are the same size in two dimensions (e.g., Figure 2.4 demonstrates this for neutral HEP and DEC). In other words, the anion–cation packing in the two dimensions of the monolayer probably resembles the planar packings shown for the DEC^+ salts in Figure 2.8. In the third dimension, the length of the alkyl substituents is very different, as shown in Figure 2.3 and also in the drawings in Figure 2.13, which depicts side-on views of hypothetical monolayers of $BUT^+NO_3^-$ and $DEC^+NO_3^-$ when they are self-assembled on the surface of a gold electrode. According to this model, the ion-pairing (really ion-clustering) energies would be the same across the series of extractant from $BUT^+NO_3^-$ to $DEC^+NO_3^-$. All of them would have two short and two long Fe···N distances (see Figure 2.8). However, since the aqueous phase would be in contact with one side of the monolayer, the *effective dielectric constant* of the medium in closest contact with the plane containing the centers of the positive and negative charges (i.e., the Fe and N atoms, respectively) would be more water-like for $BUT^+NO_3^-$ and more hydrocarbon-like for $DEC^+NO_3^-$. As discussed in Chapter 1, lowering the dielectric constant of the non-aqueous phase can have a dramatic effect on the energy and hence the equilibrium constant for ion exchange. Therefore, as the alkyl substituents on the ferrocenium cations increase in length from BUT^+ to $PENT^+$ to HEX^+ to HEP^+ to DEC^+, the dielectric constant of the medium in direct constant with the region of ionic charges decreases and the selectivity of the monolayers for ClO_4^- increases.

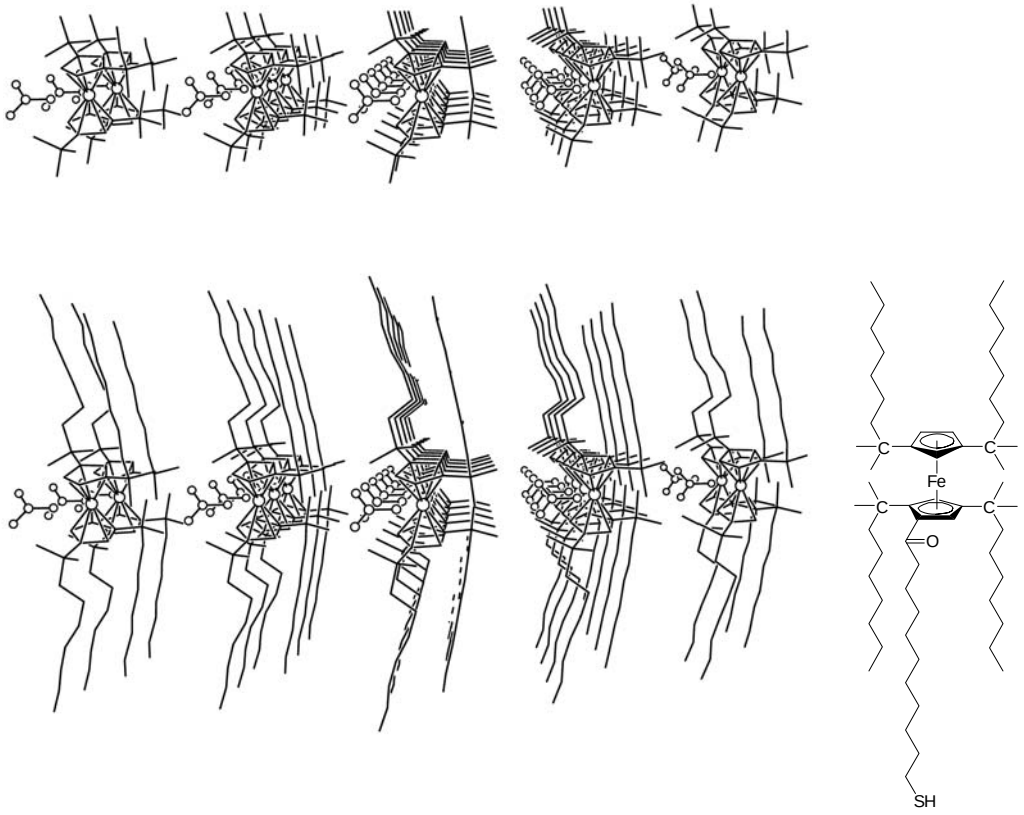

Figure 2.13. Structural models for monolayers of $BUT^+NO_3^-$ (top) and $DEC^+NO_3^-$ (bottom) when they are self-assembled on the surface of a gold electrode by a $CO(CH_2)_{10}SH$ group attached to one of the cyclopentadienyl rings of each ferrocenium cation. A drawing of the structure of the mercaptoundecanoyl substituted DEC molecule is also shown. The drawing of the $DEC^+NO_3^-$ layer is a fragment of the X-ray structure of this compound and corresponds to a side-on view of the anion–cation packing depicted in Figure 2.8. The drawing for $BUT^+NO_3^-$ is hypothetical. It shows the same packing arrangement as for $DEC^+NO_3^-$.

In summary, the "size" of the ferrocenium extractant cations does increase, but only in one dimension, from BUT^+ to DEC^+. However, whether or not the difference in size affects ion-exchange selectivities depends on whether the non-aqueous phase containing the extractant is (i) dissolved in a water-immiscible solvent, in which case $D(X^-)_{BUT^+} \approx D(X^-)_{HEP^+} \approx D(X^-)_{DEC^+}$, (ii) a three-dimensional thin film, in which case $K_d^*(X^-)_{BUT^+} < K_d^*(X^-)_{HEP^+} < K_d^*(X^-)_{DEC^+}$, or (iii) a monolayer self-assembled on an electrode surface, in which case $K_{eff}(X^-)_{BUT^+} < K_{eff}(X^-)_{HEP^+} < K_{eff}(X^-)_{DEC^+}$ but for a different reason than for the thin film.

II.1.4. A Closer Look at the Cation–Anion Interactions in Ferrocenium Salts. C–H···O Hydrogen Bonding. Weak hydrogen bonds involving CH bonds have been intensively studied recently both experimentally and theoretically.[19-22] This includes C–H···O hydrogen bond interactions involving oxoanions such as NO_3^- and ClO_4^-. Nearly all of these studies focus on aromatic CH bonds, since an H atom bonded to an sp^2 C atom is generally more acidic than one bonded to an sp^3 C atom,[23,24] exceptions like the H atoms in $CHCl_3$, CH_2Cl_2, and CH_3CN notwithstanding.[25]

The closest contacts between the cations and anions in the salts listed in Table 2.1 are not between the anion O atoms and the Fe atom. The shortest Fe···O distances in $DEC^+NO_3^-$ and $DEC^+ClO_4^-$ are 4.828 and 4.964 Å, more than twice the ca. 2 Å Fe···O distances in Fe_2O_3[26] or Fe(TPP)(ClO_4) (TPP^{2-} = tetraphenylporphyrinate(2−)).[27] Instead, the anions are "bonded" to the cations via a network of C–H···O hydrogen bonds as are the cations and anions in crystalline $Cr(C_6H_6)^+CrO_3(OCH_3)^-$[28] (these have been referred to as charge-assisted C–H···O hydrogen bonds[29]). The ferrocenium cations have a formal 1+ charge on the Fe(III) atom, and this charge is delocalized, to some extent, onto the cyclopentadienyl (Cp) ligands. This makes the three aromatic H atoms on each of the two Cp rings even more acidic than aromatic H atoms in neutral organic molecules.[30] The next most acidic CH bonds in the DEC^+ cations should be the β–H atoms on the Cp

ligands, viz. the H atoms on the β-CH_2 moiety and the two α-CH_3 groups on each of the two 2-methyl-2-nonyl substituents on each Cp ligand.

Figure 2.14 shows the environment surrounding the nitrate anions in $DEC^+NO_3^-$, $HEP^+NO_3^-$, and $BUT^+NO_3^-\cdot CHCl_3$. The CH···O distances and C–H···O angles are shown in the figure, but these are not as precise as, for example, C–C distances, in these structures because in most cases the H atoms were placed in idealized positions. The CH···O distances range from ca. 2.0 to 2.7 Å, a common range for CH···O hydrogen bonds,[20] although the 2.07 Å distance in $BUT^+NO_3^-\cdot CHCl_3$ involving the chloroform H atom may be shorter than any other $CH\cdots ONO_2^-$ in the Cambridge Structural Database in 2008 (the average for 849 such distances was reported to be 2.57 Å with a standard deviation of 0.20 Å).[20] The somewhat arbitrary "cut-off" of 2.7 Å was chosen for our study because this is the sum of van der Waals radii for an H and an O atom.[10] Some authors use an arbitrary cut-off of 2.6 Å.[28] Some statistics for the sets of hydrogen bonds for these three compounds are listed in Table 2.2. Both the average distances and the average numbers of CH···O hydrogen bonds per O atom are consistent with our earlier conclusion that anions are probably more tightly held in the lattice in BUT^+ salts than in DEC^+ salts, although the differences are small.

Figure 2.15 shows the environment surrounding the perchlorate anions in $DEC^+ClO_4^-$, $BUT^+ClO_4^-\cdot CHCl_3$, and $BUT^+ClO_4^-\cdot CH_2Cl_2$, and hydrogen-bond statistics are also listed in Table 2.2. The differences between the DEC^+ and BUT^+ salts of perchlorate are not as pronounced as they are for the nitrate salts. A more relevant comparison, however, is between the structures of $DEC^+NO_3^-$ and $DEC^+ClO_4^-$. *In both cases*, the anions are held in the lattice by *eight* CH···O hydrogen bonds with an average distance of 2.54 ± 0.03 Å. This is in sharp contrast to the significant difference in the hydrogen-bonding networks in $BUT^+NO_3^-\cdot CHCl_3$ and $BUT^+ClO_4^-\cdot CHCl_3$, in which the average CH···O distances are nearly the same but the nitrate anion is held in the lattice by *ten* CH···O hydrogen bonds and the perchlorate anion by only *five* hydrogen bonds.

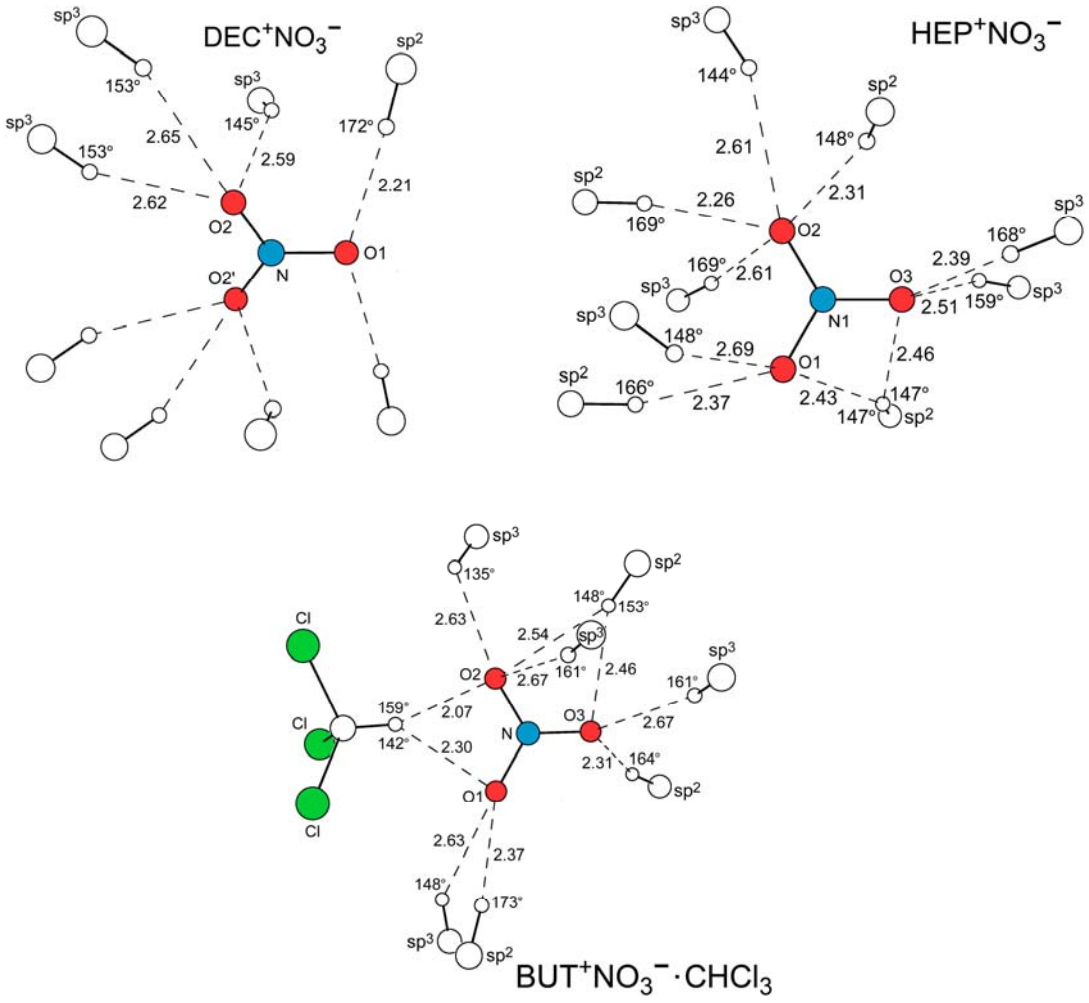

Figure 2.14. Drawings of the immediate environments of the NO_3^- anions in the X-ray structures of $DEC^+NO_3^-$, $HEP^+NO_3^-$, and $BUT^+NO_3^-\cdot CHCl_3$. The unlabeled small circles represent H atoms, which are attached to either sp^2 or sp^3 C atoms. The CH···O distances, in Å, are shown next to each hydrogen bond, and the C–H···O angles are shown next to each H atom. Note that the NO_3^- ion in $DEC^+NO_3^-$ has crystallographic C_2 site symmetry.

Table 2.2. Some statistics for CH···O(N) hydrogen bonds in ferrocenium nitrate salts[a]

cation	anion	range of CH···O distances, Å	mean CH···O distance, Å	standard deviation, Å	number of CH···O hydrogen bonds per O atom
DEC^+	NO_3^-	2.21–2.65	2.52	0.19	2⅔
HEP^+	NO_3^-	2.31–2.69	2.46	0.14	3⅓
BUT^+	NO_3^-	2.07–2.67[b]	2.47	0.20	3⅓
DEC^+	ClO_4^-	2.44–2.69	2.57	0.09	2
BUT^+	ClO_4^-	2.22–2.64[c]	2.51	0.17	1¼
BUT^+	ClO_4^-	2.49–2.69[d]	2.60	0.07	2

[a] The data are from the X-ray structures of $DEC^+NO_3^-$, $HEP^+NO_3^-$, BUT^+-$NO_3^-\cdot CHCl_3$, $DEC^+ClO_4^-$, $BUT^+ClO_4^-\cdot CHCl_3$, and $BUT^+ClO_4^-\cdot CH_2Cl_2$. In all cases, hydrogen atoms were added in idealized positions 0.96 Å from the C atom to which they are attached. [b] The two shortest distances, 2.07 and 2.30 Å, involve the CH bond of the chloroform molecule. [c] Chloroform solvate. [d] Dichloromethane solvate.

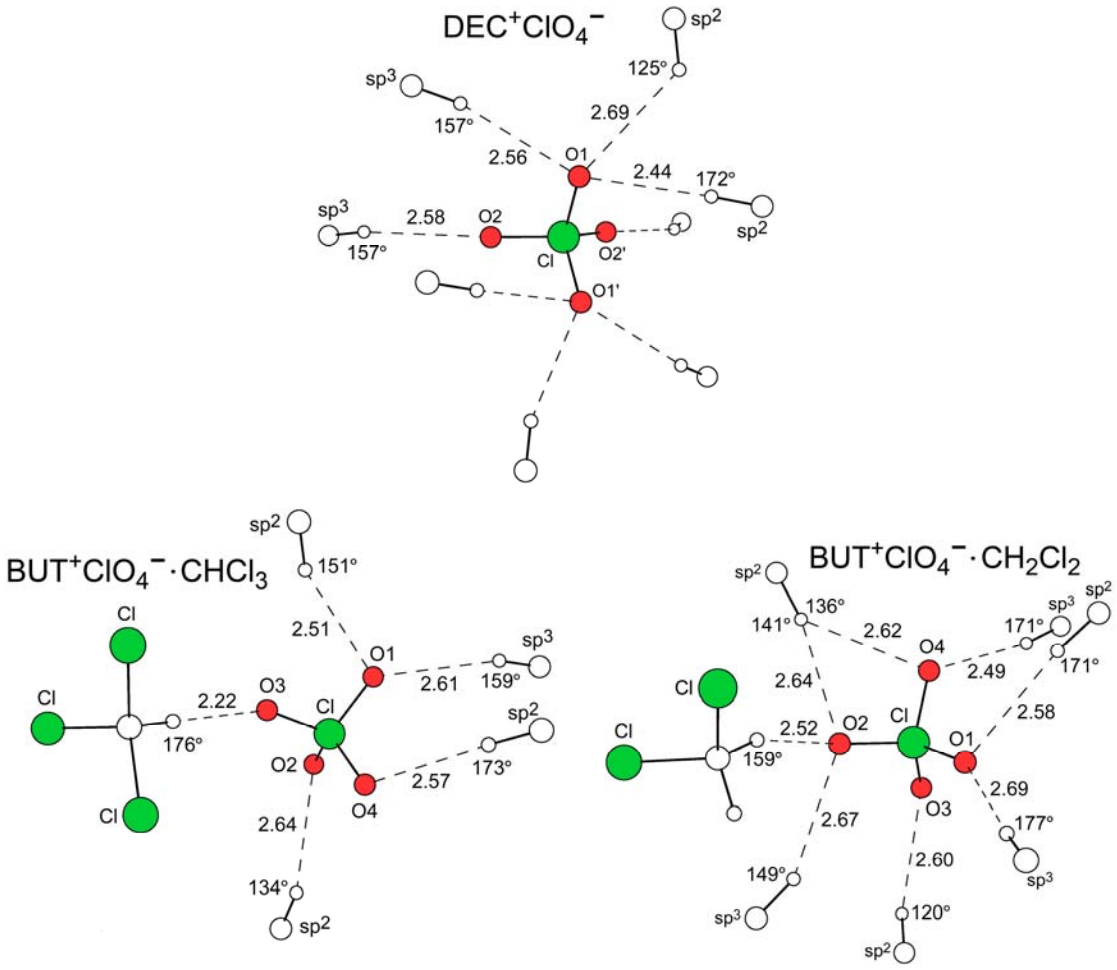

Figure 2.15. Drawings of the immediate environments of the ClO_4^- anions in the X-ray structures of $DEC^+ClO_4^-$, $BUT^+ClO_4^-\cdot CHCl_3$, and $BUT^+ClO_4^-\cdot CH_2Cl_2$. The unlabeled small circles represent H atoms, which are attached to either sp^2 or sp^3 C atoms. The CH···O distances, in Å, are shown next to each hydrogen bond, and the C–H···O angles are shown next to each H atom. Note that the ClO_4^- ion in $DEC^+ClO_4^-$ has crystallographic C_2 site symmetry.

On this basis, the DEC^+ cation should be a more selective ion-exchange cation for thin films of ferrocenium$^+NO_3^-$ salts than the BUT^+ cation, which was shown to be the case in the experiments summarized in the top plot in Figure 2.10. Note that this conclusion is based on the assumption that the cation-anion packing in thin films resembles the three-dimensional *crystalline* structures elucidated by single-crystal X-ray diffraction.

II.2. Infrared Spectra of Dry Thin Films and Crystalline Samples of DEC^+ Salts. The previous sections discussed the crystallographic characteristics of thin films and single crystals of the tetraalkylated ferrocenium salts. The next sections will focus on the description of the IR spectra and how a combination of both sets of data can be used to create a model for the thin film structures.

II.2.1. $DEC^+ClO_4^-$. There are two ways that ca. 1 μm thin films of $DEC^+ClO_4^-$ were prepared on the DiComp ATR probe for this investigation. The first method, which was reproduced many times, was to first deposit a 60 nmol thin film of $DEC^+NO_3^-$ on the diamond ATR crystal and to place that thin film in contact with an aqueous solution of $K^+ClO_4^-$ until NO_3^-/ClO_4^- anion exchange had reached completion. It was noted in Section I.1.2 that when this was done, one ν(ClO) band was observed in the first minutes of ion exchange, and that single band split into multiple bands at longer times (see Figure 2.1). The second method, which was also reproduced many times, was to directly deposit a 60 nmol thin film of $DEC^+ClO_4^-$ on the diamond ATR crystal from a 3 mM dichloromethane solution of recrystallized $DEC^+ClO_4^-$. After the dichloromethane solvent had visibly evaporated (ca. 20 s or less), ATR-FTIR spectra of the dry thin film in contact with air were recorded at regular time intervals. These spectra are shown in Figure 2.16. The single strong ν(ClO) band at 1090 cm^{-1} splits over time into *four* bands at ca. 1100 (sh), 1090 (s), 1054 (m), and 878 cm^{-1} (m). Therefore, the band splitting is not a function of the presence of an aqueous phase in contact with a thin film of $DEC^+ClO_4^-$, it is an intrinsic property of the $DEC^+ClO_4^-$ film itself.

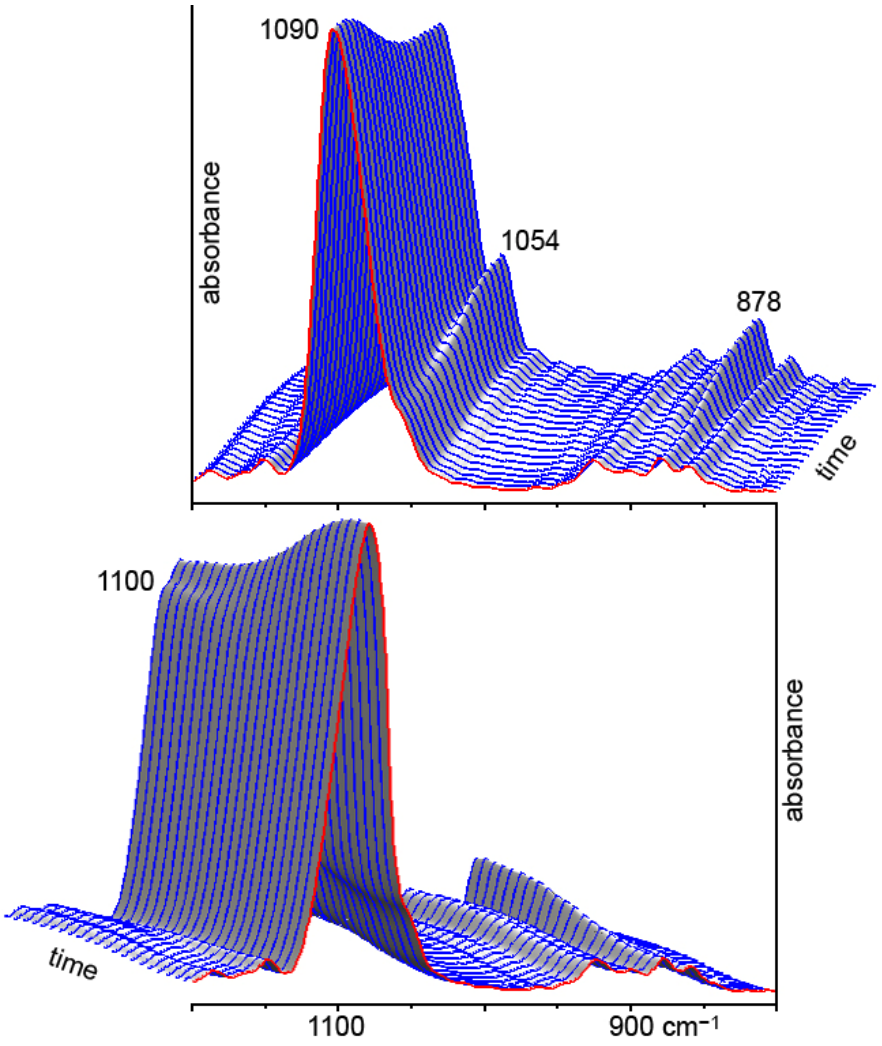

Figure 2.16. ATR-FTIR spectra of a ca. 1 μm thin film of $DEC^{+}ClO_4^{-}$ deposited on a diamond ATR crystal. The spectra were recorded every two minutes (the first spectrum is in the front). The single ν(ClO) band at 1090 cm^{-1} splits into four bands over time, at ca. 1100 (sh), ca. 1090 (s), 1054 (m), and 878 cm^{-1} (m). The thin film was in contact with air.

Our interpretation of the band splitting is that the local symmetry of the perchlorate anion changes as the thin film "anneals" over time. The free anion has T_d symmetry, and the four Cl–O stretching normal modes of vibration give rise to a Raman-active A_1 band and a triply-degenerate IR- and Raman-active T_2 band.[31,32] An ATR spectrum of aqueous $KClO_4$ showing a single ν(ClO) band at 1105 cm^{-1} is shown in Figure 2.17 along with spectra of a $DEC^+ClO_4^-$ thin film deposited from dichloromethane after less than two minutes and after 44 minutes (there were no further changes after 44 minutes) and a spectrum of microcrystalline $DEC^+ClO_4^-$. (The spectrum of aqueous $KClO_4$ is identical to that reported for aqueous $LiClO_4$ at 300 K by Mayer et al.[33]) The spectrum of microcrystalline $DEC^+ClO_4^-$ displays bands assigned to the four ν(ClO) stretching vibrations at 1100, 1089, 1051, and 879 cm^{-1}, and is very similar to the thin film after 44 minutes, in band position, band intensity, and peak width at half-height (note that the ν(ClO) band for aqueous ClO_4^- is considerably broader than the thin film band after less than one minute, probably because of the greater polarity/dielectric constant of H_2O relative to the lower-dielectric environment of the of ClO_4^- ion in the thin film[34]).

With four observed ν(ClO) bands, the effective symmetry of the ClO_4^- anion in both the annealed thin film and crystalline $DEC^+ClO_4^-$ must be C_{2v} or lower (i.e., the only subgroups of the T_d point group that are consistent with the structure of ClO_4^- and do not have E or T irreducible representations are C_{2v}, C_2, C_s, and C_1). As discussed earlier, the anion has crystallographic C_2 symmetry in crystalline $DEC^+ClO_4^-$. It is apparent that the ClO_4^- anions in thin films of $DEC^+ClO_4^-$, however the films are prepared, experience an (effective) isotropic environment at short times (< 1 min) and eventually experience the anisotropic environment consistent with the observed spectra at longer times (≥ 44 min). Clearly, the newly-formed thin film undergoes structural reorganization in the solid state so that the final thin-film structure resembles the crystal structure, at least as far as the ClO_4^- is concerned.

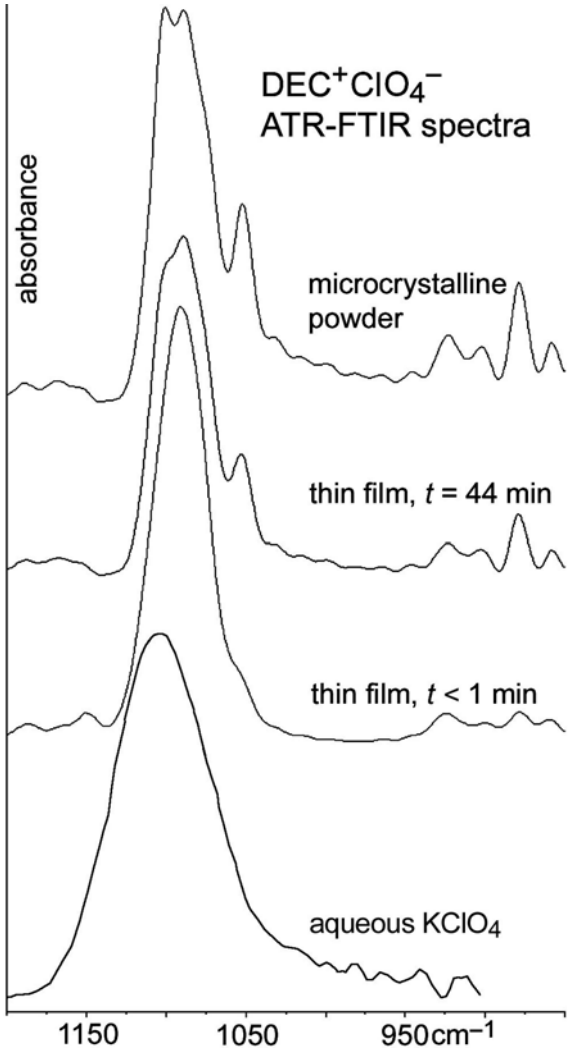

Figure 2.17. ATR-FTIR spectra of (bottom spectrum) an aqueous solution of $KClO_4$, (middle two spectra) a ca. 1 μm thin film of $DEC^+ClO_4^-$ deposited from a dichloromethane solution, and (top spectrum) crystalline $DEC^+ClO_4^-$ (no mulling agent). For the solid-state spectra, the samples were in contact with air.

The CH···O hydrogen-bonding in $DEC^+ClO_4^-$, shown in Figure 2.15, is apparently anisotropic enough to cause splitting of the triply-degenerate ν(ClO) band of the free ClO_4^- anion. The two O1 atoms each interact with three C–H bonds having CH···O distances shorter than 2.7 Å, two of which involve sp^2 hybridized C atoms. In contrast, the two O2 atoms each interact with only one C–H bond, and it is a less acidic C–H bond because that carbon atom is sp^3 hybridized. Nevertheless, the differences in hydrogen bonding interactions cause only a barely significant difference in the two types of Cl–O distances in crystalline $DEC^+ClO_4^-$, which are 1.443(2) Å for Cl–O1 and 1.429(2) Å for Cl–O2. Perhaps more significant as far as the symmetry-lowering is concerned is the fact that the O1–Cl–O1' angle, at 106.2°, is six degrees smaller than the O2–Cl–O2' angle, which is 112.4(2)°. Similar hydrogen bonding in β-alaninium perchlorate also removed the degeneracy of the T_1 ν(ClO) vibrations by lowering the site symmetry of the ClO_4^- anions. Relevant ν(ClO) peak positions are listed in Table 2.3.[35] The ranges of frequencies of the three ν(ClO) vibrations that arise from the T_1 normal modes are only 49 cm^{-1} for crystalline $DEC^+ClO_4^-$ but are 130 ± 1 cm^{-1} for crystalline β-alaninium$^+ClO_4^-$ and $KClO_4$ and 227 cm^{-1} for the matrix-isolated $LiClO_4$ ion pair. These splittings are consistent with the weak CH···O interactions between cations and anions in $DEC^+ClO_4^-$ compared with the other compounds (note that the cation–anion interactions in β-alaninium$^+ClO_4^-$ include relatively strong $NH^+\cdots OClO_3^-$ hydrogen bonds).

II.2.2. $DEC^+ReO_4^-$. A thin film of this compound freshly deposited on the diamond ATR crystal of the DiComp probe by evaporating 20 μL of a 3 mM solution also exhibited IR spectral changes over time, as shown in Figure 2.18. It is very likely that the thin film also undergoes structural reorganization over time and that the structure of the thin film eventually resembles the structure of crystalline $DEC^+ReO_4^-$. To better resolve the changes, a transmission IR spectrum of a thin film of $DEC^+ReO_4^-$

Table 2.3. Infrared ν(ClO) stretching frequencies for the ClO_4^- anion[a]

compound	ClO_4^- site symmetry	symmetric stretch (irreducible rep.)	asymmetric stretches; (irreducible rep(s))
$KClO_4$ aqueous soln.	T_d	not observed (A_1)	1105 (T_1)
$DEC^+ClO_4^-$ thin film, $t < 1$ min	T_d	not observed (A_1)	1090 (T_1)
$DEC^+ClO_4^-$ thin film, $t \geq 44$ min	C_{2v} (or lower)	878 (A_1)	1100(sh), 1090, 1054 ($A_1 + B_1 + B_2$)
$DEC^+ClO_4^-$ crystals	C_2	879 (A)	1100, 1089, 1051 (A + 2B)
β-alaninium$^+ClO_4^-$[b] crystals	C_1	940 (A)	1170, 1125, 1038 (3A)
$LiClO_4$ ion pair[c] (matrix isolated)	C_{2v}	895 (A_1)	1220, 1143, 994 ($A_1 + B_1 + B_2$)
$KClO_4$[d] (doped in $KMnO_4$)	C_s	943 (A')	1124, 1107, 1094 (A' + 2A")
$TBA^+ClO_4^-$ thin film	not known	886	1086, 1077(sh)

[a] All data from this work unless otherwise indicated; rep = representation. [b] Ref. [31]. [c] Ref. [35]. [d] Ref [32]; the frequencies listed for this compound are for the $^{35}ClO_4^-$ isotopomer.

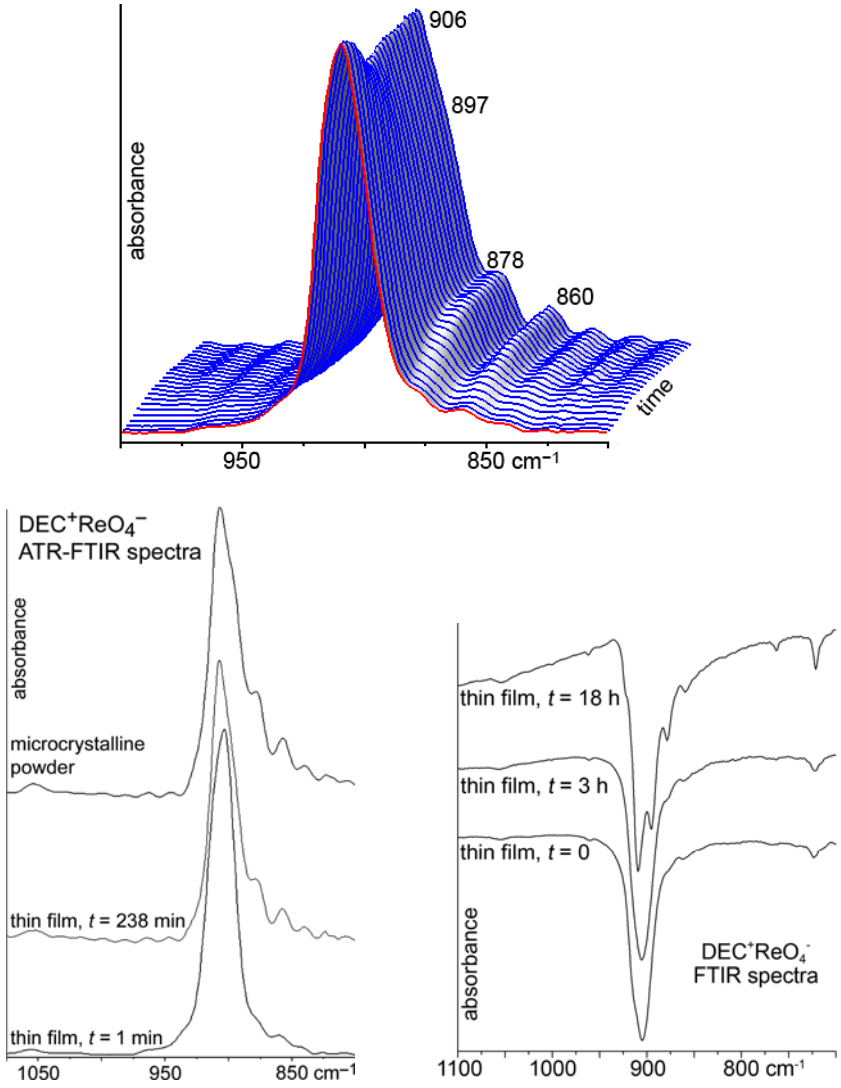

Figure 2.18. Top. ATR-FTIR spectra of a ca. 1 μm thin film of $DEC^{+}ReO_4^{-}$ deposited from a dichloromethane solution on the diamond ATR crystal. The spectra were recorded over a period of approximately four hours. **Bottom left.** The first and last ATR-FTIR spectra from the sequence of spectra at the top and the ATR-FTIR spectrum of microcrystalline $DEC^{+}ReO_4^{-}$ in contact with the diamond ATR crystal. **Bottom right.** Transmission FTIR spectrum of a ca. 1 μm thin film of $DEC^{+}ReO_4^{-}$ deposited from a dichloromethane solution on a KBr window. All of the samples were in contact with air.

deposited on a KBr window was recorded at t = 0, 3, and 18 h. The splitting of the ν(ReO) band over time is better resolved in the transmission IR spectrum than in the ATR spectrum, and resembles the splitting over time observed for thin films of $DEC^+ClO_4^-$. However, note that the structural changes that produce the band splitting were more than six times slower for thin films of $DEC^+ReO_4^-$ than for thin films of $DEC^+ClO_4^-$.

II.2.3. $DEC^+NO_3^-$. Unlike thin films of $DEC^+ClO_4^-$ and $DEC^+ReO_4^-$, thin films of $DEC^+NO_3^-$ deposited from dichloromethane solution on the diamond ATR crystal exhibited an ATR-FTIR spectrum that did *not* change over time for at least 8 h. As discussed below, a thin-film spectrum of $DEC^+NO_3^-$ is strikingly different, in both the ν(NO) and ν(CH) regions, than the IR spectrum of a sample of crystalline $DEC^+NO_3^-$, as shown in Figures 2.19–2.21. Figure 2.19 also shows spectra of the neutral molecule DEC and the salt $DEC^+ClO_4^-$ so that the medium-to-strong ν_{asym}(NO) bands of $DEC^+NO_3^-$ in each sample, in the ca. 1300–1400 cm^{-1} region, can be unambiguously assigned. The crystalline salt also exhibited a weak band at 1058 cm^{-1} that is absent from the spectrum of neutral DEC and, importantly, absent from the thin film of $DEC^+NO_3^-$, as shown in Figure 2.21.

The "free" nitrate anion in crystalline $NaNO_3$ has D_{3h} symmetry[36] and exhibits a Raman-active A_1' symmetric N–O stretch at 1067 cm^{-1} and an IR- and Raman-active E asymmetric N–O stretch at 1385 cm^{-1}.[37] In crystalline KNO_3, the anions have C_{2v} symmetry,[38] the degenerate E band is split into two bands of similar intensity at 1358 and 1343 cm^{-1},[37] and the symmetric stretch at 1055 cm^{-1} has become IR active.[39] In crystalline $DEC^+NO_3^-$, the anions have C_2 symmetry, the two ν_{asym}(NO) IR bands of similar intensity are at 1364 and 1320 cm^{-1} (see Figure 2.19), and the band at 1058 cm^{-1} shown in Figure 2.21 can be assigned to ν_{sym}(NO). Therefore, the nitrate anions in KNO_3 and crystalline $DEC^+NO_3^-$ are similar both structurally and spectroscopically. The pronounced E band splitting ($\Delta\nu$ = 44 cm^{-1} in crystalline $DEC^+NO_3^-$) is undoubtedly a

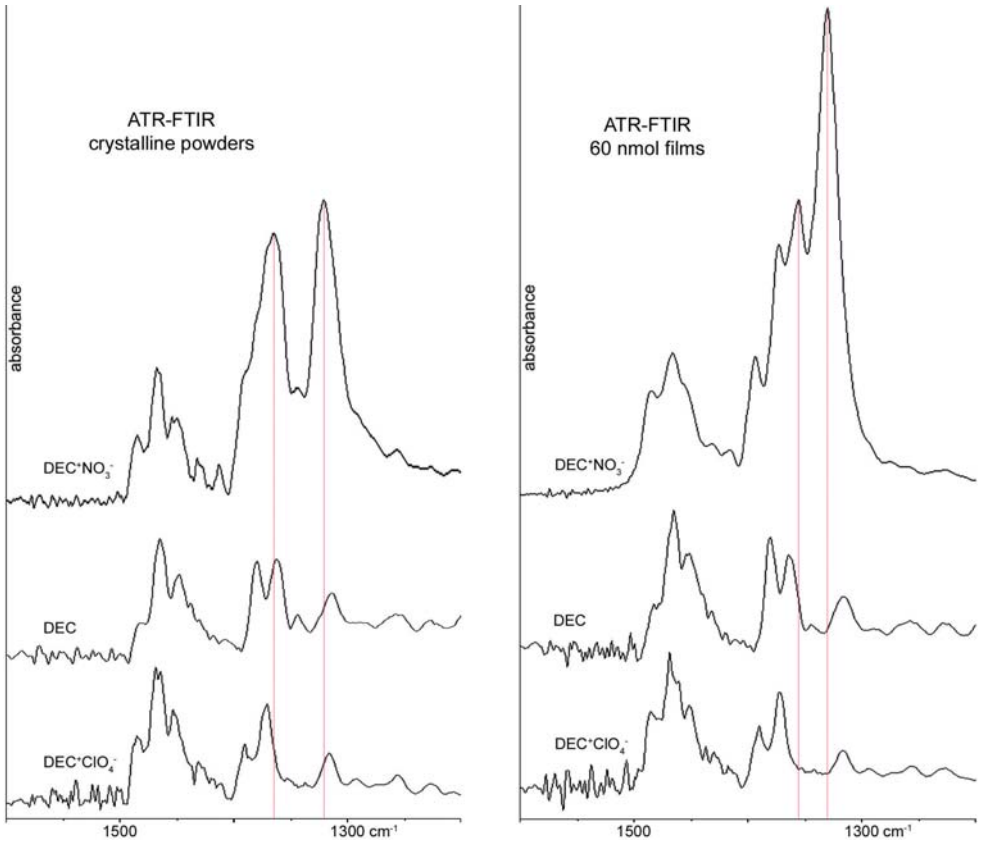

Figure 2.19. Comparison of ATR-FTIR spectra (diamond ATR crystal, 2 cm^{-1} resolution) of microcrystalline powders and ca. 1 μm thin films of $DEC^{+}NO_3^{-}$, $DEC^{+}ClO_4^{-}$, and the neutral ferrocene DEC deposited from dichloromethane solutions. The spectra of $DEC^{+}ClO_4^{-}$ and neutral DEC are shown so that the $\nu_{asym}(NO)$ bands at 1364 and 1320 cm^{-1} (microcrystalline powder) and at 1355 and 1330 cm^{-1} (thin film) can be assigned unambiguously.

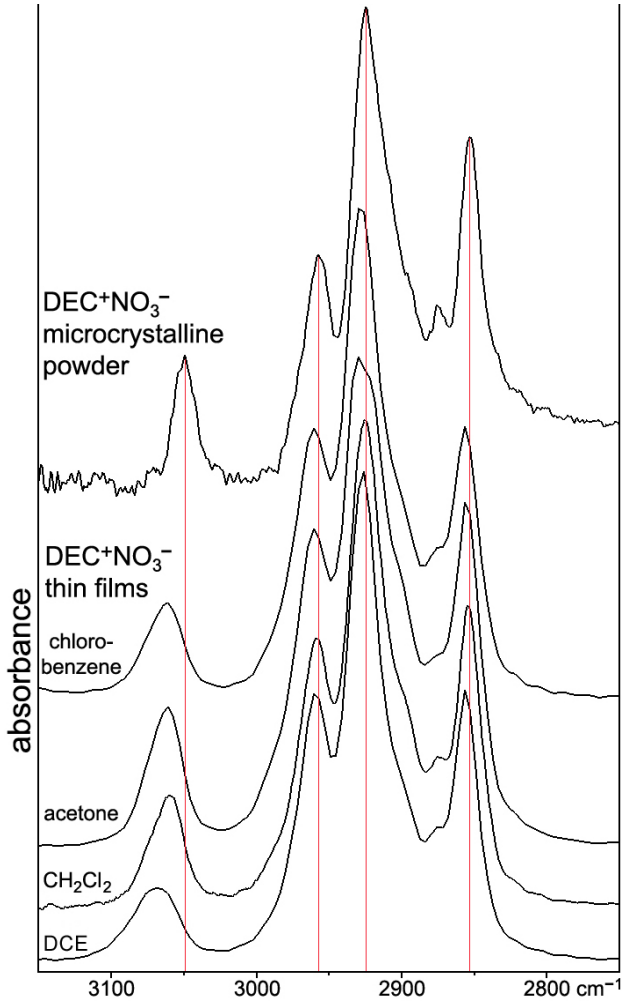

Figure 2.20. Comparison of ATR-FTIR spectra (diamond ATR crystal, 2 cm^{-1} resolution) of microcrystalline powders and ca. 1 μm thin films of $DEC^{+}NO_3^{-}$. The vertical red lines illustrate the ν(CH) band positions at 3049, 2958, 2925, and 2853 cm^{-1} in the micrystalline sample of $DEC^{+}NO_3^{-}$. The highest-energy band is at 3061, 3061, 3060, and 3068 cm^{-1} in the thin-film spectra deposited from chlorobenzene, acetone, dichloromethane, and 1,2-dichloroethane (DCE) solutions, respectively.

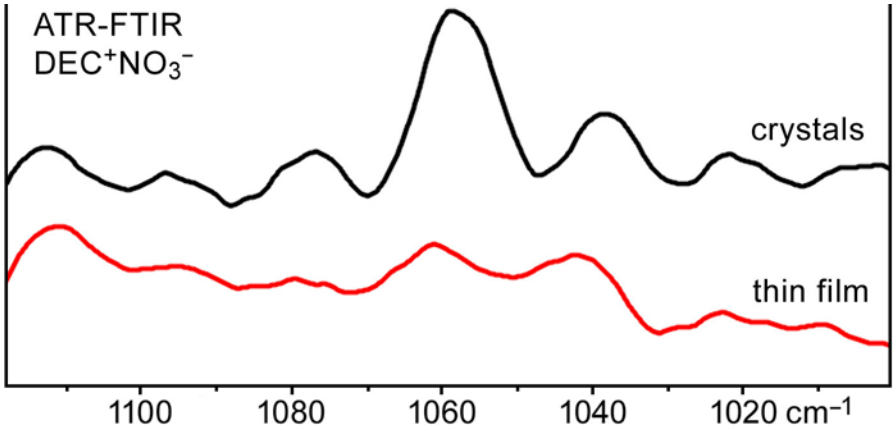

Figure 2.21. Comparison of ATR-FTIR spectra (diamond ATR crystal, 2 cm^{-1} resolution) of a microcrystalline sample (black spectrum) and a ca. 1 μm thin film of $DEC^{+}NO_3^{-}$ deposited from dichloromethane solution (red spectrum). The weak band at 1058 cm^{-1} in the spectrum of the microcrystalline salt is assigned to $\nu_{sym}(NO)$ of the NO_3^{-} anion.

function of the nearly-linear (172°) and relatively short (2.21 Å) hydrogen bonds between two symmetry-related aromatic CH bonds and O1 (see Figure 2.14). In contrast, O2 and O2' interact with less acidic aliphatic CH bonds at smaller angles (145°, 153°) and longer distances (ca. 2.6 Å).

Figure 2.19 shows that the IR spectrum of a thin film of $DEC^+NO_3^-$ deposited from dichloromethane does not exhibit two $\nu_{asym}(NO)$ IR bands *of similar intensity*. There is a very intense band at 1330 cm^{-1} (this is the most intense band in the entire spectrum) and a much weaker band at 1355 cm^{-1} ($\Delta\nu$ = 25 cm^{-1}). In addition, there is an aromatic ν(CH) band at 3060 cm^{-1} that is shifted from 3049 cm^{-1} in the crystalline salt (see Figure 2.20). Furthermore, the weak $\nu_{sym}(NO)$ band in the spectrum of the crystalline salt is absent from the thin-film spectrum (see Figure 2.21). These observations show that the local environment of the nitrate anions is significantly different in the crystalline salt and the thin film. The apparent, or effective, symmetry of the anions is clearly higher in the thin film.

II.2.4. The ν(CD) Band of $BUT^+ClO_4^-$·$CHCl_3$. The 21 cm^{-1} shift in the aromatic ν(CH) band on going from crystalline to thin-film $DEC^+NO_3^-$ is probably due to differences in the CH···O hydrogen bonds that involve the six aromatic CH bonds per ferrocenium cation (three per 1,3-dialkylcyclopentadienide(1−) ring). As discussed in Section III.5 of this chapter, an H atom bonded to an sp^2 C atom is generally more acidic than one bonded to an sp^3 C atom, exceptions like the H atoms in $CHCl_3$, CH_2Cl_2, and CH_3CN notwithstanding. There is a growing literature on shifts in ν(CH) bands for bonds involved in CH···O, CH···N, and CH···F hydrogen bonding.[19,23,40-52] In some cases, one or more ν(CH) bands shift to higher frequencies (a "blue" shift) and the band intensity is decreased.[23,40-49] However, in many cases the relevant ν(CH) bands shift to lower frequencies (a "red" shift) and the band intensity is greatly increased,[46-52] as is the case with more typical OH···X, NH···X, or FH···X hydrogen bonds (X = N, O, or F).[53] An example is the gas phase complex formed between $CHCl_3$ or $CDCl_3$ and NH_3, in which

the chloroform ν(CH) band was red shifted by 17.5 cm^{-1} and the band intensity was increased by a factor of 340 (the ν(CD) band of chloroform-d was red shifted by 12.5 cm^{-1} in the complex).[52]

Since the Strauss group had studied the X-ray structure of $BUT^+NO_3^-\cdot CHCl_3$, and it was known that the chloroform H atom was strongly hydrogen bonded to two of the three nitrate O atoms (see Figure 2.14), we decided to measure the ν(CD) shift on going from neat $CDCl_3$ to $BUT^+NO_3^-\cdot CDCl_3$. A fresh thin film of this compound was evaporated from a chloroform-d solution of $BUT^+NO_3^-$ on the silicon ATR probe (the diamond ATR crystal does not have a window in the ν(CD) region of the IR spectrum). The solvate is not stable at 25 °C, so the band due to hydrogen-bonded $CDCl_3$ diminished over time (ca. 45 min). Nevertheless, a band at 2221 cm^{-1} was observed, as shown in Figure 2.22. This band was absent from a fresh thin film of the $CHCl_3$ solvate. Since neat chloroform-d has a band at 2255 cm^{-1}, the ν(CD) band in $BUT^+NO_3^-\cdot CDCl_3$ had been red shifted by 34 cm^{-1}, one of the largest shifts ever reported for a hydrogen-bonded complex of chloroform-d.[50] Figure 2.22 also shows that a thin film of $DEC^+NO_3^-$ evaporated on the silicon ATR crystal from a chloroform-d solution does not incorporate a solvent molecule in the solid thin film.

II.2.5. The Aromatic ν(CH) Bands of DEC and DEC^+ Salts. The observed shift in the ν(CD) band of chloroform-d in $BUT^+NO_3^-\cdot CDCl_3$ suggested the comparison and analysis of the aromatic ν(CH) region of a thin film of neutral DEC to those of thin films of DEC^+ salts of various anions. Relevant ATR-FTIR spectra are shown in Figures 2.23 and 2.24. All of the spectra in Figure 2.23 were taken on 60 nmol thin films, and the highest intensity aliphatic ν(CH) band at ca. 2925 cm^{-1} in each spectrum (not shown) had about the same absorbance value.

It can be seen that the aromatic band(s) of neutral DEC and of DEC^+Cl^- are extremely weak compared to the band for a thin film of $DEC^+NO_3^-$ or fresh thin films of

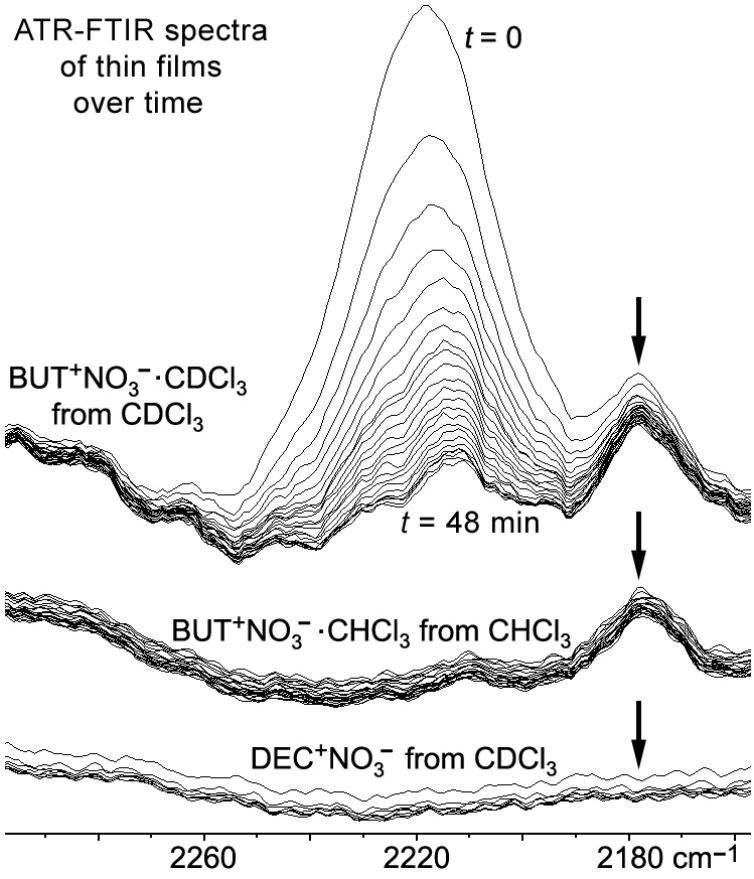

Figure 2.22. ATR-FTIR spectra of thin films deposited on a silicon ATR crystal from chloroform or chloroform-d solutions over time.

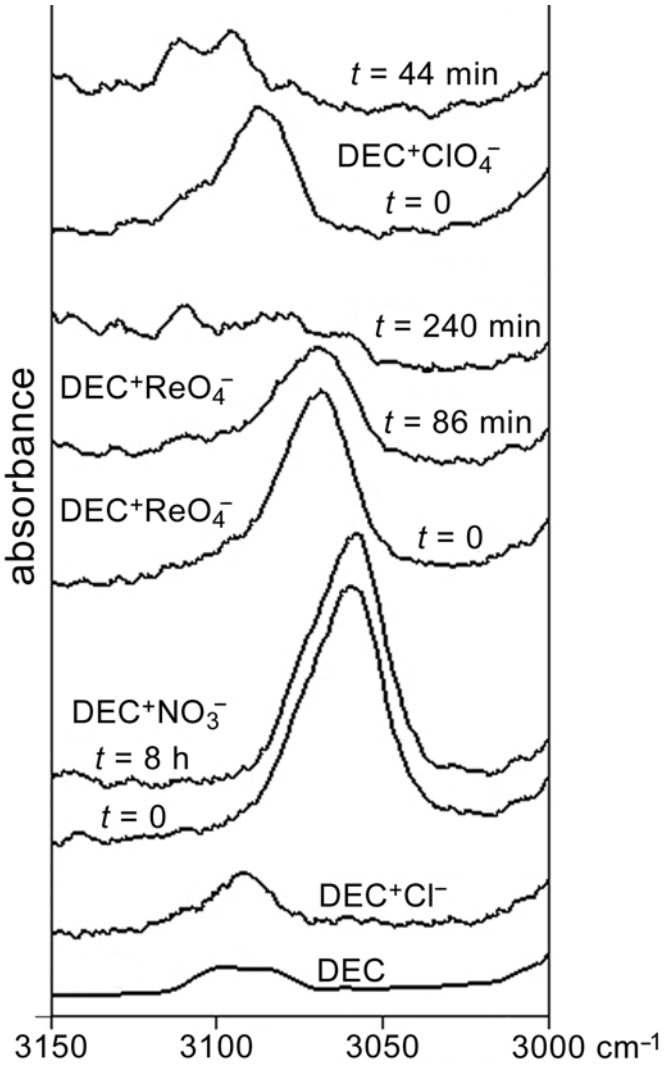

Figure 2.23. Comparison of the aromatic ν(CH) bands for DEC and several DEC^+ salts. All of the samples were 60 nmol thin films deposited on a diamond ATR crystal from dichloromethane solutions.

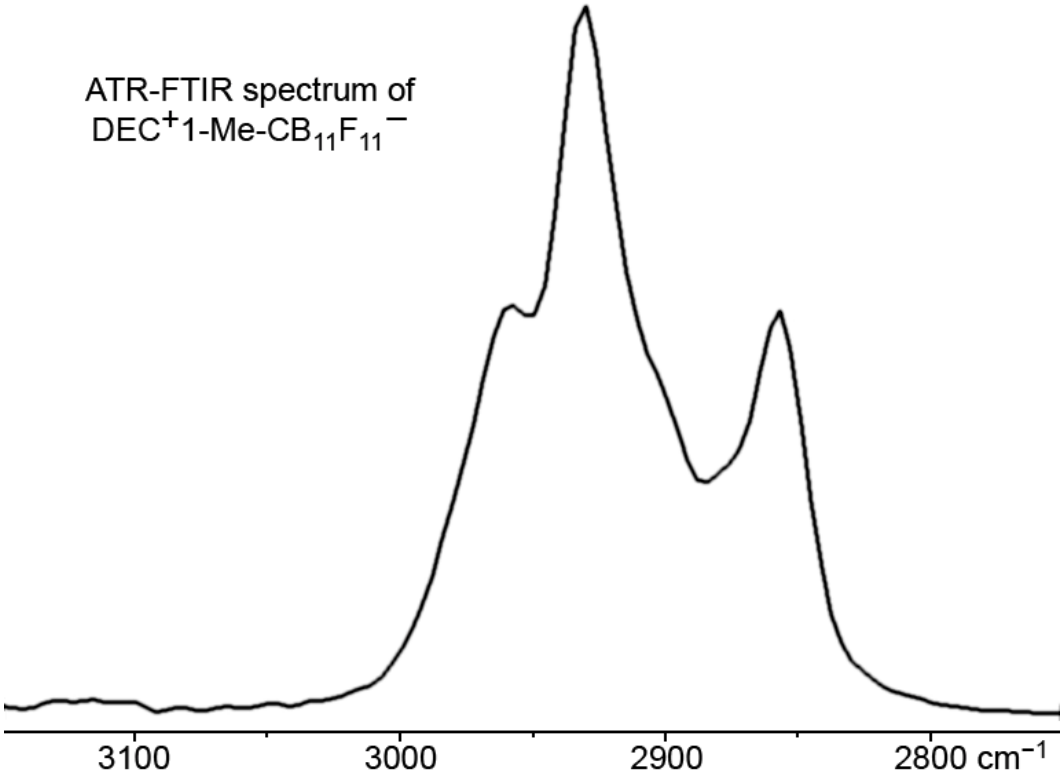

Figure 2.24. The ν(CH) region for a thin film of $DEC^{+}1\text{-Me-}CB_{11}F_{11}^{-}$. Note the absence of an observable band or bands in the aromatic ν(CH) region.

$DEC^+ClO_4^-$ or $DEC^+ReO_4^-$. This is probably because there is *no* CH···X hydrogen bonding in DEC and *only very weak* CH···Cl^- hydrogen bonding in DEC^+Cl^-. This conclusion is supported by the spectrum of DEC^+1-Me-$CB_{11}F_{11}^-$ shown in Figure 2.24. The fluorocarborane anion in this salt is extremely weakly coordinating and should therefore be a very poor hydrogen-bond acceptor, hence the aromatic ν(CH) band or bands for this salt are so weak that they are not discernable. On the other hand, the relatively intense aromatic ν(CH) bands of $DEC^+NO_3^-$, $DEC^+ClO_4^-$, and $DEC^+ReO_4^-$ are indicative of relatively strong hydrogen bonding between the aromatic CH bonds and the O atoms of the oxoanions.

The aromatic ν(CH) regions of the IR spectra for thin films of $DEC^+ClO_4^-$ and $DEC^+ReO_4^-$ evolved over time, resulting in multiple bands at higher wavenumbers. The times involved are similar to those required to produce the spectral changes in the ν(ClO) and ν(ReO) regions of the spectrum, respectively, discussed previously. Whatever structural change(s) lowered the symmetry of the oxoanions and split the one T_2 ν(ClO) and ν(ReO) band in the fresh thin films into three bands, also results in the replacement of one aromatic ν(CH) band with multiple bands.

II.3. A Comprehensive Model for the Structure of Thin Films of DEC^+ Salts. It is clear from the data discussed in this chapter that a thin film of $DEC^+NO_3^-$ deposited on an ATR crystal from a dichloromethane solution does not have the same structure as the crystalline salt, which consists of interdigitated layers of DEC^+ cations separated by parallel layers of NO_3^- anions. Our interpretation of these data is as follows. As a solution of $DEC^+NO_3^-$ in a volatile solvent, such as dichloromethane, rapidly dries, producing a thin film of the compound, the anions and cations do not have time to orient themselves into the lowest-energy solid-state structure, which is presumably the structure of the crystalline salt (and presumably it is the interdigitation of the cations that is the slow step). In a freshly-formed thin film of $DEC^+NO_3^-$, $DEC^+ClO_4^-$, or $DEC^+ReO_4^-$, the anions are in a nearly isotropic environment. In the latter two salts, the thin films anneal

over time to form structures that are spectroscopically indistinguishable from the crystalline salts. It is not clear at this time why the solid-state structural changes are significantly slower for $DEC^+ReO_4^-$ than for $DEC^+ClO_4^-$. It is also not clear at this time why a thin film of $DEC^+NO_3^-$ does not undergo a similar solid-state reorganization at 25 °C.

Although it seems likely that the alkyl "arms" of the DEC^+ cations are not interdigitated with one another in the freshly-formed thin films, this does not suggest that the thin-film structures are disordered. In fact, there is ample evidence for both short-range and long-range ordering of the cations and anions in the thin films. First, the thin film IR spectra indicate a single type of environment for the oxoanions (i.e., a very broad band or series of ν(NO), ν(ClO), or ν(ReO) bands is not observed). Second, these spectra also indicate a single type of environment for the aromatic CH bonds (i.e., there appears to be one relatively symmetric aromatic ν(CH) band for each of the three thin films). Furthermore, the crystal structures suggest that *more* of the aromatic CH bonds are involved in hydrogen bonding to the anion O atoms in the thin films than in the crystalline salts. The relatively intense ν(CH) bands for the thin films indicates that some of the aromatic CH bonds are participating in hydrogen bonding, and the isotropic nature of the anions requires that each oxygen atom interacts, somewhat equally, with at least one aromatic CH bond. It is possible that the DEC^+ cations with "folded" alkyl arms can pack similarly to BUT^+ or $BUT2^+$ cations in their salts, allowing more aromatic CH bonds to interact with the anions. This is shown in Figure 2.25 for $BUT2^+ReO_4^-$. Note that the cations are oriented in two different perpendicular directions. This may allow for a better "use" of the aromatic CH bonds for hydrogen bonding to the O atoms. In contrast, once the alkyl arms become interdigitated, as in the crystal structures, all of the DEC^+ cations are oriented in the same direction, as shown in Figure 2.26 for $DEC^+ReO_4^-$. Figure 2.27 is a comparison of the cation-anion layers in crystalline $DEC^+ReO_4^-$ and $BUT2^+ReO_4^-$.

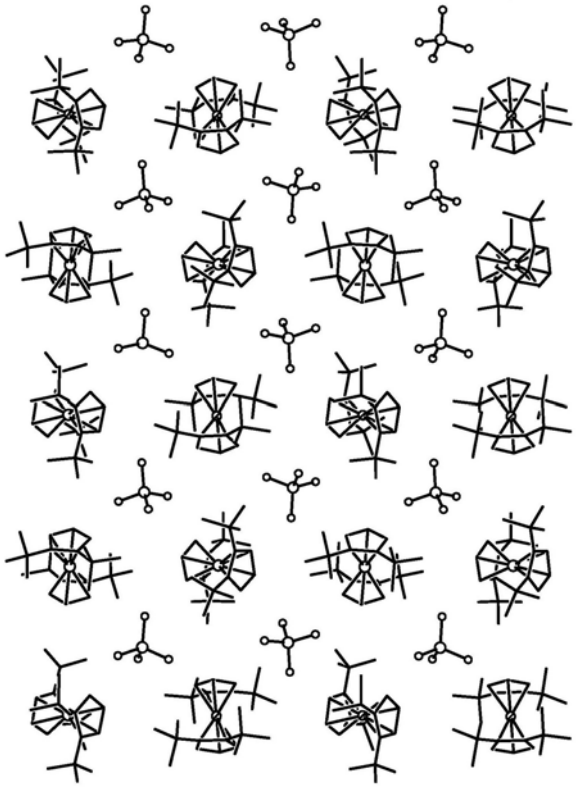

Figure 2.25. The packing of cations and anions in a layer of $BUT2^{+}ReO_4^{-}$. Note that there are two nearly perpendicular orientations of the $BUT2^{+}$ cations.

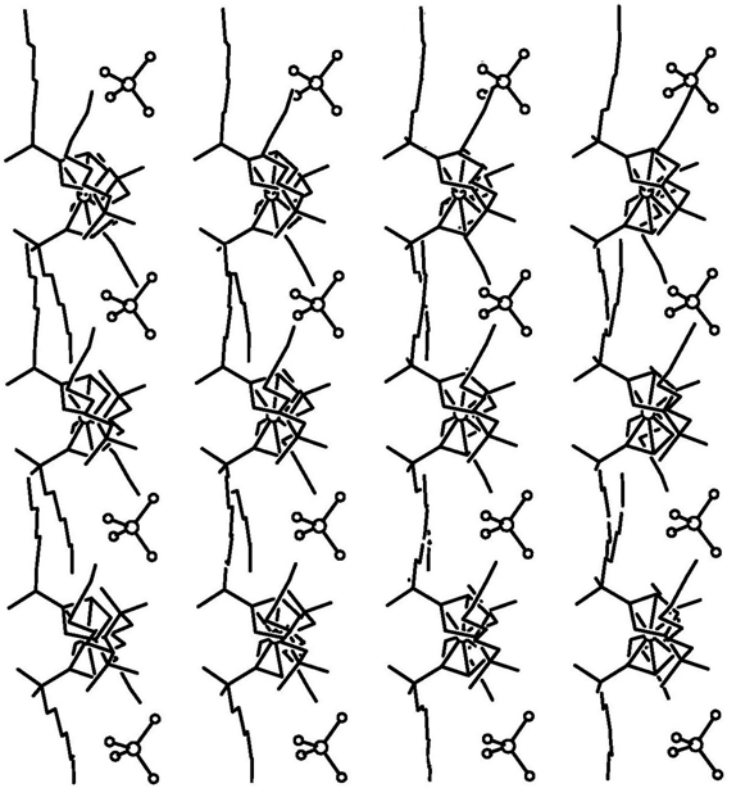

Figure 2.26. The packing of cations and anions in a layer of $DEC^{+}ReO_4^{-}$. Note that there is only one orientation of the DEC^{+} cations.

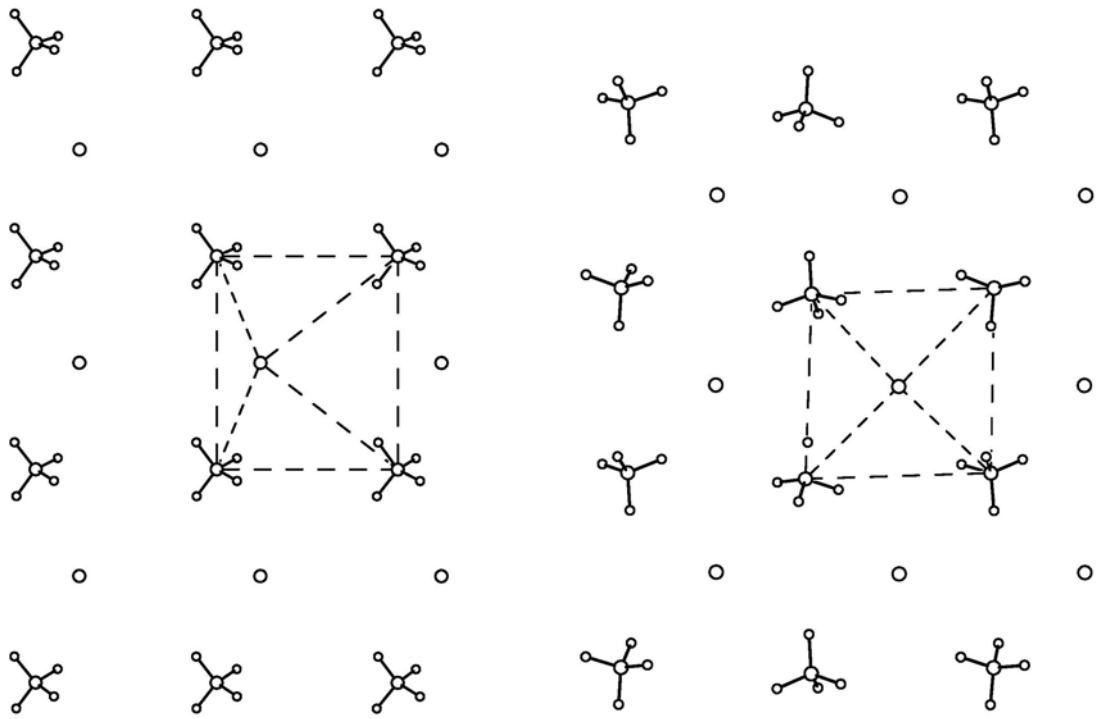

$DEC^{+}ReO_4^{-}$ $BUT2^{+}ReO_4^{-}$

Figure 2.27. Comparison of the packing of cations and anions in a layer of $DEC^{+}ReO_4^{-}$ (left) and $BUT2^{+}ReO_4^{-}$ (right).

There are only two "short" Fe···Re distances in $DEC^{+}ReO_4^{-}$ but four such distances in $BUT2^{+}ReO_4^{-}$. The ReO_4^{-} anions in $BUT2^{+}ReO_4^{-}$ appear to be in a more isotropic environment than in $DEC^{+}ReO_4^{-}$. For example, all four O atoms in $BUT2^{+}ReO_4^{-}$ are hydrogen bonded to at least one aromatic CH bond, as shown in Figure 2.28.

There is another indication that the structure of the freshly-formed thin films are ordered. Ion exchange reactions proceed fairly rapidly, as shown in Figure 2.1. If the thin films were a jumbled mass of cations and anions, one would not expect the ion-exchange process to be as rapid or as uniform as it appears to be.

II.4. Investigation of Film Morphology using Atomic Force Microscopy (AFM). AFM images of thin films made with two of the tetraalkylated ferrocenes discussed in this chapter, deposited on different surfaces, were obtained using the instrument in the Van Orden Research Group. Two kinds of substrates were chosen: Mica-on-Glass substrates and Silicon Wafers. Both $DEC^{+}NO_3^{-}$ and $DEC^{+}ClO_4^{-}$ were analyzed by making films with two different amounts of material in the same volume: 6 nmol and 60 nmol, on the mica substrates. Only $DEC^{+}NO_3^{-}$ was analyzed on the Si wafers. A metal mask or washer was pressed against the Si wafers to simulate the well dimensions of the Si probe, and deposit the solution in the center. This was done in order to mimic the interactions that a film deposited on the probe experiences, both with the crystal and with the stainless steel enclosure. The results are shown in Figure 2.29 and Figure 2.30. Even when the resolution is not molecular, it can nonetheless be seen that the film doesn't present a uniform surface, but regions or "islands" where the solution coalesces. This phenomenon would indicate a better interaction between the molecules of the solution itself compared to its interaction with the crystal; it seems to be enhanced by the presence of dust particles on the surface of the substrate. The mica substrates results show that when going from a thinner film to a thicker one, the $DEC^{+}NO_3^{-}$ thin film surface changes from small clusters of material uniformly distributed on the surface, with thicker areas on

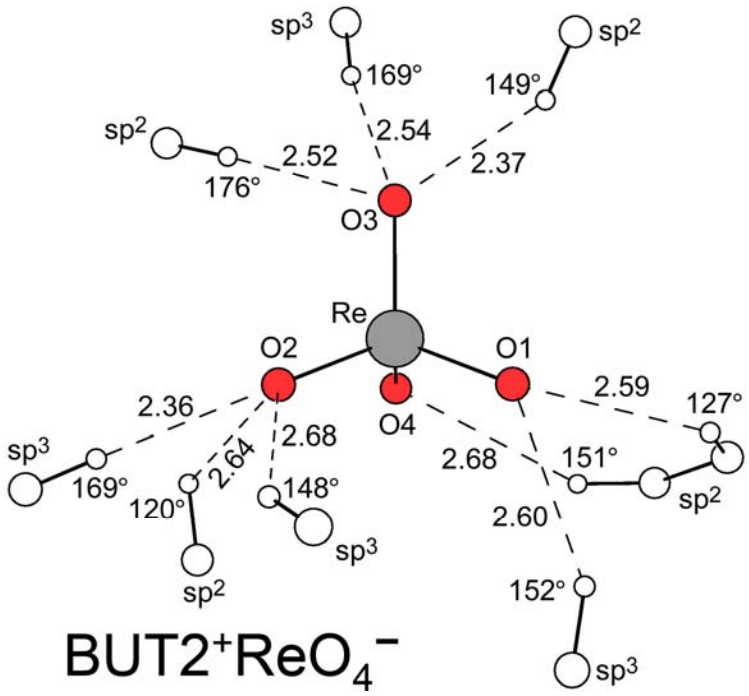

Figure 2.28. Hydrogen bonding to the perrhenate anion in the X-ray structure of $BUT2^{+}ReO_4^{-}$.

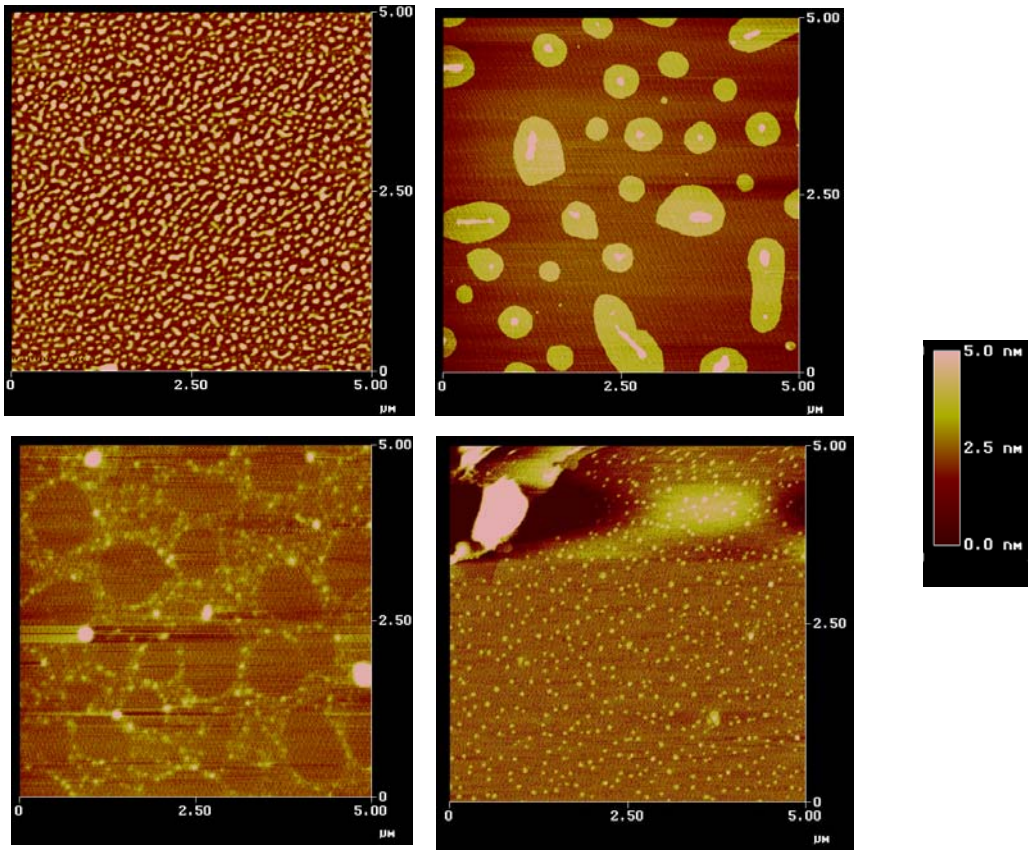

Figure 2.29. AFM images of $DEC^{+}NO_3^{-}$ (left) and $DEC^{+}ClO_4^{-}$ (right) films made with 6 (top) and 60 (bottom) nmol of ferrocenium salts, deposited on mica substrates.

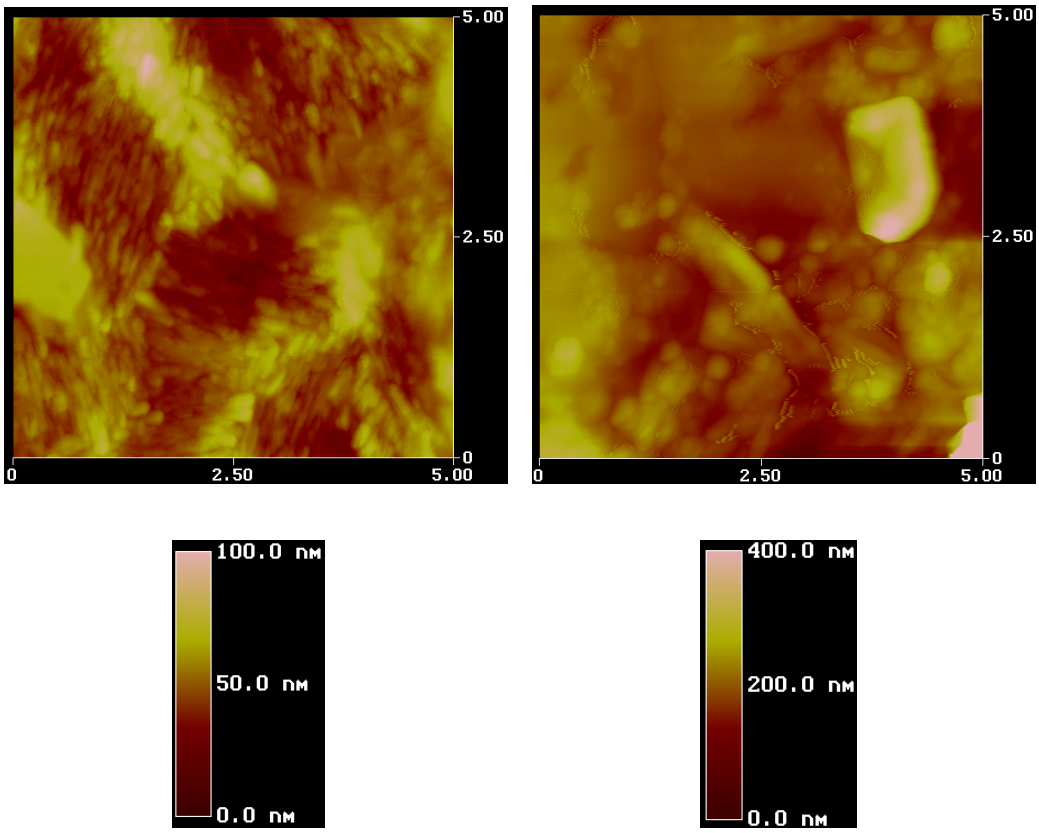

Figure 2.30. AFM images of $DEC^{+}NO_3^{-}$ films made with 6 (left) and 60 (right) nmol of ferrocenium salts, deposited on silicon wafers using a metallic mask to form a well.

the center of these clusters, to big round well-like areas with less material in them. $DEC^+ClO_4^-$, on the other hand, presents big clusters in the thinner film (bigger than those for the more concentrated solution of $DEC^+NO_3^-$), with a thicker area in the center, while the thicker film show smaller, more uniformly distributed clusters. This suggests that the trend in uniformity observed for $DEC^+NO_3^-$ (thinner films are more uniform) is opposite to the one observed for $DEC^+ClO_4^-$. When the $DEC^+NO_3^-$ film was further investigated on the Si wafers (figure 2.30) using a metal mask, the well-like morphology was observed for the thinner film, while the thicker film showed a combination of uniformly covered areas and clusters very close to each other. Again, greater uniformity was observed for the thinner film compared to the thicker one.

These results show that the use of the metal mask to create a probe-like environment affects the thickness of the film: the $DEC^+NO_3^-$ films on the silicon wafer required an observation from ca. 300 nm away from the substrate surface in order to observe the surface morphology (vs. 4nm for the thicker film on mica). It is also apparent that for $DEC^+NO_3^-$, the "density" of the materials as the films form affects the surface morphology: when the films were deposited on the mica substrates, the solution spread as it evaporated, which means the molecules where further apart from each other as the film dried. However, when the films were deposited on the silicon wafers, within the well formed by the mask, the solution was contained in a small volume and during the drying process the molecules were able to interact with each other more closely. This explains why the thinner film deposited in the well (silicon) show microscopic surface features similar to those observed in the thicker film deposited without the solution being confined (mica), but not shown for thinner films deposited without confinement: round, well-like features with less material in them.

The most important result was, however, that there are clear differences in the microscopic features between the surface of a $DEC^+NO_3^-$ film and that of a $DEC^+ClO_4^-$ film, both in morphology of the features themselves and in the uniformity of films with

different thicknesses. This is consistent with the discussion presented above: as an organic solution of these salts dries (and even after the solvent has evaporated completely), the film forms different for $DEC^+NO_3^-$ and for $DEC^+ClO_4^-$, as evidenced by the IR spectra of these films.

III. Experimental Section

III.1. Reagents, Solvents, and Solutions. All reagents and solvents were ACS grade or better unless stated otherwise. All solutions used were prepared in Class A volumetric glassware. The distilled deionized water (dd-H_2O) used for solution preparation had an initial resistivity of 18 MΩ cm.

III.1.1. Preparation of 1,1′,3,3′-tetrakis(*t*-butyl)ferrocenium Perchlorate ($BUT^+ClO_4^-$) and Crystal Structure Determinations. The following reagents/solvents were used as received (common name/abbreviation; formula; vendor are indicated in parenthesis): dichloromethane (Fisher Scientific), silver chloride (Aldrich), hexanes, mixture of isomers (Fisher Scientific), ethanol/EtOH (AAPER or PHARMCO); chloroform (Fisher Scientific). The polyalkylated ferrocene 1,1',3,3'-tetrakis-(*t*-butyl)ferrocene (BUT) was synthesized according to literature methods by other members of the Strauss Research Group.

III.1.2. Experiments with 1,1′,3,3′-tetrakis(*t*-butyl)ferrocenium (BUT^+) and 1,1′,3,3′-tetrakis(2-methyl-2-nonyl)ferrocenium (DEC^+) Thin Films. The following reagents/solvents were used as received (common name/abbreviation; formula; and vendor are indicated in parenthesis): dichloromethane (Fisher Scientific), dichloroethane (Fisher Scientific), acetone (Mallinckrodt), benzene (Fisher Scientific), chloroform (Fisher Scientific), chloroform-d ($CDCl_3$; Cambridge Isotope Laboratory, Inc).

III.2. Instrumentation. Distilled, dionized water (dd-H_2O) was purified using the Barnstead NANOpure system, Thermo Scientific (Dubuque, IA); IR spectra were recorded using the ATR-FTIR spectrometer described (ReactIR-1000, Mettler-Toledo,

Columbus, OH) that was equipped with either an 18-bounce diamond (DiComp®) ATR crystal or a 30-bounce silicon (SiComp®) ATR crystal, mated to a ZnSe optical focusing element and housed in a 1.3 cm thick × 7.6 cm diameter stainless-steel DuraDisk™ (Mettler-Toledo, Columbus, OH). The wetted surface of the crystals was a circular area 0.9 cm in diameter. The electronic gain was either 2 (DiComp® probe) or 1 (SiComp® probe). A liquid-nitrogen-cooled mercury cadmium telluride (MCT) detector was used. The spectral window was 4000 to 600 cm^{-1} with a nominal spectral resolution of either 2 or 8 cm^{-1}. Happ-Ganzel apodization was used with no post-run spectral smoothing. X-ray diffraction data from crystals of 1,1′,3,3′-tetrakis(*t*-butyl)ferrocenium (BUT^+) were recorded on a Bruker Kappa APEX II CCD diffractometer employing Mo Kα radiation (graphite monochromator). Absorption and other corrections were applied by using SADABS. The structures were solved by using direct methods and refined (on F^2, using all data) by a full-matrix, weighted least squares process. Standard Bruker control and integration software (APEX II) was employed, and Bruker SHELXTL software was used for structure solution, refinement, and graphics. For the AFM experiments a Bioscope AFM instrument mounted on the stage of a Zeiss Axiovert inverted optical microscope was used, together with Nanoscope III controller and software V.4.42r9 (Digital Instruments).

III.3. Study of Modified Ferrocenium Salts

III.3.1. Preparation of 1,1′,3,3′-tetrakis(*t*-butyl)ferrocenium Perchlorate ($BUT^+ClO_4^-$). The salt was prepared from the corresponding ferrocene (BUT) using an adapted procedure developed by a previous member of the Strauss Research Group.

III.3.2. Crystal Structure Determinations. A quarter of a glass tube (length=25 cm, ID≈4mm) was filled with a saturated solution of 1,1′,3,3′-tetrakis(*t*-butyl)ferrocenium perchlorate ($BUT^+ClO_4^-$) in either CH_2Cl_2 or $CHCl_3$. Hexenes were slowly added to the tube until it was half full, carefully creating an interface between the

two otherwise miscible solutions. The tube was left undisturbed for 48 hours, capped with a rubber stopper and Parafilm™. The crystals were analyzed using x-ray diffraction.

III.3.3. Atomic Force Microscopy (AFM) Experiments. Two kinds of substrates were used for the deposition of samples in the AFM determinations: Mica-on-Glass substrates and Silicon Wafers, which were used as received. Two ferrocenium salts were studied: 1,1′,3,3′-tetrakis(2-methyl-2-nonyl)ferrocenium Nitrate ($DEC^{+}NO_3^{-}$) and Perchlorate ($DEC^{+}ClO_4^{-}$). The thin films were of two different thicknesses, based on the amount of compound deposited on the substrate: 6 nmol and 60 nmol.

III.3.3.a. Mica-on-Glass Substrates. The substrates consisted on square glass slides containing a circular portion of mica attached to the center of one of the surfaces. Adhesive tape was used to carefully remove one layer of mica at a time, stripping it from the substrate. An aliquot of 20 μL of the solution containing the ferrocenium salt of interest was deposited in the center of this mica layer using an automatic Eppendorf™ pipette. Evaporation of the solvent was allowed for ca. 5 minutes and the samples were analyzed by AFM.

III.3.3.b. Silicon Wafers. A stainless steel washer was manually pressed against the wafers, in order to reproduce the metallic well where the films are formed on the ATR crystal probes. The pressure was maintained while an aliquot of 20 μL of the solution containing the ferrocenium salt of interest was deposited in the center of the washer using an automatic Eppendorf™ pipette. Evaporation of the solvent was allowed for ca. 5 minutes and the samples were analyzed by AFM.

III.3.4. Attenuated Total Reflectance Fourier Transform Infrared (ATR-FTIR) Spectroscopy Experiments. Solutions of the ferrocenium salts in an organic solvent were prepared within 24 hours of analysis. Both the diamond and the silicon ATR crystals were used.

III.3.4.a. **Dry Thin Film Experiments.** A background of either the diamond or the silicon ATR crystals in air was obtained before depositing the films. Subsequently,

an aliquot of a solution containing the ferrocenium salt of interest was placed on the ATR probe, and the solvent was allowed to evaporate. Infrared spectra were obtained at 2 cm^{-1} resolution, being each spectrum, in general, an average of 128 scans. In the case of the study of $DEC^{+}NO_3^{-}$ thin films, collections with 16 scans as average were performed, which allowed for spectra collection every ca. 30 seconds. These parameters allowed for monitoring of the $DEC^{+}NO_3^{-}$ film during initial seconds of formation, period during which the regular analysis (128 scans) was collecting data to display the first spectrum. In all cases collection of data was started as soon as there was no more evidence of the presence of solvent to the naked eye (<20 seconds). The development of IR bands of interest was monitored for periods of up to 8 hours, interrupting the collection once the bands stopped changing with time.

IV. Conclusions

The extensive analysis presented here explains several spectroscopic behaviors of the modified ferrocenium salts used in the Strauss research Group, some of which had been observed for years without a clear explanation of their causes. The author also:

(i) presents a cohesive discussion of different crystallographic and electrochemical parameters of several treaalkylated ferrocenium salts, synthesized and characterized by previous members of the Strauss Research Group, to prove that relative cation size does increase, but only in one dimension, from BUT^{+} to DEC^{+}, and also that this difference in size affects ion-exchange selectivities depending what the non-aqueous phase containing the extractant is (either a water-immiscible solvent, a three-dimensional thin film or a monolayer self-assembled on an electrode surface);

(ii) investigated crystallographic and spectroscopic data to show the effects of C–H...O hydrogen bonding in the cation–anion interactions in ferrocenium salts, explaining why the DEC^{+} cation is a more selective ion-exchange cation for thin films of ferrocenium$^{+}NO_3^{-}$ salts than the BUT^{+} cation;

(iii) developed a comprehensive model for the structure of thin films of DEC^+ salts, based on atom distances from the crystallographic data, which explain the observed apparent differences and similarities between the structure of a thin film (deposited on an ATR crystal) and the crystalline salt of $DEC^+NO_3^-$ and $DEC^+ClO_4^-$ (or $DEC^+ReO_4^-$), respectively;

(iv) used atomic force microscopy to observe the morphology of surfaces of $DEC^+NO_3^-$ and $DEC^+ClO_4^-$ films, which had never been done before, and found results consistent with the hypothesis that there is a clear difference in the way that organic solutions of these two salts molecularly arrange as solvent evaporates to form very different thin films.

V. References

(1) Griffiths, P. R.; de Haseth, J. A. *Fourier Transform Infrared Spectrometry*; John Wiley & Sons: New York, 1986.

(2) Hebert, G. N.; Odom, M. A.; Bowman, S. C.; Strauss, S. H. *Anal. Chem.* **2004**, *76*, 781-787.

(3) Strauss, S. H.; Odom, M. A.; Herbert, G. N.; Clapsaddle, B. J. *J. Am. Water Works Assoc.* **2002**, *94*, 109-115.

(4) Collette, T. W.; Williams, T. L.; Urbansky, E. T.; Magnuson, M. L.; Hebert, G. N.; Strauss, S. H. *Analyst* **2003**, *128*, 88-97.

(5) Leigh, T. *J. Chem. Soc.* **1964**, 3294.

(6) Hughes, R. P.; Kowalski, A. S.; Lomprey, J. R. *Organometallics* **1994**, *13*, 2691-2695.

(7) Chambliss, C. K. Investigation and Development of Liquid-Liquid Extraction Systems for the Removal of Pertechnetate from Aqueous Nuclear Waste Simulants. Ph.D. Dissertation, Colorado State University, 1998.

(8) Clark, J. F. Design, Synthesis, and Evaluation of Redox-Recyclable Organometallic Extractants for the Recovery of Ionic Radionuclides from Aqueous Waste Streams. Ph.D. Dissertation, Colorado State University, 1999.

(9) Clapsaddle, B. J. Synthesis and Characterization of Tetraalkylated and Functionalized Polyalkylated Ferrocenes and Their Applications for the Selective Redox-Recyclable Extraction and Detection of Aqueous Anions. Ph.D. Dissertation, Colorado State University, 2002.

(10) Bondi, A. *J. Phys. Chem.* **1964**, *68*, 441-451.

(11) Boese, R.; Blaser, D.; Kuhn, S.; Stubenrauch, S. *Z. Kristallogr.* **1993**, *205*, 282-284.

(12) Keller, A. *Phil. Mag.* **1957**, *2*, 1171-.

(13) Brown, R. J. C.; Powell, B. M.; Stuart, S. N. *Acta Crystallogr.* **1993**, *C49*, 214-216.

(14) Odom, M. A. Development of Strategies for the Detection, Extraction, and Recovery of Aqueous Anions Using Highly Selective Redox-Recyclable Materials. Ph.D. Dissertation, Colorado State University, Fort Collins, CO, 2001.

(15) Wickleder, M. S. *Z. Anorg. Allg. Chem.* **2003**, *629*, 1466-1468.

(16) Wartchow, R.; Berthold, H. J. *Z. Kristallogr.* **1978**, *147*, 307-317.

(17) Sawada, H. *Mat. Res. Bull.* **1993**, *28*, 867-870.

(18) Granzin, J. *Z. Kristallogr.* **1988**, *184*, 157-159.

(19) Barnes, A. J. *J. Molec. Struc.* **2004**, *704*, 3-9.

(20) Hay, B. P.; Bryantsev, V. S. *Chem. Commun.* **2008**, 2417-2428.

(21) Pedzisa, L.; Hay, B. P. *J. Org. Chem.* **2009**, *74*, 2554-2560.

(22) Coletti, C.; Re, N. *J. Phys. Chem. A* **2009**, *113*, 1578-1585.

(23) Scheiner, S.; Grabowski, S. J.; Kar, T. *J. Phys. Chem. A* **2001**, *105*, 10607-10612.

(24) Nolasco, M. M.; Ribeiro-Claro, P. J. A. *ChemPhysChem* **2005**, *6*, 496-502.

(25) Graul, S.; Squires, R. R. *J. Am. Chem. Soc.* **1990**, *112*, 2517-2529.

(26) Pinakidou, F.; Katsikino, M.; Paloura, E. C.; Kavouras, P.; Kalogirou, O.; Komninou, P.; Karakostas, T. *Nuclear Instr. Methods Phys. Res. B* **2006**, *246*, 170-175.

(27) Reed, C. A.; Mashiko, T.; Bentley, S. P.; Kastner, M. E.; Scheidt, W. R.; Spartalian, K.; Lang, G. *J. Am. Chem. Soc.* **1979**, *101*, 2948-2958.

(28) Braga, D.; Grepioni, F.; Tagliavini, E.; Novoa, J. J.; Mota, F. *New J. Chem.* **1998**, 755-757.

(29) Grepioni, F.; Cojazzi, G.; Draper, S. M.; Scully, N.; Braga, D. *Organometallics* **1998**, *17*, 296-307.

(30) Bordwell, F. *Acc. Chem. Res.* **1988**, *21*, 456-463.

(31) Pandiarajan, S.; Rajaram, R. K.; Ramakrishnan, V. *J. Raman Spectrosc.* **2005**, *36*, 785-790.

(32) Pejov, L.; Petrusevski, V. M. *J. Phys. Chem. Solids* **2002**, *63*, 1873-1881.

(33) Mitterbock, M.; Fleissner, G.; Hallbrucker, A.; Mayer, E. *J. Phys. Chem. B* **1999**, *103*, 8016-8025.

(34) Turner, J. J. *Coord. Chem. Rev.* **2002**, *230*, 213-224.

(35) Ritzhaupt, G.; Devlin, J. P. *J. Chem. Phys.* **1975**, *62*, 1982-1986.

(36) Wyckoff, R. W. G. *Phys. Rev.* **1920`**, *16*, 149-157.

(37) Waterland, M. R.; Stockwell, D.; Kelley, A. M. *J. Chem. Phys.* **2001**, *114*, 6249-6258.

(38) Nimmo, J. K.; Lucas, B. W. *J. Phys. C: Solid State Phys.* **1973**, *6*, 201-211.

(39) Karpov, S. V.; Shultin, A. A. *J. Phys. Chem. Solids* **1968**, *29*, 475-480.

(40) Hobza, P.; Havlas, Z. *Theor. Chem. Acc.* **2002**, *108*, 325-334.

(41) Reimann, B.; Buchhold, K.; Vaupel, S.; Brutschy, B.; Havlas, Z.; Spirko, V.; Hobza, P. *J. Phys. Chem. A* **2001**, *105*, 5560-5566.

(42) van der Veken, B. J.; Herrebout, W. A.; Szostak, R.; Shchepkin, D. N.; Havlas, Z.; Hobza, P. *J. Am. Chem. Soc.* **2001**, *123*, 12290-12293.

(43) Michielsen, B.; Herrebout, W. A.; van der Veken, B. J. *ChemPhysChem* **2008**, *9*, 1693-1701.

(44) Michielsen, B.; Herrebout, W. A.; van der Veken, B. J. *ChemPhysChem* **2007**, *8*, 1188-1198.

(45) Brisdon, A. K.; Flower, K. R.; Pritchard, R. G. *Inorg. Chem.* **2007**, *46*, 7189-7192.

(46) Diana, E.; Stanghellini, P. L. *J. AM. CHEM. SOC.* **2004**, *126*, 7418-7419.

(47) Scheiner, S.; Kar, T. *J. Phys. Chem. A FIELD Full Journal Title:Journal of Physical Chemistry A* **2008**, *112*, 11854-11860.

(48) Scheiner, S.; Kar, T. *J. Phys. Chem. A* **2002**, *106*, 1784-1789.

(49) Delanoye, S. N.; Herrebout, W. A.; van der Veken, B. J. *J. Am. Chem. Soc.* **2002**, *124*, 7490-7498.

(50) Huber, S.; Knozinger, H. *J. Mol. Catal. A* **1999**, *141*, 117-127.

(51) Douglas, D. C.; McHale, J. L. *J. Phys. Chem. A* **1997**, *101*, 3070-3077.

(52) Hippler, M. *J. Chem. Phys.* **2007**, *127*, 084306-1-10.

(53) Buckingham, A. D.; Del Bene, J. E.; McDowell, S. A. C. *Chem. Phys. Lett.* **2008**, *463*, 1-10.

Chapter 3

Detection of Anions in Aqueous Solutions Using Thin-Film Coated ATR-FTIR Probes

I. Introduction

I.1. Applications of the ATR-FTIR technique. In Chapter 1, an analytical technique based on ATR-FTIR spectroscopy was introduced. The Strauss Research Group has used this technique in the past for the detection and quantification of anionic pollutants, applying the "time-dependent exchange method".[1,2] In this chapter, variations of the original method introduced by the author are presented, including the use of novel extracting salts, investigation of multi-analyte experiments and the optimization of traditionally used parameters.

I.1.1. The Time-dependent Exchange Method for Quantification. The name "time-dependant" arises because the quantification of the analyte is achieved by monitoring the exchange, with time, of anions between an aqueous sample and a solid thin film. The extractant is an anionic compound, deposited by evaporation on the probe of the ATR-FTIR spectrometer and then placed in contact with an aqueous sample containing the analyte. The anion exchange takes place based on the hydration energy of the anions participating in the exchange, as explained in Chapter 1. However, only some sites in the film are subject to exchange. All exchange reactions proceed until all available sites in the film have undergone exchange, given enough time and that sufficient analyte is available. This means that Beer's law does not apply for this system and this method would not be suitable for quantification. However, the rate of exchange is directly proportional to the analyte concentration originally in the sample.[3] The

exchange is monitored with time, analyzing the initial (first ten minutes) absorbance change (d*A*/d*t*) for a particular IR band of the analyte. This change, which constitutes the initial rate of exchange, is correlated to the analyte concentration in the sample. Using different samples with standard analyte concentrations, a calibration curve is created for each particular analyte-film pair. This analytical method permits for higher limits of detection (LOD) by just allowing the exchange to take place for longer time. This method proves that despite popular belief to the contrary, IR spectroscopy is a suitable analytical method for the detection and quantification of aqueous anions at sub-micromolar concentrations.[3]

This time-dependent exchange method will be better illustrated through an example presented in Section II.1.1.

I.1.2. The Extractants. The nature of the compound used as the extractant plays an important role in the exchange. Three different type of extractants were used for exchange experiments: 1,1′,3,3′-tetrakis(2-methyl-2-nonyl)ferrocenium salts (DEC^+X^-), 1,3-bis(diphenylphosphino)propanedichloronickel(II) ($NiCl_2$(dppp)) and 1,1′,3-tris(2-methyl-2-nonyl)-3′-N(N,N-dimethyl-N-heptylammonium)ferrocenium (Hp-aza-DEC^+).

I.1.2.a. **DEC^+X^-.** In order for the modified ferrocenium salts to be suitable for anion exchange from aqueous solutions, the thin films made out of them must be water insoluble, as they are placed directly in contact with the aqueous sample for the duration of the experiment (ca. 1 h). Some ferrocenium salts are water-insoluble, like those with long hydrocarbon chains attached to the cyclopentadienyl rings such as DEC^+X^-, which makes these compounds hydrophobic. Other salts, however, like BUT^+X^-, dissolve in water, which make them unsuitable for making thin films to be used in this kind of heterogeneous exchange.

Thin films of DEC^+X^- have been the bases for detection, extraction and quantification of anions in aqueous solutions for several years in the Strauss Research Group. Mainly $DEC^+NO_3^-$, which given the high hydration energy of NO_3^- constitutes a

very useful compound to extract other analytes from water (see Chapter 1). Although $DEC^+NO_3^-$ is stable indefinitely in the solid state at 25 °C, previous investigations by other co-workers in the Strauss Research Group at CSU revealed that thin films of $DEC^+NO_3^-$ are not stable indefinitely when in contact with water at 25 °C. It was proposed that a reaction such as the following might be responsible for this behavior:[3,4]

$$3\ DEC^+NO_3^-(s) \xrightarrow{H_2O} 2\ DEC(s) + FeO(OH) + 3\ NO_3^-(aq) + \text{other organic products}$$

This proposal was consistent with the known reduction/decomposition of some substituted ferrocenium cations in the presence of nucleophilic anions (e.g., Cl^-, Br^-, I^-, CN^-) even in the absence of water,[5-8] as exemplified by the following reaction:

$$3\ DEC^+Cl^-(CH_2Cl_2) \longrightarrow 2\ DEC(CH_2Cl_2) + FeCl_3(s) + \text{other organic products}$$

Among the strategies followed to deal with the $DEC^+NO_3^-$ instability was the use of thinner films than those traditionally used in our research group; the hypothesis being that a thinner film would have all available exchange-sites closer to the surface, which would accelerate the exchange process and hence the amount of time the film is in contact with the aqueous solution.

For certain experiments in which $\Delta\Delta G°_{hyd}$ between the sample and the film anions allowed the exchange (see Chapter 1), thin films of $DEC^+ClO_4^-$ were used.

I.1.2.b. **$NiCl_2$(dppp).** For the detection of free cyanide (CN^-), the use of DEC^+X^--coated probes was not possible, as described in the next sub-section. Instead, the compound 1,3-bis(diphenylphosphino)propanedichloronickel(II) ($NiCl_2$(dppp)), shown in Figure 3.1b, was used to complex free aqueous cyanide. This extractant, unlike the DEC^+ salts, is not redox recyclable, but a Cl^-/CN^- ligand exchange takes place, with

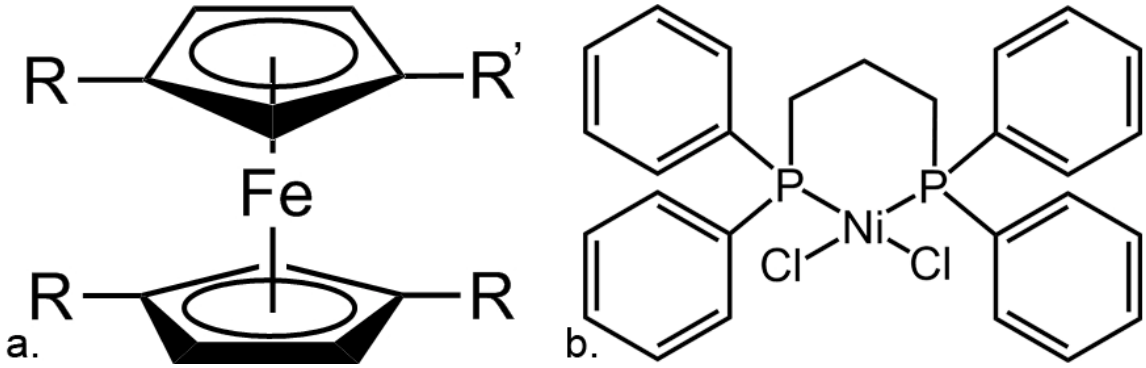

Figure 3.1. General structures of the ion-exchange extractants used make thin films on the ATR probes in order to quantify anions in aqueous solutions.

a. 1,1′,3,3′-tetrakis(2-methyl-2-nonyl)ferrocenium salts **(DEC$^+$)** when R = R' = 2-methyl-2-nonyl and 1,1′,3-tris(2-methyl-2-nonyl)-3′-N(N,N-dimethyl-N-heptylammonium) ferrocenium **(Hp-aza-DEC$^+$)** when R = 2-methyl-2-nonyl and R' = N(N,N-dimethyl-N-heptylammonium.

b. 1,3-bis(diphenylphosphino)propanedichloronickel(II) **($NiCl_2$(dppp))**

the essentially irreversible formation of a new water-insoluble complex, NiCl(CN)(dppp), as studied by Elisha Kosak[9] and Gretchen Hebert[3], both former members of the Strauss Research Group, and shown in Equation 3.1.

$$NiCl_2(dppp)\,(s) + CN^-\,(aq) \longrightarrow NiCl(CN)(dppp)\,(s) + Cl^-\,(aq) \qquad 3.1$$

The use of this nickel complex as a thin-film coating on silicon ATR crystals for the detection of low concentrations of free cyanide will be discussed in this chapter. An ATR-FTIR method using a Ni-based organometallic ligand-exchange complex, including determination of a LOD for free (uncomplexed) CN^-, has been previously reported by the Strauss Research Group.[10] Table 3.1 presents the thermodynamic radii and the calculated hydration energies ($\Delta G°_{hyd}$) for selected anions, as they appear in an important review by Moyer and Bonnesen.[11] When looking at these values it becomes clear, based on the previous discussion introduced in Chapter 1, why it is not possible to use the DEC^+ salts to detect CN^-: this anion has a higher $\Delta G°_{hyd}$ than either of the anions in these salts (NO_3^-, ReO_4^- or ClO_4^-). Also, the presence of CN^- presents the possibility of causing nucleophilic decomposition of the ferrocenium complex, as explained in the previous section.

I.1.2.c. **Hp-aza-DEC$^+$I$^-$.** This compound was synthesized to circumvent the previously mentioned $DEC^+NO_3^-$ instability issues in the presence of certain nucleophiles. A novel extractant, based on the cation 1,1′,3-tris(2-methyl-2-nonyl)-3′-N(N,N-dimethyl-N-heptylammonium)ferrocenium (Hp-aza-DEC^+), possess a similar structure to DEC^+ (Figure 3.1a), but with the positive charge placed on a nitrogen atom instead of the iron. This compound was mainly used for exchange in an attempt to detect and quantify ppm concentrations of dodecylsulfate (DDS^-), the anion in the ionic detergent sodium dodecylsulfate (SDS), in aqueous media obtained from certain

biological experiments. SDS is used as a promising decellularization/antigen-clearing

Table 3.1. Ion Size and Hydration Energies for Selected Anions[a]

Anion X^-	Thermochemical radius, nm	$\Delta G_h(X^-)$ calculated with eq. 3.4, kJ mol^{-1}
NO_3^-	0.196	−314
ClO_4^-	0.144	−259
ReO_4^-	0.174	−240
CN^-	0.191	−322

[a] Ref. [11]

agent by many researchers, including Dr Christopher Orton at the Veterinary Teaching Hospital, Colorado State University.[12-14] The samples from the experiments conducted by Orton et al. were suspected to contain SDS, but it was unknown in what concentrations. The samples, which had been used to soak tissue samples treated with the detergent, contained other components (see Table 3.2), including Cl^-, which render the media unstable for $DEC^+NO_3^-$ films. Dr Orton's Research group and the Strauss Research Group embarked in the development of an analytical method that allowed for the determination of DDS^- in these biological samples. These experiments are explained in detail in Chapter 4.

I.1.3. The Samples. The volume of choice for the aqueous samples used for ion-exchange experiments in the Strauss Research Group has traditionally been 100 mL, referred to in this report as "large volume". The reason behind the volume choice is that when an analyte is being quantified in a sample, it is desired that its concentration in the bulk of the sample does not change. The use of a large volume where the target analyte concentration is obtained with a large amount of compound allows for an insignificant diminishing of this concentration in the bulk. Thus, the sample does not become depleted of the analyte during the measurement and its concentration can be considered essentially constant for the duration of any experiment. Nevertheless, the author demonstrates in the present chapter that linear calibration curves can be created in a volume of 1 mL. In this way, a new methodology which came to be termed "small-volume experiments" was developed as part of this work.

The majority of the ion-exchange experiments performed in the Strauss Research Group dealt with the detection of a single analyte, either by it being the only species present in the sample or by studying samples with other species which do not interfere with the ATR-FTIR detection. In the present work the effect of $\Delta\Delta G°_{hyd}$ on selectivity was tested, by performing a series of multiple-anion experiments using $DEC^+NO_3^-$, $DEC^+ClO_4^-$ and $DEC^+ReO_4^-$ in several exchanges.

Table 3.2. Soaking solution composition and components concentration.

component	concentration
phosphate	10.4 mM
sodium chloride	1193.9 mM
potasium chloride	2.8 mM
aprotinin	9.2×10^{-2} % v/v
ethylenediaminetetraacetic acid	0.1 % w/v
trizma hydrochloride buffer	1050 mM
penicillin G	1×10^{4} U/mL
streptomycin sulfate	10 mg/mL
amphotericin B	25 mg/mL

To prepare this solution, a 1 L PBS solution was prepared in dd-water, and then used to dissolve/dilute the rest of the components to a final volume of 250 mL. This final solution was used to soak tissue samples in a precise soaking regime, as described in the experimental section.

I.2. The Analytical Problem. The analytes quantified and studied in the exchange experiments described in this chapter were cyanide (CN^-), perchlorate (ClO_4^-), perfluoro-*n*-octanesulfonate ($C_8F_{17}SO_3^-$; $PFOS^-$), perrhenate (ReO_4^-), and dodecylsulfate (DDS^-). It was found by former members of the Strauss Research Group that some of these anions can be detected at low concentrations ($\leq$ 0.06 μM) by ATR-FTIR, with chemically modified probe crystals.[1]

Cyanide. This anion has traditionally been introduced in the environment by the mining industry, which utilizes the coordination capabilities of this anion to form complexes with precious metals to extract traces of Au and Ag from ore.[15,16] In more recent times, the major cyanide releases to water are discharges from metal finishing industries, iron and steel mills, and organic chemical industries.[17]

In aqueous solutions with pH < 9.2, evolution of the gas, HCN, can be observed. This acid has shown significant health risks even at low concentrations, causing nerve damage or thyroid problems and death within minutes occurs from exposure to high concentrations.[18,19] The Environmental Protection Agency (EPA) has listed CN^- under the National Primary Drinking Water Regulations, setting a maximum contaminant level (MCL) of 0.2 mg/L [20]

Cyanide determinations commonly used are classified in three groups: "total cyanide" techniques measure free, weakly-coordinated, and strongly-coordinated CN^-, "Weak Acid Dissociable" (WAD) techniques measure the former two kinds, and "free cyanide" techniques measure free CN^- and HCN. No regulatory standards exist to date for most of these determinations, which constitutes a significant problem when analyzing samples from mining industry. The accurate determination of cyanide is difficult for various reasons. Depending on the pH of the solution, cyanide is present both in molecular form (HCN) and ionic form (CN^-). Also, cyanide is a good complexing reagent and reacts with almost all cations resulting in complexes with widely varying properties, such as

stabilities, solubilities and rates of reaction. Cyanide also breaks down in sunlight and air, so that sampling and sample treatment become very important aspects to consider in the methodologies.[21] The EPA has approved a flow injection method to determine total cyanide concentration in solution (including weak or intermediate-strength metal cyano complexes; e.g., Zn^{2+}, Cu^{+}, Cd^{2+}, Hg^{2+}, Ni^{2+}, and Ag^{+}). This method has a limit of detection (LOD) of 0.02 μM CN^{-} (analysis time ca. two minutes, not including any of the preparation steps) and a linear range of 0.05–130 μM.[22] The presence of sulfide in the solution interferes with the CN^{-} determination (it causes a false positive response), and more importantly, this method will not determine cyanide from complexes of Co, Au, Pd, Pt, Ru, and Fe which are thermodynamically or kinetically stable. In order to release cyanide from complexes with these metals, harsher conditions of digestion in the presence of intense UV radiation are necessary prior to detection.[23]

Perchlorate (ClO_4^{-}). This anion, highly soluble and stable in water, is found in the environment primarily due to the defense and aerospace industries and to military operations,[24,25] where perchlorate salts are widely utilized as oxidants in munitions and solid fuels for rockets. It is also used on a large scale as a component of automobile air bag inflators,[26] in addition to many other uses.

Since the late 1990s, perchlorate has been detected in human and cow's milk samples, and vegetable samples throughout the United States,[27-31] in surface, ground and drinking-water samples from several western states including Utah, California, Arizona, and Nevada, and there have been confirmed releases of perchlorate in at least 20 states within the United States.[32] The contamination of the Colorado River with perchlorate was the subject of a cover story article in *Chemical and Engineering News* in 2003, which described the widespread use of this perchlorate-tainted water for drinking and irrigation.[33] In the last couple of years Sanchez et. al. published several articles on their findings on perchlorate in edible crops that used water from the Colorado River as their irrigation source.[34,35] The concern over perchlorate arises from its ability to interfere with

iodine uptake into the thyroid gland, which may cause a decreased synthesis of thyroid hormones, and may potentially affect metabolism as well as normal growth and development.[36-38] Although a problem in the past,[39] nitrate fertilizers (from Chilean caliche) are not generally seen as a major source of perchlorate in the environment in recent times.[40] Their use has diminished to less than 0.2% of current U.S. fertilizer consumption[41] as a result of the low cost of synthetically produced nitrogen sources, and since 2001, new processing methods have reduced the perchlorate content in these fertilizers to <0.01%.[42]

The EPA added perchlorate to the Contaminant Candidate List for drinking water in 1998[43] and to the Unregulated Contaminant Monitoring Regulation list in 1999.[44] In 2005, the National Academy of Sciences (NAS) recommended a reference dose (RfD) of 0.7 mg kg^{-1} per day for perchlorate.[45] In 2009, the US Environmental Protection Agency (EPA) released an interim health advisory level for perchlorate of 15 μg L^{-1} or parts per billion (ppb).[46] Several states also have advisory levels of perchlorate, ranging from 1 to 18 ppb.[47]

Perrhenate (ReO_4^-). This anion does not constitute an environmental hazard, but it was studied as a surrogate for the radioactive contaminant pertechnetate (TcO_4^-).[48] Perrhenate and pertechnetate are isoelectronic, so ReO_4^- has been used in this study to model the radioactive anion without having to manipulate ^{99}Tc, which has a long half-life (210,000 years) and is very mobile in most oxidizing systems in the environment when in the form of the pertechnetate ion.[49] It exists over the complete pH range of natural waters and it is highly soluble and not strongly sorbed.[50]

A vast amount of solid and liquid radioactive waste has been generated since the world's first full-scale nuclear reactors and processing plants, established for the production and isolation of plutonium-239, began operating at the Hanford Site River in southeastern Washington. The remediation of these radioactive wastes is of current interest at the U.S. Department of Energy (DOE). One plan was to separate the waste into

primarily solid (sludge containing insoluble high-activity waste (HAW) species as well as nonradioactive solids) and aqueous liquid portions (tank supernatant and water-soluble species derived from HAW sludge washings).[51] The water soluble fraction can be further separated and treated, and then added to the HAW portion, leaving an aqueous solution containing both low-activity waste (LAW) species and other nonradioactive species. The LAW and HAW fractions resulting from these pretreatment steps would then be separately mixed with glass precursor additives or glass frit and then would be vitrified for long-term storage. However, TcO_4^- constitutes a problem, remaining in the LAW after pretreatment.

Previous members of the Strauss Research Group have investigated the use of ferrocenium salts as extracting materials to eliminate ReO_4^-, and by extension TcO_4^-, from nuclear simulants.[4]

Perfluoro-n-octanesulfonate ($C_8F_{17}SO_3^-$; PFOS$^-$). Salts of $PFOS^-$ were used for years in many consumer and industrial formulations, including fabric treatments, anti-static agents, paper coatings approved for food contact, shampoos, insecticides, and aqueous film-forming foams (AFFFs),[52] which were used for fire-fighting practices.[53-56] Effluents from these practices were not pre-treated in any way before being discharged to wastewater treatment facilities or to the environment, which may be responsible for the presence of $PFOS^-$ in localized environments.

The $PFOS^-$ anion is a very stable species, like many other perfluorinated chemicals.[57] It is resistant to thermal degradation and chemical attack in aqueous solution,[58] and to degradation in wastewater treatment systems, because it causes excessive foaming which inhibits nitrification.[59] Recent studies have been done that report very low concentrations of $PFOS^-$ (i.e., 0.7 pM to 0.2 nM) in Japanese surface and groundwater.[60,61]

Salts of $PFOS^-$ have shown significant toxic effects to the thyroid, abnormal fetal development and newborn development, and even mortality, in cynomolgus monkeys,[62] rabbits,[63] rats,[64] some invertebrates,[65] and zooplankton.[66] There is growing evidence that

$PFOS^-$ is toxic to higher organisms, and it has been found in the tissues of many species around the globe, including eagles from the Baltic Sea coastal area and areas around the Great Lakes,[67,68] various fish, birds and dolphins in Italy, Korea, Japan, India, the United States and the Southern emisphere,[69-73] polar bears in Alaska,[74,75] sea otters in California[76], and seals in the Northwest Atlantic region and Antartica.[73,77] This research clearly shows that $PFOS^-$ is distributed globally in the environment. This anion has also been found in birds egg yolk and marine animal puppies, demonstrating that the chemical is transferred down the food chain.[68,78,79] One study[80] reports that $PFOS^-$ has been found in sea otters from Alaska from 1992 to 2007, and that an overall decrease in the anion's concentration was observed after 2001. These results are consistent with the decision of 3M Company to discontinue $PFOS^-$ production in 2000,[81,82] due to the widespread presence and persistence of $PFOS^-$ in the environment as well as the discovery of its toxicity. In 2002, the EPA regulated its production and use in the United States.[52]

Lauryl sulfate ($C_{12}H_{25}SO_4^-$, dodecylsulfate, DDS^-). Sodium dodecylsulfate (SDS) is commonly used as a treatment agent in preparing proteins for sodium dodecyl sulfate polyacrylamide gel electrophoresis (SDS-PAGE). This technique is widely used in biochemistry, forensics, genetics and molecular biology to separate proteins according to their electrophoretic mobility. SDS denatures secondary and non–disulfide–linked tertiary structures, and it applies a negative charge to each protein proportionally to their masses. This gives a near uniform negative charge along the length of the polypeptide. Samples with identical charge-to-mass ratios are separated by size.[83] The electrostatic repulsion that is created by SDS binding causes proteins to unfold into a rod-like shape, thereby eliminating differences in shape as a factor of separation in the gel.

Due to the great affinity of DDS^- for proteins, this detergent is also used as a promising agent in decellularization/antigen-clearing treatments.[12,13] The initial and crucial step to obtain an optimal tissue matrix is decellularizion, which creates xenogenous tissues. Samples are immersed in a solution of typically 0.1% SDS

concentration for a period of generally 24 hours, but controversy exists throughout the literature about whether this treatment generates problems when recellularization is attempted.[84,85] It is unknown whether DDS^- stays in the tissue after decellularization procedures are finished, and whether the presence of the detergent creates a toxic environment for the new cells. Clarifying this concern is what made DDS^- an anion of interest to the author, as it will be discussed in more detail in Chapter 4.

II. Results and Discussion

II.1. ATR-FTIR Detection and Quantification of Pollutants using DEC^+ Salts. Further developments of the time-dependent exchange method performed by the author are presented next. Research was carried out to investigate whether reliable, consistent data can be obtained (i) for smaller volumes than 100 mL, (ii) when films "thinner" than 60 nmol of extractant are used, and (iii) when the analyte is in the presence of interfering substances.

II.1.1. Perfluoro-*n*-octanesulfonate Quantification in Small Volumes. The time-dependent exchange method was previously used for the quantification of $PFOS^-$ using a $DEC^+NO_3^-$ film and the Si probe. These results showed that the surfactant can be detected in aqueous solutions at concentrations as low as 0.06 μM^2 using the large-volume system. After successfully reproducing published results, the experiments were attempeted using the small-volume system developed by the author. In these experiments, a sample volume of 1 mL was used instead of the 100 mL used in the large-volume experiments. A $DEC^+ClO_4^-$ film was used as the extractant to quantify $PFOS^-$ in water samples. A calibration curve was constructed by analyzing standard solutions of $PFOS^-$ and monitoring the exchange with time (Figure 3.2). The apparently linear A(1270 cm^{-1}) vs. time plot for the first 10 minutes of ion exchange was fit to a straight line, the slope of which was the dA/dt (actually $\Delta A/\Delta t$) value for that particular concentration (Figure 3.3).

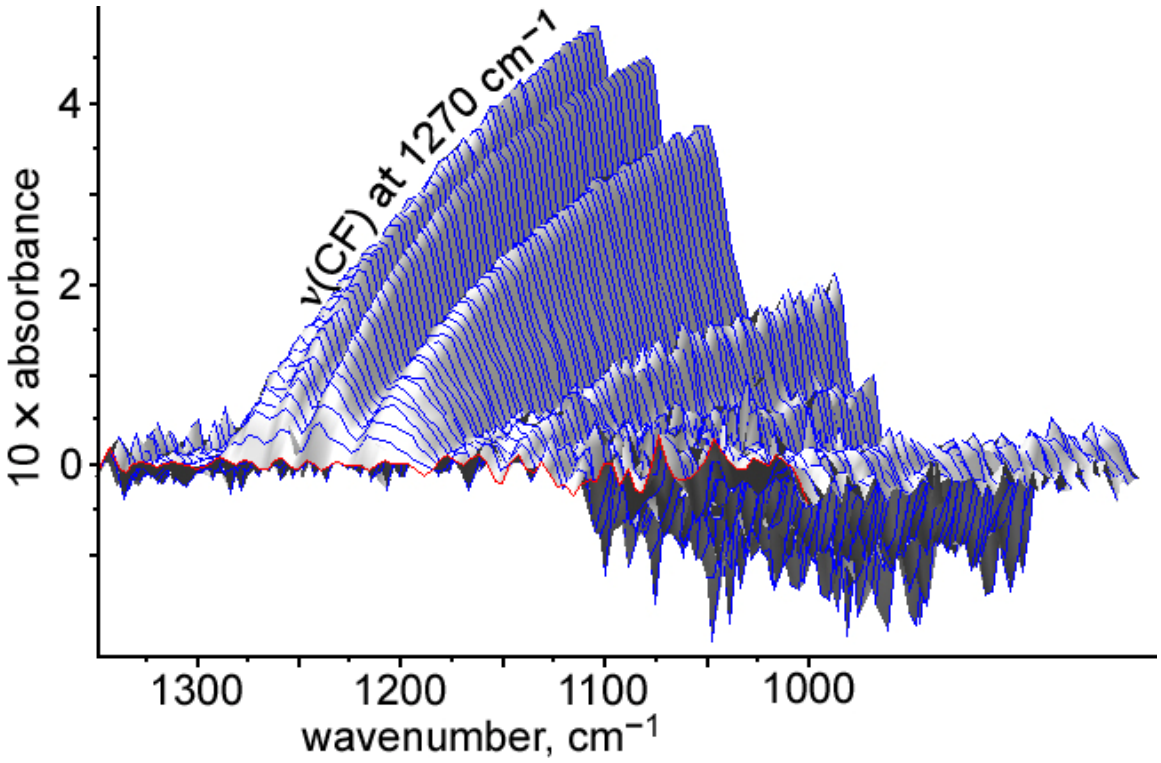

Figure 3.2. Set of infrared spectra of an originally $DEC^{+}ClO_4^{-}$ thin film, in contact with a small volume potassium perfluoro-*n*-octanesulfonate ($PFOS^{-}$) solution, recorded as a function of time. The 1000-1350 cm^{-1} region shows the ν(CF) bands of $PFOS^{-}$, increasing as this anion is introduced into the film.

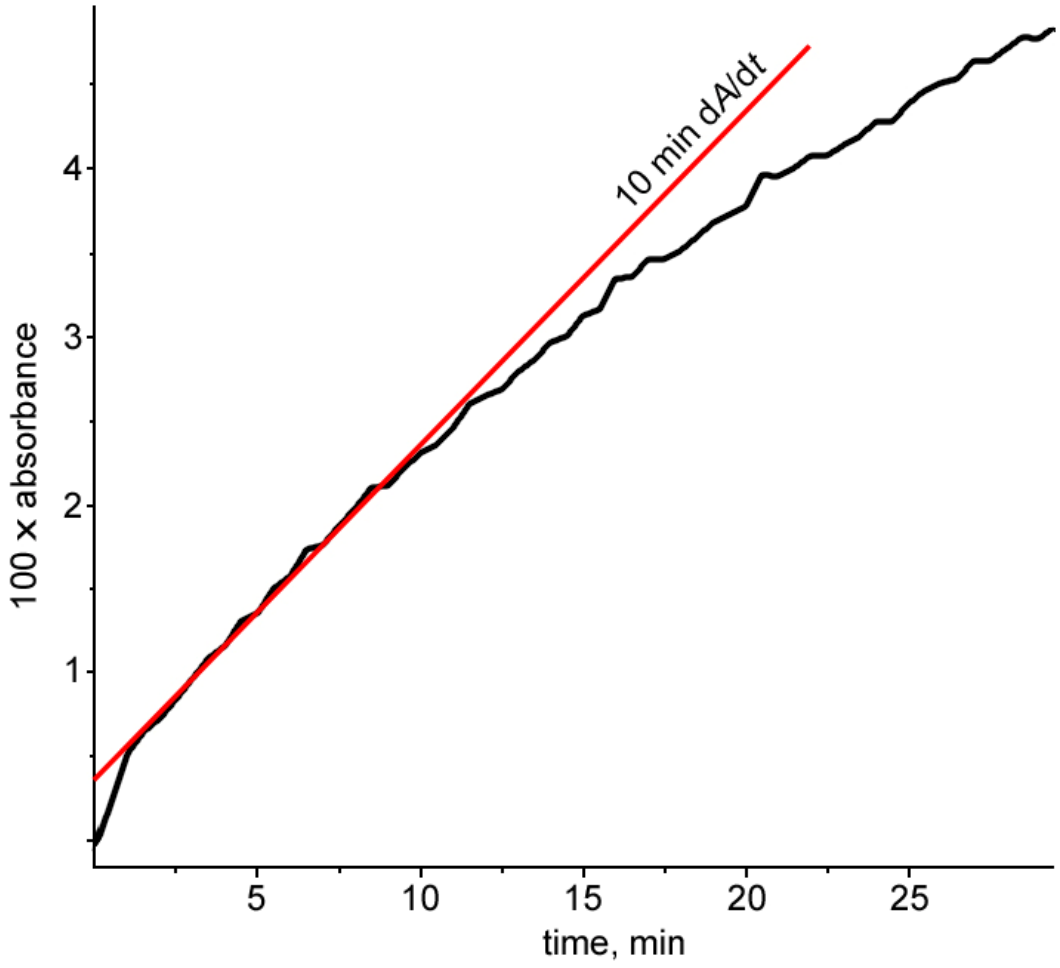

Figure 3.3. Profile (absorbance vs. time) for the main perfluorooctanesulfonate ($PFOS^-$) ν(CF) band, at 1270 cm^{-1}. A linear fit is shown for the data collected during the initial 10 minutes of $PFOS^-$ exchange from a 1 mL solution into a film originally of $DEC^+CO_4^-$. The slope of the fitted line represents d*A*/d*t*, which is proportionl to the concentration of $PFOS^-$ in the sample.

The different d*A*/d*t* values were graphed versus analyte concentrations for different samples. The calibration curve is shown in Figure 3.4. Although a limit of detection was not determined for this method, it can be observed that the range of concentrations analyzed is quite high (10-50 μM) compared to that for the 100-mL system using $DEC^{+}NO_3^{-}$ films (0.06-1 μM). Such a high-range was investigated to address the fact that the depletion of analyte in the system is more obvious with smaller concentrations. However, when observing the signal for the ν(CF) band for the lowest concentration measured (10 μM; Figure 3.2) it can be seen that the signal-to-noise ratio (SNR) would probably allow for the determination of a concentration 10 times smaller (1 μM).

These data show that the small-volume experiments can be used to quantify $PFOS^{-}$ in 1 mL of aqueous samples, and that the analyte depletion due to volume size does not affect the exchange to an extent that impedes a linear behavior with concentration.

II.1.2. Anion Detection Experiments using Different Film Thicknesses. In order to test the effect of film thickness in the quantification of anions using the time-dependent exchange method, the detection of 50 μM ReO_4^{-} using a ClO_4^{-} film was performed. In one of the experiments, the probe-coating film was made with 60 nmol of ClO_4^{-} (amount typically used by the author for this method) while in the other experiment the amount of compound used was 10 times smaller. Although calibration curves were not built for this system, a direct comparison of the exchange profiles for the 907 cm^{-1} band of perrhenate is shown in Figure 3.5. This figure shows that although the number of exchange sites in the films is different, hence the difference in the final absorbance once the system has stopped changing, the slope for the initial portion of the curve is comparable, which is expected considering the analyte concentration was the same in both cases. The figure also shows that the amount of sites available for exchange is not directly proportional to the film thickness: the absorbance reached by the "thicker

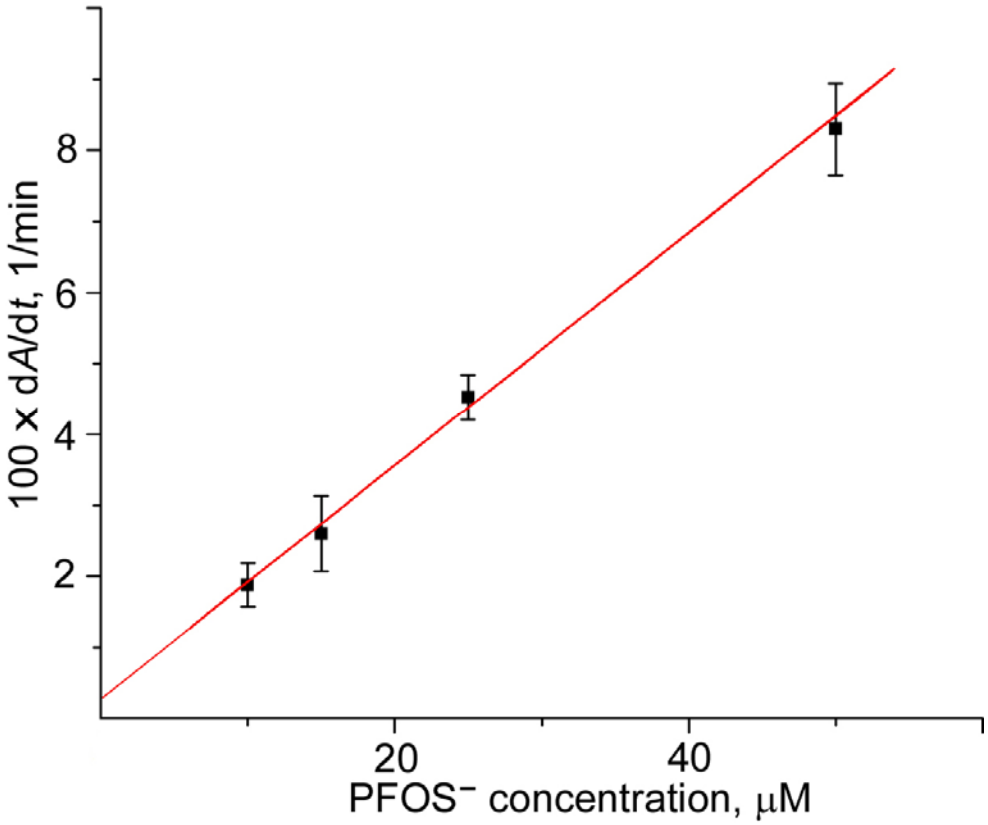

Figure 3.4. Calibration curve for perfluoro-*n*-octanesulfonate ($PFOS^-$) in small-volume samples, using a $DEC^+ClO_4^-$ thin film. The dA/dt values are plotted against $PFOS^-$ concentration. The errors shown for the d*A*/d*t* values are ±1σ.

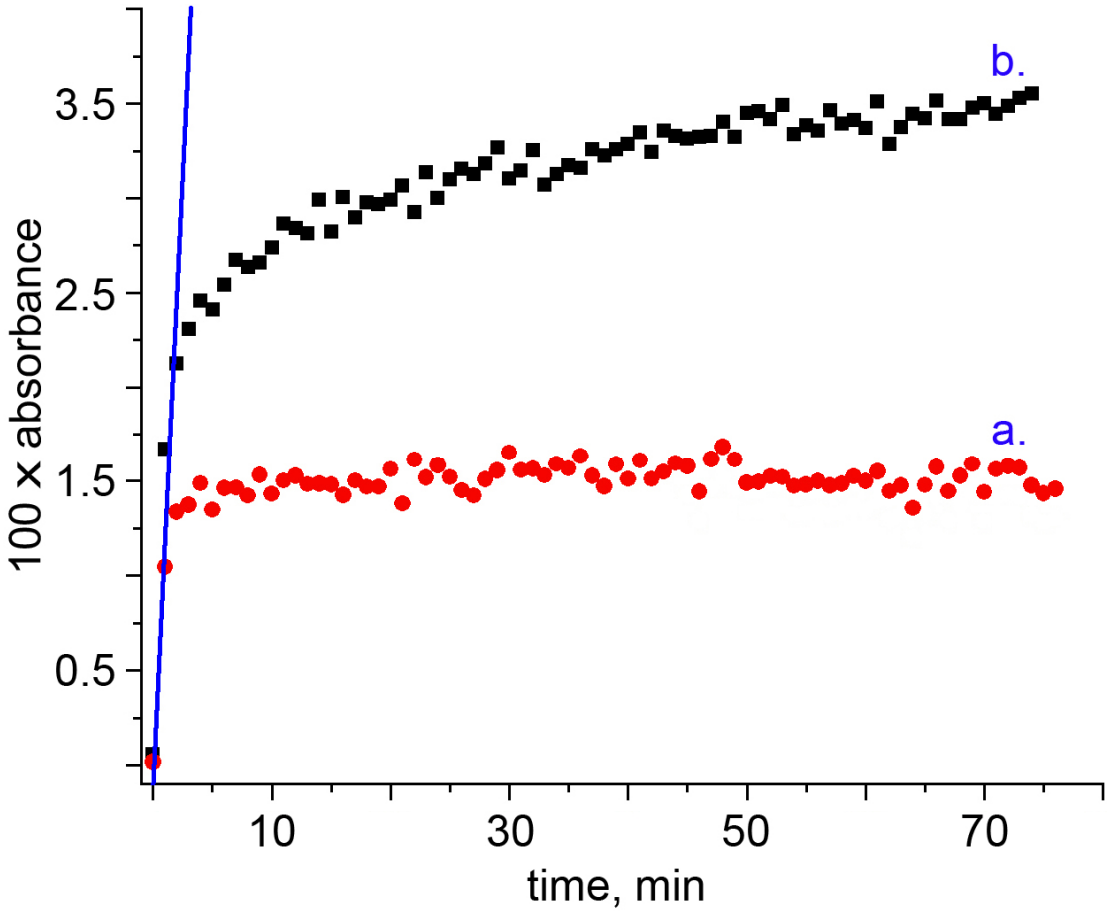

Figure 3.5. Profiles (absorbance vs. time) for the main perrhenate (ReO_4^-) ν(ReO) band, at 905 cm^{-1}, being exchanged from a solution into two films originally of $DEC^+CO_4^-$, with two different thicknesses A linear fit is shown for the data collected during the initial 4 minutes of the exchange. **a.** Profile for a thin film made with 6 nmol of $DEC^+CO_4^-$. **b.** Profile for a thicker thin film made with 60 nmol of $DEC^+CO_4^-$.

film system" (60 nmol of compound, ca. 778 layers, considering a layer spacing of ca. 0.9 nm from X-ray crystallography) once stability has been reached (curve "b") is not 10 times bigger than the one reached by the "thinner film system" (6 nmol of compound, ca. 78 layers, curve "a").

These data show that ReO_4^- can be detected by a film ten times thinner than the thickness of choice, and probably be quantified with the same system.

II.1.3. Multiple-Anion Detection using Different Film Thicknesses. In order to further study the effect of $\Delta\Delta G°_{hyd}$ on selectivity, $DEC^+NO_3^-$ films were used in competition experiments, consisting in placing two anions at a time in solution and monitoring the exchange into the $DEC^+NO_3^-$ film. For a wet films of $DEC^+NO_3^-$, $DEC^+ClO_4^-$, and $DEC^+ReO_4^-$ the monitored signals were ν(NO) = 1,332 cm^{-1}, ν(ClO) = 1,100 cm^{-1}, and ν(ReO) = 903 cm^{-1}, respectively. According to Table 3.1, the calculated $\Delta G°_{hyd}$ for the anions used in this section, in kJ mol^{-1}, should be (in absolute value):

$$NO_3^- (-314) > ClO_4^- (-259) > ReO_4^- (-240)$$

These $\Delta G°_{hyd}$ values were obtained using equation 3.4[11]

$$\Delta G^\circ_{hyd} = \frac{Bz^2}{r + 0.017}\left(1 - \frac{1}{\varepsilon}\right) + 7.9 \qquad 3.4$$

where B is the proportionality constant −69.47 kJ nm mol^{-1}, z is the ionic charge, *r* is the thermochemical radius (Table 3.1) and ε is the dielectric constant, which for water equals 78.

These thermodynamic data explain the observed experimental results: when treating a 60 nmol thin film of $DEC^+NO_3^-$ in aqueous solutions containing, for example, ≥ 10 μM ClO_4^-, ReO_4^-, or *n*-$C_8F_{17}SO_3^-$ ($PFOS^-$), complete replacement of NO_3^- in the

film with the concomitant production of a wet 60 nmol thin film of $DEC^+ClO_4^-$, $DEC^+ReO_4^-$, or DEC^+PFOS^- takes place.

In answering the question of whether an aqueous solution of one of these anions, when put in contact with a film, will undergo ion exchange and result in complete replacement, the $\Delta G°_{hyd}$ values for ClO_4^- and ReO_4^- should be considered. It is not surprising that these anions have similar hydration energies and ReO_4^- has a somewhat smaller hydration energy than ClO_4^-, since ReO_4^- is larger (the Re–O bonds in ReO_4^- are 1.74 Å and the Cl–O bonds in ClO_4^- are 1.44 Å, see Table 3.1). As far as ion pairing between these two anions and DEC^+ cations in the solid state is concerned, ClO_4^- should have a somewhat larger ion-pairing energy because the cation–anion center-to-center distances in $DEC^+ClO_4^-$ are shorter than those in $DEC^+ReO_4^-$ (two of these distances are 5.560(2) and one is 8.288(2) Å vs. two of them being 5.648(2) and one being 8.512(2) Å, respectively). Therefore, these two anions should be quite similar in their ability to be transferred from water to a thin film containing DEC^+ cations.

II.1.3.a. Competition Experiments. In one of the competition experiments performed, a thin $DEC^+NO_3^-$ film was deposited on the diamond probe and treated with a solution containing 50 μM of both aqueous $K^+ClO_4^-$ and aqueous $K^+ReO_4^-$. ATR-FTIR spectra were recorded every 1 minute until there was no further change in several consecutive spectra (total analysis time = 3 h). Since the spectra were recorded after scanning the wet thin film of $DEC^+NO_3^-$ as the spectral background, the recorded spectra (1400–800 cm^{-1} range) show the appearance of a negative 1,332 cm^{-1} ν(NO) band and two positive bands, a 1,100 cm^{-1} ν(ClO) band and a 903 cm^{-1} ν(ReO) band, over time (along with other, less intense ν(ClO) or ν(ReO) bands). The final spectra (i.e., complete ion exchange; no further spectral change) are shown in Figure 3.6. Before the ν(ClO) and ν(ReO) bands could be compared directly, a parameter that we have termed "relative

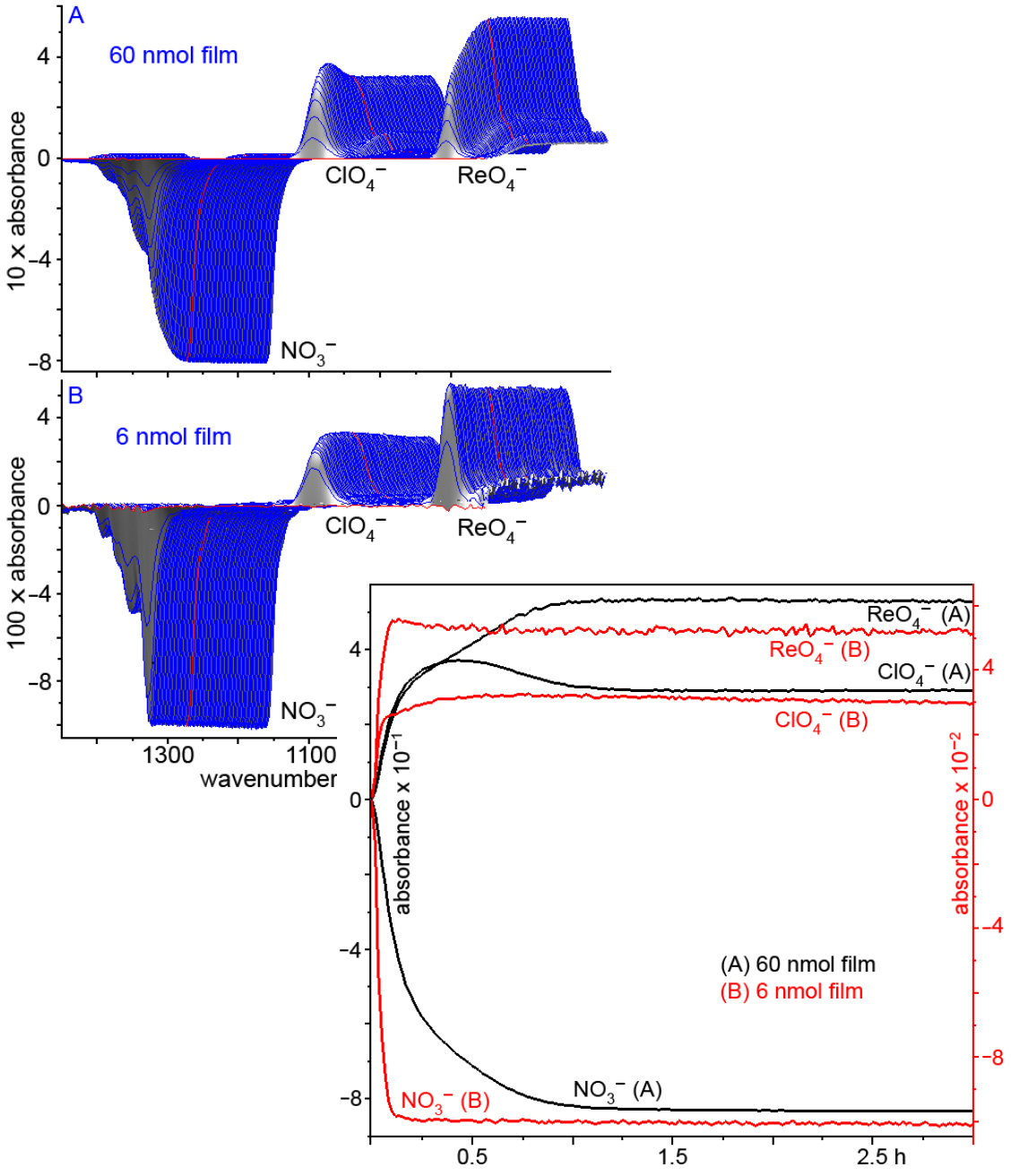

Figure 3.6. Set of IR spectra and profiles for two competition experiments. **Top Left.** Set of infrared spectra of two competition experiments between perrhenate and perchlorate anions to exchange into a $DEC^{+}NO_3^{-}$ film with two different film thicknesses. **Bottom Right.** Profiles in the two competition experiments shown on the top left for 1332 cm^{-1} ν(NO) band , 903 cm^{-1} ν(ReO) and 1100 cm^{-1} ν(ClO). **A.** 60 nmol film. **B.** 6 nmol film.

extinction coefficient of anion X" or "ε(X^-)" needed to be determined. This determination was performed as follows: individual experiments were carried out, in which both aqueous ClO_4^- and aqueous ReO_4^- were extracted from solution by a $DEC^+NO_3^-$ film deposited on the Di probe. The maximum absorbances for both ν(ClO) and ν(ReO) were determined and the ratio of each of these absorbances vs. the maximum ν(NO) absorbance was calculated. This ratio is denoted ε(X^-), where X^- was either ClO_4^- or ReO_4^-. The results of these calculations show that ε(ClO_4^-) = 1.195, while ε(ReO_4^-) = 1.527. The relative concentration of X^- at any given time during the exchange can then be determined by measuring the maximum absorbance and dividing by the ε(X^-) value at that time. A plot of time vs. relative concentration of both ClO_4^- and ReO_4^- for this competition experiment was created and is shown in Figure 3.7.

One question that persisted before this work, regarding the ion-exchange behavior of thin DEC^+X^- films, was whether or not they reach thermodynamic equilibrium with the solutions in which they are immersed at approximately the same rate as the ion-exchange process itself. That question has now been answered.

The competition experiments were tried with thinner films, namely with films containing 6 and 2 nmol of anion. This would be equivalent to a nominal film thickness of ≈ 0.07 and ≈ 0.02 μm, respectively, for films made with any of the salts, assuming a uniform cylinder and considering the diameter of the probing crystal (0.9 cm) and the densities obtained from X-ray crystallography (ca. 1.1, 1.2 and 1.3 g cm^{-3} for $DEC^+NO_3^-$, $DEC^+ClO_4^-$ and $DEC^+ReO_4^-$, respectively). It was observed that their exchange behaviors were comparable to that of the thick films (nominal thickness ≈ 0.7 μm for all of the DEC^+ salts), as shown in Figure 3.6. As was expected for the thin films, they achieve an equilibrium state faster than thick films, because there are fewer sites that can undergo ion exchange. This feature could in turn make them extremely useful for applications in quantitative extractions of analytes from water, as in this kind of experiment d*A*/d*t* values are calculated using the first 10-15 min of an experiment.

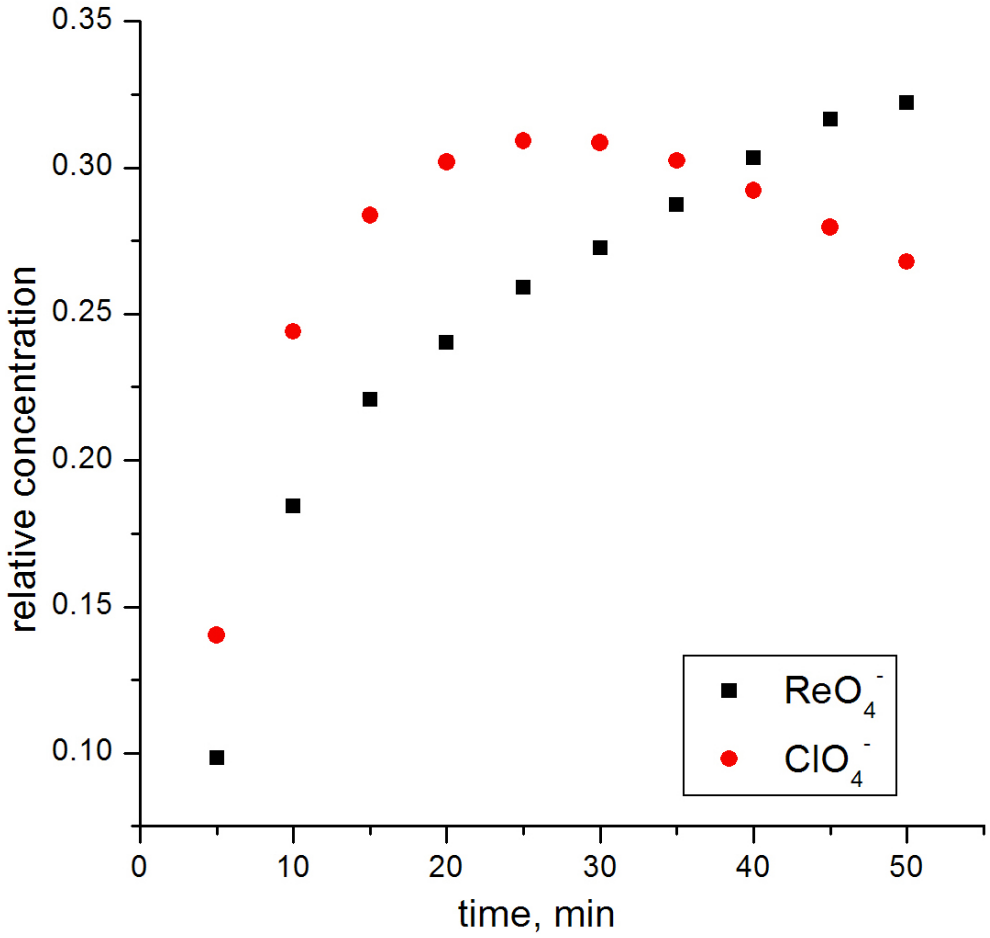

Figure 3.7. Profiles (absorbance vs. time) for the main ν(ReO) band for perrhenate (905 cm^{-1}, squares) and ν(ClO) band for perchlorate (at 1094 cm^{-1}, circles), for a competition experiment of these anions exchanging into an originally $DEC^{+}NO_3^{-}$ thin film.

Even though the signal-to-noise ratio (SNR) for the spectra was not calculated, it can be appreciated that with the 2 nmol films, the IR signal from the analytes is > 3, (Figure 3.6). This means that even approximately 22 layers of ferrocenium salt on the ATR crystal are enough to accurately detect anions in water by ATR-FTIR, and reproduce the thick films results (ca. 778 layers, considering a layer spacing of ca. 0.9 nm from X-ray crystallography). The above calculations were made assuming that in the film, the ferrocenium salts layers stagger on the probe with the alkyl chain "parallel" to the surface.[86] This assumption, and the values for interlayer separation obtained from crystallography, gave rise to the number of layers reported here.

II.1.4. Free Dodecylsulfate Quantification? The author found that although the stability of $DEC^{+}NO_3^{-}$ films in contact with low-concentration aqueous SDS solutions (and no other dissolved substances) is sufficient to use this extractant to detect DDS^{-} (in concentrations as low as 0.75 μM),[87] it could not be used to quantify the anion in a complex biological matrix (soaking solution; SS) used to soak SDS-treated tissues. A $DEC^{+}NO_3^{-}$ film decomposed even faster when exposed to this media compared to when it was exposed to dd-H_2O, as illustrated in Figure 3.8. The SS, which contains the ingredients listed in Table 3.2, presented a challenge that required two new analytical strategies. One of them required the synthesis of a new extractant that was more stable in SS. The synthesis and characterization of this new extractant are described below in this chapter, in section II.3, and the "new-strategy" quantification experiments are described in detail in Chapter 4, section II.1.2.a.

II.2. ATR-FTIR Quantification of Free Cyanide using a Ni Complex. Craig Johnson is a research geologist at the US Geological Survey (USGS). The Strauss Research Group embarked on a collaboration with his group to use our ferrocenium-salt-coated-probe ATR-FTIR technique to measure free CN^{-} content in water samples. The Johnson research Group was investigating the use of ultra violet (UV) light to liberate

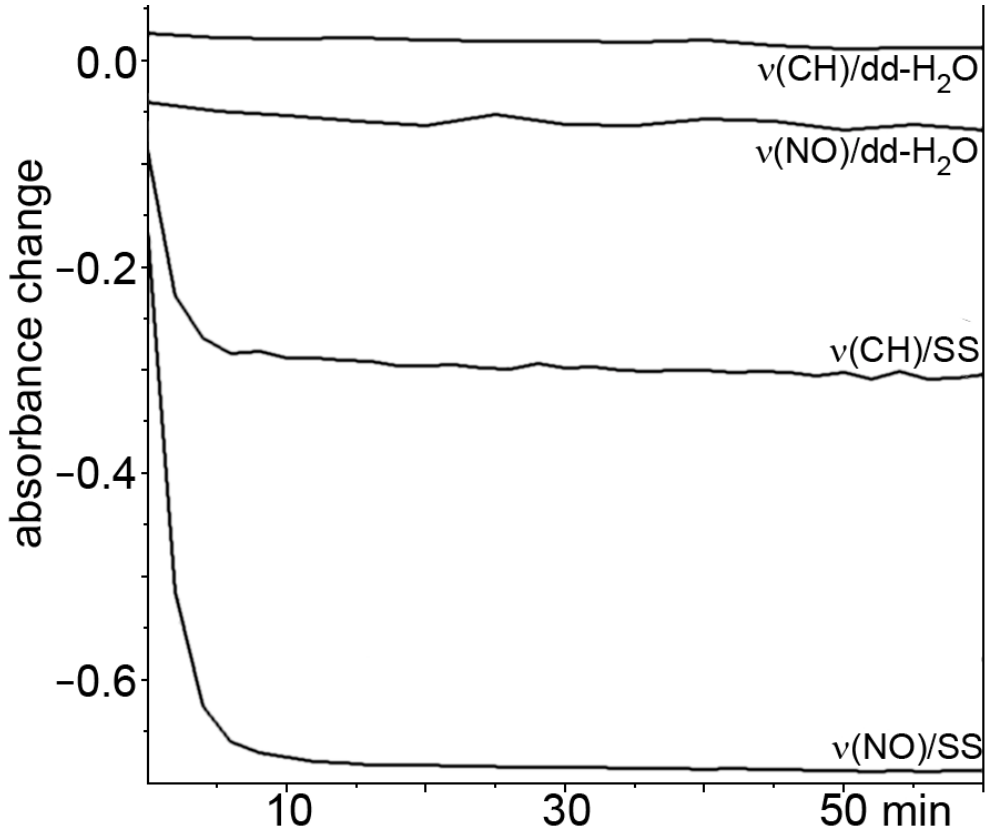

Figure 3.8. Profiles (absorbance vs. time) for the main nitrate ν(NO) band, as two $DEC^{+}NO_3^{-}$ thin films are exposed to dd-water or soaking solution (SS).

CN^- from a strong metal-cyanide complex, using a picric acid colorimetric weak acid dissociable (WAD) method to detect free cyanide.[88] As already mentioned, $DEC^+NO_3^-$ cannot be used as the extractant, since CN^- is more strongly hydrated than NO_3^-.[89] Therefore, 1,3-bis(diphenylphosphino)propanedichloronickel(II) ($NiCl_2$(dppp)) was used, which not only eliminated the effects of $\Delta\Delta G°_{tr}$, but also solved the problem of potential nucleophilic decomposition of the ferrocenium salt by CN^-. The determinations were performed at a pH > 9.2, and the Si ATR crystal was used, since the Di ATR crystal absorbs strongly in the region where the ν(CN) band is observed (ca. 2100 cm^{-1}).

A calibration curve was built for the detection of free CN^- in water using $NiCl_2$(dppp) films (linear portion 0.1-5.0 μM, shown in Figure 3.9). This curve was used to quantify the concentration of free CN^- in real samples (as described in section III.3.2.b). These samples had been amended with potassium hexacyanocobaltate(III), $K_3[Co(CN)_6]$, and exposed to UV light for various periods of time (0, 1, 8, 24, 48 and 96 hours), which produced photodissociation of the cobalt complex in varying degrees, and consequently generated varying amounts of free CN^-. The samples were protected from light until analyzed. The final concentrations of free CN^- in each sample were calculated. A plot of UV exposure vs. free CN^- concentration was built, and compared with the one obtained by Craig Johnson et al. using their WAD method to detect free cyanide. This comparison is shown in Figure 3.10. The results are comparable within experimental error (error bars = one estimated standard deviation). They show that coated-probe ATR-FTIR can be used to detect free CN^- in water samples. The technique is, as a whole, simple and fast, not requiring sample pretreatment except for a dilution step, necessary to reduce the free CN^- concentration to the calibration-curve range.

II.3. ATR-FTIR Quantification of Free Dodecylsulfate using Me-Aza-DEC^+I^-.

II.3.1. Preliminary Experiments.

II.3.1.a. Me-Aza-DEC^+I^- synthesis. The synthesis of this salt consisted of five steps (see Figure 3.11), using ferrocene as the starting material.

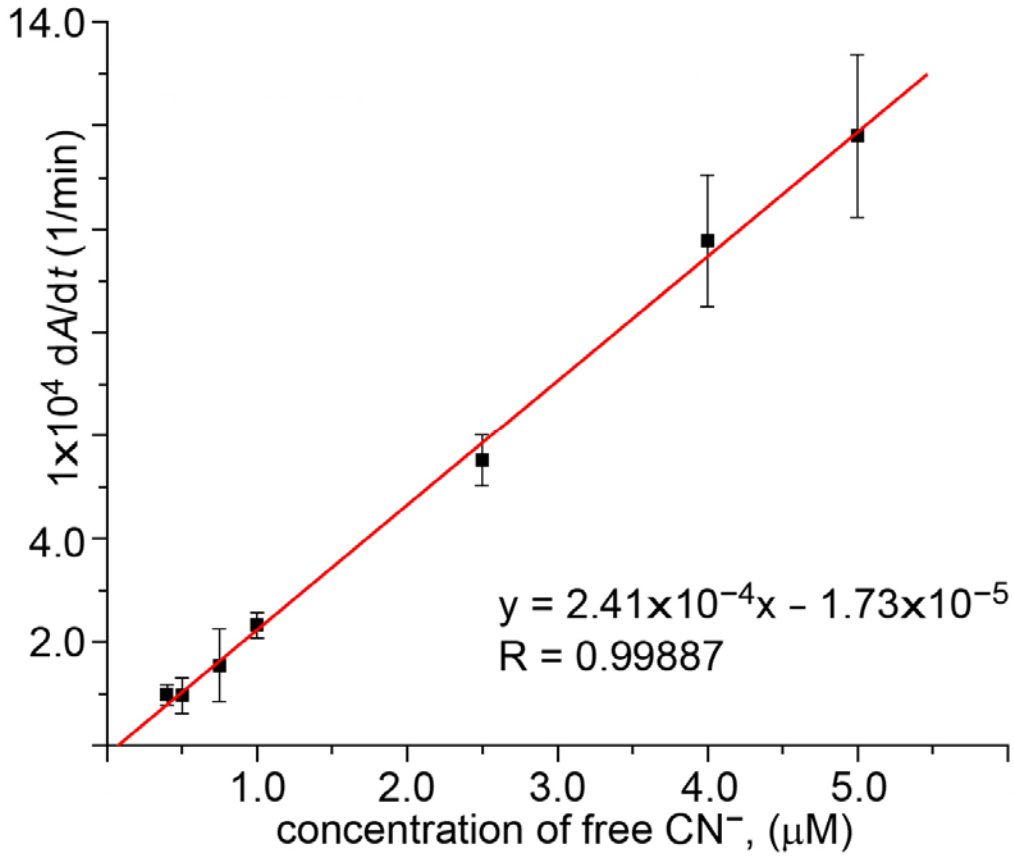

Figure 3.9. Calibration curve for Cyanide (CN^-) in a pH-10 water samples, using a $NiCl_2$(dppp) thin film. The d*A*/d*t* values are plotted against CN^- concentration. The errors shown for the d*A*/d*t* values are ±1σ.

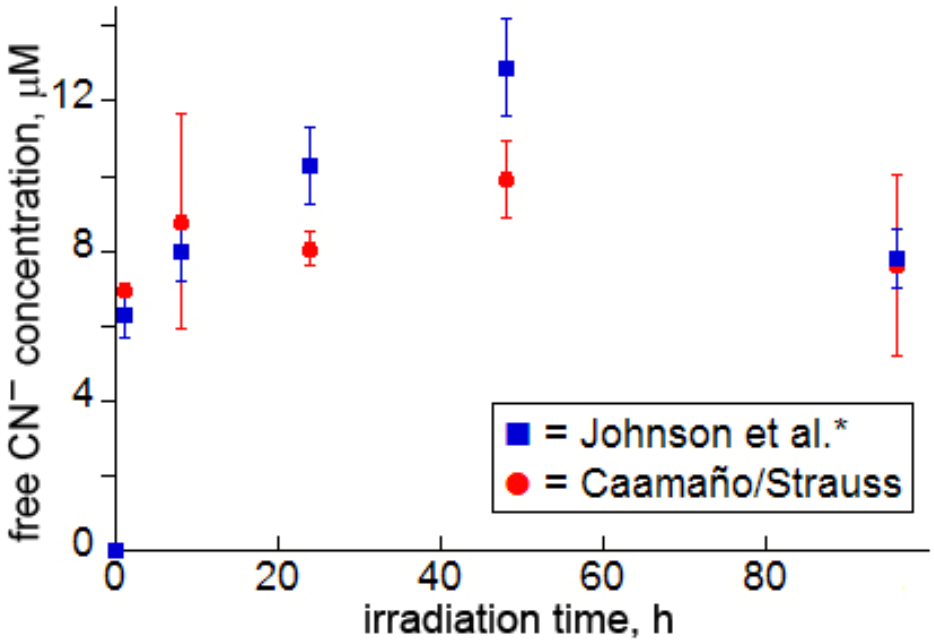

Figure 3.10. Concentration of free cyanide (CN^-) vs. irradiation time when comparing quantification CN^- methods in real samples. ■. Data obtained by Johnson et. al. using the picric acid WAD colorimetric method ●. Data from this work, obtained using ATR-FTIR spectroscopy through the time-dependent method and with a $NiCl_2$(dppp) thin film. The errors shown for the concentration values are ±1σ

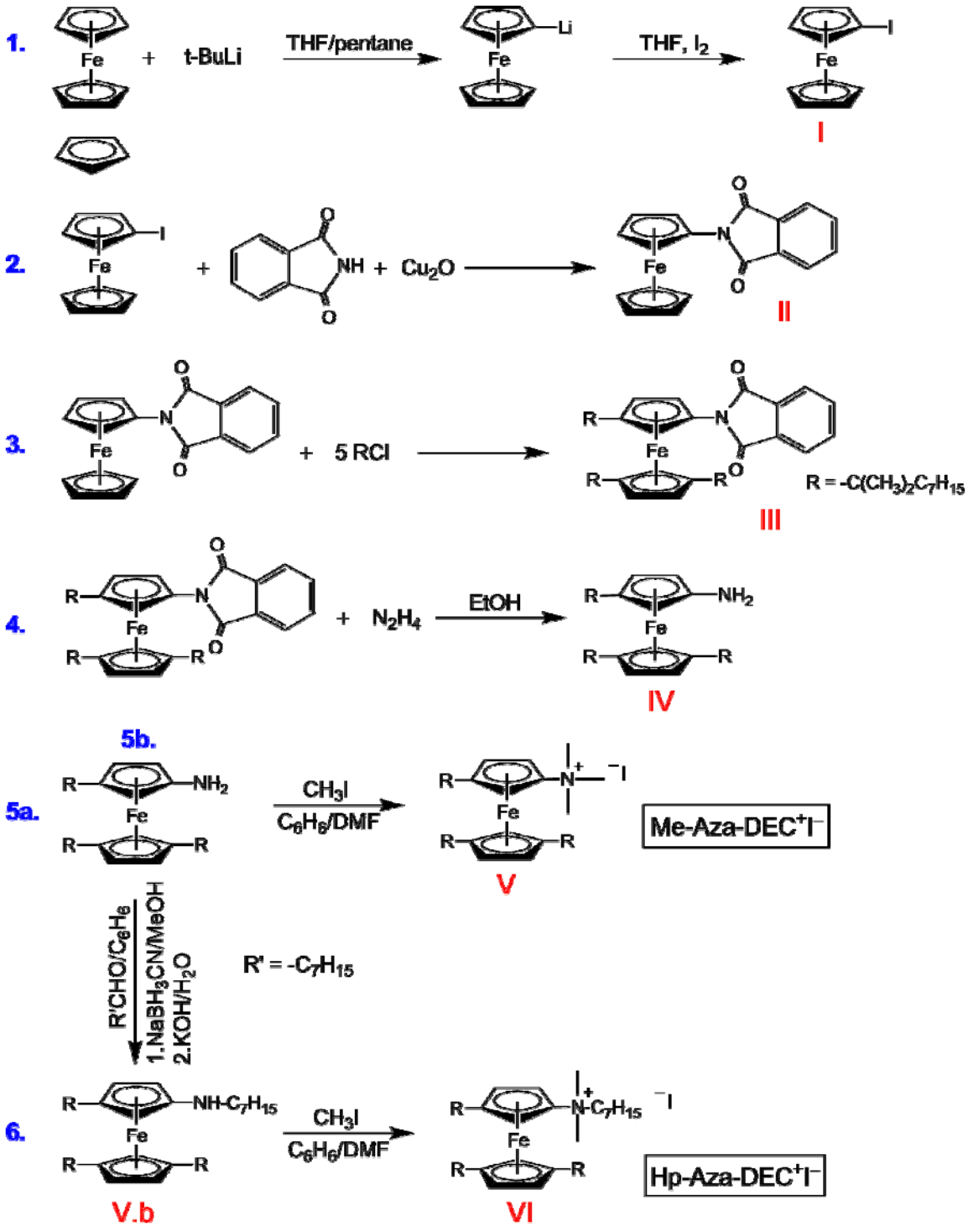

Figure 3.11. Synthesis of Me-Aza-DEC^{+}I^{-} and Hp-Aza-DEC^{+}I^{-}

Step 1: Halogenation of Ferrocene. This step of the synthesis consisted of initially synthesizing lithiumferrocene by slowly mixing $FeCp_2$ in THF with t-BuLi in an ice bath, while stirring. Secondly, addition of pentane and iodine in THF gave the target compound: iodoferrocene. Purification was performed by addition of ether and several washes of the organic phase with sodium thiosulfate solution and dd-H_2O. The organic phase was dried over $MgSO_4$ and analyzed by ^{1}H-NMR. The spectrum showed a mixture of the mono-substituted product (I; 60%), the di-substituted product (II; 25%).and ferrocene (unreacted starting material; 16%).

Step 2: Protection of Carbon 1. The halogenated ferrocene from the previous step was set to reflux under N_2 together with H(phthilamide), copper (I) oxide and pyridine for approximately 1.5 days. Once the sample was cool, the solvent was evaporated in a vacuum line and ethyl acetate was added to the mixture while stirring. A chromatographic separation was performed, producing two fractions, the second of which was analyzed by ^{1}H-NMR. The spectrum revealed the presence of the target compound: the phthalimide-protected compound (II); the sample also contained H(phthalimide) and ferrocene.

Step 3: Alkylation of Carbons 3, 1' and 3'. A portion of the second fraction obtained in the previous step, containing the pthalimide-protected compound, was mixed with $ZnCl_2$ and CH_2Cl_2 in a inert atmosphere. Mantaining these conditions, a Friedel-Craft alkylation was performed using $C_{10}H_{21}Cl$ under reflux. After 2.5 hours a portion of the reaction mixture was filtered, stirred over Fe powder for 20 min and dryed in the Schlenk line. The color of the mixture is still green. A portion of the mixture was analyzed by ^{1}H-NMR; a broad peak in the p-region did not show any features. After 27 hours of reaction, a sample was washed with a 10% H_2O/KOH solution (after which it turned caramel color), dried over Mg_2SO_4, treated with Fe powder and dried in the line. An ^{1}H-NMR spectrum showed the target trialkylated compound (III) and no presence of the starting material. Another portion of the crude was analyzed by (+)ESI-MS, which

confirmed the presence of III and the absence of starting material. Purification of the sample was performed by column chromatography and five fractions were collected. A hexanes:CH_2Cl_2 mixture eluted the target compound, which was evaporated down: a brown oil resulted. All recrystallization attempts from different solvents (MeOH, EtOH, EtOH + 2% H_2O) were unsuccessful and the compound precipitates as oil. The yield of this reaction step was calculated to be 54%.

Step 4: Replacement of the Pthalimide with an Amine. The trialkylated compound (III) obtained in the previous step was mixed with hydrazine hydrate and EtOH and set to reflux for 40 min. Hexanes were used to extract the product into the organic phase, which was then washed several times and dried under vacuum, yielding 280 mg of product. A ^{1}H-NMR spectrum shows the target compound (IV) in the product mixture is highly pure.

Step 5: Trimethylation of the Amine Group. Most of the product obtained in the previous synthesis (IV) was dissolved in a 1:1:1 iodomethane:benzene:DMF mixture and refluxed under N_2 for 7 hours. Any remainder CH_3I left was eliminated by briefly drying under vacuum. The sample was redisolved in hexanes and washed several times, evaporated under vacuum and finally purified using column chromatography. Two fractions were collected, being MeOH the solvent that eluted Me-aza-DEC$^+$I$^-$. This fraction was evaporated down and dried with benzene twice. The mass of the product was 108.7 g. In order to calculate the purity of the product, a series of precise dilutions of the starting material (IV) and the target compound (V; Me-aza-DEC$^+$I$^-$) were carefully prepared and analyzed by (+)ESI-MS. According to these experiments (see description under D.5 in the experimental section), the purity of Me-aza-DEC$^+$I$^-$ was 88%. A second purification produced 96.6 mg of product, resulting in an 88.9% recovery after the second purification. The (+)ESI-MS experiment was repeated, revealing the purity of Hp-aza-DEC$^+$I$^-$ (V) of 91.7%.

II.3.1.b. Hp-Aza-DEC$^+$I$^-$ Synthesis: Reductive Alkylation followed by Methylation of the Amine Group. The first four steps in the synthesis of this salt were the same as explained before for the Me-aza-DEC$^+$I$^-$ salt. In the last step, however, the reductive alkylation of the amine was performed as an intermediate step to obtain the final product: Hp-aza-DEC$^+$I$^-$.

Although the purity of both Hp-aza-DEC$^+$I$^-$ and Me-aza-DEC$^+$I$^-$ after the final step were high, both final products contained some of the unreacted amine ferrocenyl (IV; see Figure 3.11.4) which was probably responsible for the lack of success in obtaining crystals of either of the two salts. (Attempts to crystallize the compounds from toluene, dichloromethane and acetonitrile were unsuccessful). Furthermore, the amine ferrocenyl proved to be air sensitive. The presence of small amounts of this compound in the final products of the synthesis caused them to decompose in air, which eventually rendered solutions made for ATR-FTIR experiments unusable for thin-film depositions: although stock solutions of the products were kept under N_2 when not in use, decomposition was inevitable and eventually new stock solutions had to be prepared. Separations were attempted with no success.

Despite some of the difficulties experienced during the synthesis, Me-aza-DEC$^+$I$^-$ proved to be the most stable in SS for the duration of each experiment (1 hour), as shown next in the suitability experiments and Table 3.3. The synthetic steps were carried out twice, and Me-aza-DEC$^+$I$^-$ obtained from both syntheses displayed the same properties and exchanging abilities in ATR-FTIR experiments: calibration curve datapoint values were comparable with both compounds.

II.3.1.c. Suitability experiments: choosing an extractant to quantify DDS$^-$. Two aspects of Hp-aza-DEC$^+$I$^-$ and Me-aza-DEC$^+$I$^-$ were studied: i) stability in water and ii) ability to detect and quantify DDS$^-$.

Stabilities in dd-water or SS were tested by comparing the dry film bands

Table 3.3. Suitability Experiments Results

System	Feature	Hp-Aza-DEC$^+$I$^-$	Me-Aza-DEC$^+$I$^-$
Thin film	IR-active impurities	yes	no
H_2O equil	ν(CH) stop changing (min)	15	2
	stable*	no	yes
SS equil	ν(CH) stop changing (min)	60	2
	stable*	no	yes
Exchange in H_2O	capable to detect DDS^-	yes	yes
Exchange in SS	capable to detect DDS^-	yes	yes
	capable to quantify DDS^- **	na	yes

*Determined by whether a spectrum of the dry film after 8h-equilibration with water showed the same band intensities as the initial film. **Determined by whether the construction of a successful, reproducible calibration curve was possible.

before and after a water equilibration experiment. The films ability to detect and quantify DDS^- was determined by monitoring the ν(SO) bands (at 1224 and 1254 cm^{-1}) in an exchange experiment and by attempting to use one of these bands to build a calibration curve. A summary of these experiments is shown in Table 3.3. The first disadvantage encountered in the use of Hp-aza-DEC^+I^- was the presence of IR-active impurities. Intense bands are observed in the 1070-1270 cm^{-1} region, where the ν(NC) band is present. These bands would complicate the detection of DDS^-; specifically, a major band observed at 1272 cm^{-1} is the main isochronous interference. The Me-aza-DEC^+I^- film does not show any impurities in this region. Furthermore, films of Hp-aza-DEC^+I^- proves to be unstable in water, as both the interfering bands and the ν(CH) bands at ca. 2900 cm^{-1} decrease during equilibration (both in dd-water and SS), suggesting that the films decompose. The ν(CH) bands in the Me-aza-DEC^+I^- film barely change during the first 2 minutes of equilibration, which is expected as the film layers "adjust" to the presence of water (this is the reason to perform the equilibration in the first place).

Although both films were able to detect DDS^-, both in dd-water and SS, only the Me-aza-DEC^+I^- salt was used to successfully build a calibration curve to be used in the quantification of the detergent's anion in SS. Although the construction of a calibration curve was not attempted with the Hp-aza-DEC^+I^- salt, the presence of an IR-active impurity with a band that decreases in the presence of both dd-water and SS, at the same wavenumber as where the ν(SO) bands from DDS^- are present, suggests that the construction of a calibration graph with this salt would not render a useful linear portion.

The Me-aza-DEC^+I^- salt was then the compound of choice to quantify DDS^- in SS, as described next.

II.3.2. Free Dodecylsulfate Quantification. Section II.3.1 described the synthesis of two salts, similar to DEC^+ salts, and the experiments performed to determine which one of them presented more suitable properties to detect and quantify DDS^- in dd-water. Both these salts contain the $(Fc'NR_3)^+$ cation, which maintains the Fe atom in its

reduced form and places the positive charge on a N atom, in a different part of the molecule instead, which, given the enhanced stability of Fe(II) vs. Fe(III), was expected to improve the overall stability of the salts. The best salt according to the suitability experiments (Section II.3.1.c), Me-aza-DEC^{+}I^{-}, was used to quantify DDS^{-} in SS.

The calibration curve obtained for the quantification of DDS^{-} with a Me-aza-DEC^{+}I^{-} film in contact with a SS sample is shown in Figure 3.12. For concentrations below 10 μM, the d*A*/d*t* values were calculated using data from the first 15 minutes of the exchange (most linear portion for these data). For concentrations above 10 μM the d*A*/d*t* values were calculated using the data for which A(1224 cm^{-1}) vs. time appeared to be linear, which was generally less than the first 15 minutes of the ion exchange. The A(1224 cm^{-1}) vs. time data for the first 10-15 minutes of ion exchange were used to calculate d*A*/d*t*. The need to use two different methods arouse because for DDS^{-} concentrations above 10 μM the exchange occurs so fast that the data depart from linearity before the first 15 minutes of ion exchange have elapsed. When real samples were analyzed (see Chapter 4), dilutions were performed so that the concentration being determined would always be included within the initial, more precise portion of the calibration curve (below 5 μM).

III. Experimental Section

III.1. Reagents, Solvents, and Solutions. All reagents and solvents were ACS grade or better unless stated otherwise. All solutions used were prepared in Class A volumetric glassware. The distilled deionized water (dd-H_2O) used for solution preparation had an initial resistivity of 18 MΩ cm. Syntheses which involved air-sensitive compounds were carried out under a purified dinitrogen atmosphere using standard Schlenk techniques.[90] In all cases, stirring and heating were done using a magnetic stirrer and a hot plate.

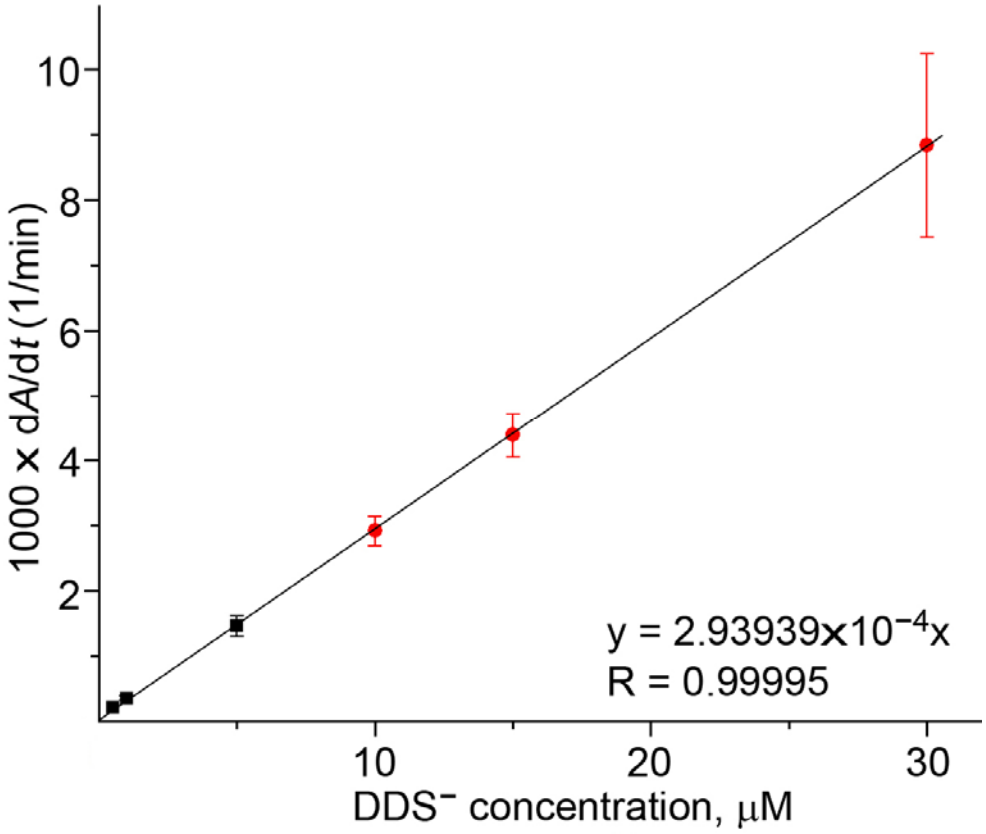

Figure 3.12. Calibration curve for Dodecylsulfate (DDS^-) in soaking solution samples, using a Me-Aza-DEC^+I^- thin film. The dA/dt values are plotted against DDS^- concentration. The errors shown for the d*A*/d*t* values are ±1σ.

III.1.1. ATR-FTIR Determinations. The ferrocenium salts 1,1',3,3'-tetrakis-(2-methyl-2-nonyl)ferrocenium nitrate/perchlorate/perrhenate ($DEC^+NO_3^-$, $DEC^+ClO_4^-$ and $DEC^+ReO_4^-$) were synthesized according to literature methods[5,6] by other members of the Strauss Group. Potassium cyanide (Fisher Scientific), sodium hydroxide (Fisher Scientific) and 1,3-bis(diphenylphosphino)propane-dichloronickel(II) ($NiCl_2$(dppp), Aldrich) were used as received. The salts Hp-aza-DEC^+I^- and Me-aza-DEC^+I^- were synthesized as described next by the author in collaboration with Igor V. Kuvychko.

III.1.2. Synthesis of Hp-Aza-DEC^+I^- and Me-Aza-DEC^+I^-. The following reagents/solvents were used as received (common name/abbreviation; formula; and vendor are indicated in parenthesis): bis(η^5-cyclopentadienyl)iron (ferrocene/$FeCp_2$; Lancaster synthesis or Alfa Aesar), 2-lithio-2-methylpropane (t-BuLi; solution in pentane, Alfa Aesar), pentane (Fisher Scientific), iodine (J. T. Baker Chemical CO), diethyl ether (Fisher Scientific), sodium thiosulfate (Fisher Scientific), magnesium sulfate anhydrous (Fisher Scientific), isoindole-1,3-dione (H(phthalimide); $C_8H_5O_2N$; Aldrich), copper(I) oxide (Acros), pyridine (Aldrich), ethyl acetate (Fisher Scientific), silica gel (70-230 mesh, 60Å, Sigma-Aldrich), acetonitrile (Mallinckrodt), thionyl chloride ($SOCl_2$; Aldrich), dichloromethane (Fisher Scientific), 1-chlorodecane (Aldrich), iron powder (Aldrich), hexanes (mixture of isomers, Fisher Scientific), methanol (MeOH; Fisher Scientific), ethanol (EtOH; 200 proof absolute, AAPER or PHARMCO), hydrazine hydrate (N_2H_4; Aldrich), iodomethane (stabilized with copper, Aldrich), benzene (Sigma-Aldrich), N,N-dimethylformamide (DMF; B&J brand), petroleum ether (Fisher Scientific), heptan-1-ol (n-heptanol; Fisher Scientific), Sodium cyanoborohydride ($NaBH_3CN$; Aldrich) and ammonium hydroxide (Mallinckrodt). Zinc chloride ($ZnCl_2$, Fisher Scientific), was dried with $SOCl_2$. Tetrahydrofuran (THF; C_4H_8O; Fisher), was distilled from Na and benzophenone.

III.2. Instrumentation. The IR spectra were recorded using an ATR-FTIR spectrometer (ReactIR-1000, Applied Systems Inc., Millersville, MD) equipped with a silicon (SiComp) or diamond (DiComp) ATR probe (Applied Systems Inc, Millersville, MD) and a Mercury Cadmium Telluride detector. The spectral window was 4000-650 cm^{-1} with a nominal spectral resolution of 8 cm^{-1}. The wetted surface of both the silicon and diamond ATR crystals was a circular area 0.9 cm in diameter. Electrospray ionization (ESI) mass spectra were recorded using a ThermQuest Finnagan LCQ-DUO spectrometer (acetonitrile eluent, 0.3 $mL \cdot min^{-1}$ flow rate). Nuclear magnetic resonance of protons (^{1}H-NMR) spectra were collected using either an Bruker Inova-300 or Inova 400 (25 °C, TMS internal standard).

III.3. ATR-FTIR Quantification: Time-Dependent Exchange Method. All the analytical experiments in this section followed a basic common method, which was adjusted for each specific procedure. A description of this general method is presented next, after which a more detailed explanation of each system is offered.

III.3.1. The General Procedure. A fresh (i.e., less than 24 hours old) solution of the extractant in an organic solvent was used to prepare each one of the thin films, which were made by delivering an aliquot of solution onto one of the probes using a micro-syringe. Once the solvent had evaporated (ca. 30 sec), the dry, thin film was monitored for impurities and reproducibility. The thin-film coated probe was immersed in an aqueous solution for a period of time, to permit the film to equilibrate with the new media. A background of the thin film in water was collected. At this point, the experiments were performed in different ways, depending on whether the measurement was of a standard solution to build a calibration curve, of a real sample, of a small-volume experiment or of a multiple-anion experiment.

III.3.2. Perfluoro-*n*-octanesulfonate Quantification in Small Volumes. The general procedure described previously was used with the following specifications: the

films were made with 60 nmol of $DEC^+ClO_4^-$, using dichloromethane as the solvent; the Si probe was used; an average of 64 scans was used to produce each spectrum.

Although the $PFOS^-$ quantification experiments were performed in small volumes, the large-volume experiments done for detection are also described next:

III.3.2.a. Large-Volume Experiments. The thin-film coated probe was submerged in 100 mL of dd-H_2O with stirring (at ~200 rpm), and equilibration with water was allowed for 10 minutes. After completion of the water equilibration, a background spectrum was recorded. Then, a volume of aqueous solution containing $PFOS^-$ was added (having previously removed the same volume of water to maintain the same final volume), so that the final concentration was the desired one. Data were collected for a 15 minutes. These experiments were used for detection and comparison; no quantification (calibration curve or real samples determinations) were carried on.

III.3.2.b. Small-Volume Experiments. The thin film coated probe was submerged in 100 μL of dd-H_2O for the water equilibration, after which 900 μL of solution containing the $PFOS^-$ were added, so that the final concentration was the desired one. The result was a 1 mL drop on top of the probe, which was covered to avoid evaporation. No stirring was performed. A calibration curve was constructed by graphing the initial (10 minutes) d*A*/d*t* values for one of the $PFOS^-$ ν(CH) bands (1270 cm^{-1}) versus the particular analyte concentration for each standard sample. No real samples were analyzed in these experiments. All determinations were performed in triplicate.

III.3.3. Anion Detection Experiments using Different Film Thicknesses. The general procedure described previously was used with the following specifications: the films were made with 60 or 6 nmol of $DEC^+ClO_4^-$, using dichloromethane as the solvent; the thin-film Di probe was submerged in 100 mL of dd-H_2O, with stirring (at ~60 rpm); an average of 64 scans was used to produce each spectrum. The concentration of analyte was 50 μM. In any other respect, these experiments were performed as previously described for the large-volume experiments (section III.3.2.a.).

III.3.4. Multiple-Anion Detection using Different Film Thicknesses. The general procedure described previously was used with the following specifications: the films were made with 60, 6 or 2 nmol of salt, using dichloromethane as the solvent; the thin-film coated Di probe was submerged in 100 mL of dd-H_2O, with stirring (at ~60 rpm); an average of 64 scans was used to produce each spectrum. Equilibration with water was allowed for a certain amount of time, depending on the anion present in the film (viz., 10 minutes for NO_3^- or ReO_4^-, and 20 minutes for ClO_4^-). After completion of the water equilibration, a background spectrum was recorded. A volume of aqueous solution containing the two analytes of interest was added to the water used for the equilibration (having previously removed the same volume of water to maintain the same final volume), so that the final concentration of analytes was the desired one. Data were collected until the three anions (the extractant's anion and the two competing analytes) bands stopped changing with time. These experiments were used for detection and comparison; no quantification (calibration curve or real samples determinations) were carried on.

III.3.5. Free Cyanide Quantification. The general procedure described previously for the ATR-FTIR time-dependent exchange method was used, with the following specifications: the films were made with 100 nmol of $NiCl_2$(dppp), using dichloromethane as the solvent; the thin-film coated Si probe was submerged in pH 10 dd-H_2O (the pH was adjusted with aqueous NaOH) to equilibrate the film, with stirring (at ~220 rpm); an average of 64 scans was used to produce each spectrum. Equilibration with water was allowed for 10 minutes.

At this point, the samples were treated differently depending on whether they were standards to build a calibration curve or real samples.

III.3.5.a. Calibration-Curve Experiments. The water equilibration was performed in 100 mL of pH 10 water. After collecting the background of the thin film in pH 10 water, a volume of standard aqueous CN^- solution (also pH 10) was added to the

water (having previously removed the same volume of water to maintain the same final volume), as to obtain the final desired concentration of CN^-. Data were collected for 30 minutes and the initial d*A*/d*t* value at 2104 cm^{-1} (ν(CN) band) for the first 15 minutes was determined. A linear calibration curve was constructed by graphing this value for each experiment vs. the concentration of free CN^-. A new thin-film coating of the ion-exchange extractant was used for every analysis, and all analyses were performed in triplicate and averaged to produce one datapoint in the calibration curve.

III.3.5.b. Real-Sample Experiments. The samples analyzed in this section of the present work were tap water samples (from Columbia MO) that had been amended with potassium hexacyanocobaltate(III), $K_3[Co(CN)_6]$. They were sent in plastic, 125 mL dark bottles, to protect them from light. They had not been subjected to any kind of pretreatment, except they had been exposed to UV light for varying times, which drove varying degrees of photodissociation of the cobalt complex. The exposure periods were as follow: 0, 1, 8, 24, 48 and 96 hours. The water equilibration was performed in 30 mL of pH 10 water, and after that 30 mL of the real sample was added (this twofold dilution of the samples was considered when performing final calculations). The pH of the real samples was adjusted to ~10 (by addition of a NaOH aqueous solution) before the analysis.

Once the final concentrations of CN^- were calculated for all the samples, a plot of UV exposure vs. free CN^- concentration was created.

III.3.6. Dodecylsulfate Quantification. Two salts were synthesized, as described ahead in section III.4.2. Both compounds were tested, and the most suitable salt to determine free DDS^- in SS was chosen, as described in section III.4.3 ahead. The general procedure described previously for the ATR-FTIR time-dependent exchange method was used, with the following specifications: the films were made with an aliquot of Me-aza-DEC^+I^- in dichloromethane solution, using volumes that would produce a film in which the absorbance of the main ν(CH) band would be between 0.8 and 0.9 (*ca.*, 150 nmol);

the thin-film coated Di probe was submerged in 100 mL of aqueous, homogenous SS to equilibrate the film, with stirring (at ~60 rpm); an average of 128 scans was used to produce each spectrum. Equilibration with SS was allowed for 15 minutes.

At this point, the samples were treated differently depending on whether they were standards to build a calibration curve or real samples.

III.3.6.a. Calibration-Curve Experiments. In these experiments, a volume of a standard SS containing SDS was added to the SS used for the equilibration (having previously removed the same volume of SS to maintain the same final volume), so that the final concentration was the desired one. Spectra were collected for 1 hour. For each spectrum, the initial d*A*/d*t* value at 1221 cm^{-1} (one of the ν(SO) bands of DDS^-) was determined as explained next, and a calibration curve was constructed by graphing this value for each spectrum vs. the concentration of SDS. For the determination of d*A*/d*t* in the DEC^+X^- experiments, the first 10-15 minutes of an exchange reaction were used to calculate d*A*/d*t*. In contrast, for the determination of d*A*/d*t* in the Me-aza-DEC^+I^- experiments, the data were chosen using two different criteria: for concentrations below 10 μM the d*A*/d*t* values were calculated using data from the first 15 minutes of the exchange (most linear portion for these data); while for concentrations above 10 μM the d*A*/d*t* values were calculated using the data that better adjusted to a straight line, which was (in most cases) less than 15 min. A new thin-film coating of the ion-exchange extractant was used for each analysis, and all analyses were performed in triplicate and averaged to produce one datapoint in the calibration curve.

III.3.6.b. Real-Sample Experiments. These experiments were carried out in the same manner as the calibration-curve experiments, but adding a portion from one of the "tissue soaking regime" washes to the SS used for the equilibration instead of standard SS. The volume was chosen so that the SDS concentration of the new diluted media would be in the lower part of the calibration curve (<10 μM), which was the most precise portion of the curve.

Final washout SDS concentrations were reported as μM/g of tissue/100 ml of SS. Total amounts of SDS washed out from treated bovine pericardium over 96 h were calculated and reported as mg/g of tissue.

III.4. Preliminary Experiments for the Quantification of Free Dodecylsulfate

III.4.1. Soaking Solution Preparation. One package of PBS was added to 1 L flask and dissolved in 1 L dd-H_2O. Aprotinin (0.23 mL), Triz (10 mL), H_4EDTA (0.25 mg), AAS (25 μL) and PBS solution were mixed to a final total volume of 250 mL. Sonication was used to aid dissolution of all solids. The solution was filtered using a 0.2 μm size filter and stored in a refrigerator when not in use.

III.4.2. Synthesis of Hp-Aza-DEC$^+$I$^-$ and Me-Aza-DEC$^+$I$^-$. The reaction scheme for the synthesis of Hp-aza-DEC$^+$I$^-$ and Me-aza-DEC$^+$I$^-$.is shown in Fig 3.12. The synthesis of Hp-aza-DEC$^+$I$^-$ is shown in the first 5 horizontal steps (1-5a). The preparation of Me-aza-DEC$^+$I$^-$ required an intermediate step before the final one was performed, which is shown vertically (5b). Steps 3, 4 and 5b are modifications of reactions originally performed by Dr. Stephanie Bowman in the Strauss Research Group.

Step 1: Halogenation of Ferrocene (reaction in Figure 3.11.1).[91] In a two neck flask with a stir bar, 148 mmol (27.505 g) of $FeCp_2$ were placed. THF (170 mL) was added and the flask was immersed in an ice bath and set to stir. An addition funnel was used to slowly add 170 mmol of t-BuLi in a period of approximately 30 min, followed by 300 mL of pentane. After 1.5 h the solution was orange-brown, and a yellow precipitate could be seen at the bottom. An extra 100 mL of pentane were added and the solution was decanted. Approximately 250 mL of THF and 157 mmol (40.16 g) of iodine were added. The solution was allowed to reach room temperature (45 min) and 150 mL of ether were added. The mixture was washed with a sodium thiosulfate solution (32.67 g in 300 mL of dd-H_2O). The organic phase was washed with dd-H_2O and dried over $MgSO_4$. The ^{1}H-NMR spectrum showed 60% of the mono-substituted product (I), 16% of ferrocene (unreacted starting material) and 25% of the di-substituted product.

Step 2: Protection of Carbon 1 (reaction in Figure 3.11.2).[92] A 44.4 mmol (13.867 g) portion of the halogenated ferrocene crude was set to reflux under N_2 together with 72.9 mmol (7.109 g) of H(phthalimide), 21.9 mmol (3.145 g) of copper (I) oxide and 85 mL of pyridine for approximately 1.5 days. Then the heat was turned off, the mixture cooled down and evaporated in a vacuum line. 50 mL of ethyl acetate were added to the mixture while stirring. A 4-cm long silica gel column (ID 11 mm) was prepared and used to separate 2 mL of the reaction crude. Two fractions were eluted with ethyl acetate and acetonitrile. The second fraction was analyzed by ^{1}H-NMR, which revealed this fraction contains the phthalimide-protected compound (II), H(phthalimide) and ferrocene.

Step 3: Alkylation of Carbons 3, 1' and 3' (reaction in Figure 3.11.3). In the glove box, 2.5128 g of $ZnCl_2$, 5 mmol (1.6560 g) of the second fraction from the above reaction (containing the pthalimide-protected compound) and approximately 15 mL of CH_2Cl_2 were added to a 1-L two-neck round bottom flask. The flask was connected to a condenser and to the Schlenk line, evacuated immediately and back-filled with N_2. The alkylating agent used was $C_{10}H_{21}Cl$; 25.7 mmol (4.5333 g) were added with stirring and the flask was heated under N_2 (reflux started 10 min later). After 2.5 hours a portion of the reaction mixture was filtered, stirred over Fe powder for 20 min and dryed in the Schlenk line. The color of the mixture is still green. A portion of the mixture was analyzed by ^{1}H-NMR; a broad peak in the p-region did not show any features. After 27 hours of reaction, a sample was washed with a 10% H_2O/KOH solution (after which it turned caramel color), dried over Mg_2SO_4, treated with Fe powder and dried in the line. A new ^{1}H-NMR spectrum was taken, which showed the target trialkylated compound (III) and no presence of the started material. Another portion of the crude was analyzed by (+)ESI-MS. Purification of the sample was performed by column chromatography: a separation column (internal diameter of 55 mm) was packed with 9.5 in of silica gel. Five fractions were collected after running five different solvent systems, as follows: f1 – hexanes, yellow; f2 – 5:1 hexanes:CH_2Cl_2, red-brown; f2a – 1:1 hexanes:CH_2Cl_2, finish

eluting f2; f3 – ethyl acetate, brown; f4 – MeOH, yellow-green. The two hexanes:CH_2Cl_2 fractions were combined and rotavaped down. A brown oil resulted. Yield: 54%. Recrystallization attempts from different solvents (from MeOH, EtOH, EtOH + 2% H_2O) did not work: the compound precipitates as oil.

Step 4: Replacement of the Pthalimide with an Amine (reaction in Figure 3.11.4). A portion of 0.55 mmol (0.412 g) of the trialkylated compound (III) was mixed with 2 mL of hydrazine hydrate and 5 mL of EtOH and they were set to reflux. After 40 min the reflux was stopped and the reaction mixture was diluted with dd-H_2O and extracted with hexanes. The organic layer was washed several times and dried under vacuum. The mass of the product was 280 mg. A ^{1}H-NMR spectrum shows the target compound (IV) in the product mixture is highly pure.

Step 5 in the Synthesis of Me-Aza-DEC$^+I^-$: Trimethylation of the Amine Group (reaction in Figure 3.11.5a). Most of the product obtained in the previous synthesis (IV) was dissolved in a 1:1:1 iodomethane:benzene:DMF mixture and refluxed under N_2. The reaction was allowed to proceed for 7 hours. The reaction mixture was placed under vacuum for 5 min to eliminate any remainder CH_3I left. More hexanes were added and washed with water several times. The sample was evaporated under vacuum and purified using column chromatography: a separation column (internal diameter of 11 mm) was packed with 45 mm of silica gel. Two fractions were collected after running two different solvent systems, as follows: f1 – 1:1 petroleum ether: ethyl acetate; f2 – MeOH (both addition of solvent to the column contained 2 drops of ammonium hydroxide per 100 mL of solvent). Fraction f2 was evaporated down and dried with benzene twice. The mass of the product was 108.7 g. A 2.2 mg sample of f2 was mixed with 2 mg of the starting material (IV) in an exact amount of 3 drops of hexanes. (+)ESI-MS was used to calculate the purity of the quaternary ammonium sample in f2, which resulted to be 88%. Further purification of this fraction was performed as previously. The final mass of the sample in f2-2 was 96.6 mg, resulting in an 88.9% recovery after the second purification. The

(+)ESI-MS experiment was repeated, revealing a product purity, the Me-aza-DEC$^+$ (V) of 91.7%.

Step 5 in the Synthesis of Me-Aza-DEC$^+$I$^-$: Reductive Alkylation of the Amine Group of the Amine Group (reaction in Figure 3.11.5b).[93] After steps 1-4 of the synthesis were repeated, most of the product obtained in step 4 (IV) was dissolved in benzene mg of n-heptanol were added. The mixture was refluxed for 30 minutes, which turned it dark brown. A 2 mL aliquot of MeOH and 0.3050 g of sodium cyanoborohydride were added and the mixture was stirred. A 1 mL aliquot of benzene and a 3 mL aliquot of a 10% aqueous KOH solution were added. The color of the mixture changed to orange. Extraction with 3 mL of benzene was carried on and the solvent was evaporated under vacuum. This procedure was repeated several times in order to eliminate any traces of water. Presence of the target compound (V.b) was confirmed by ^{1}H-NMR analysis.

Step 6 in the Synthesis of Hp-Aza-DEC$^+$I$^-$: Methylation (reaction in Figure 3.11.6). The product from step 5 (V.b) was dissolved in a 1:1 benzene:DMF mixture, after which 1 mL of iodomethane was added, and reflux under N_2 was allowed to proceed for 2.5 days. During this time, the reaction mixture was periodically monitored using (+)ESI-MS and thin layer chromatography (TLC), and also all three solvents (total of 4 mL, 4 mL and 11 mL of benzene, DMF and MeI, respectively) were added in 1-2 mL increments, as needed, in order to maintain the initial volumes, which decreased due to evaporation. Several water and water:hexanes washes were performed. The sample was evaporated under vacuum, which left a brown oily solid, and purified using column chromatography: a separation column (internal diameter of 11 mm) was packed with 155 mm of silica gel. Two fractions were collected after running two different solvent systems, as follows: f1 – 1:1 petroleum ether: ethyl acetate; f2 – MeOH (both solvent mixtures contained 2 drops of ammonium hydroxide per 100 mL of solvent mixture).

Fraction f2 was evaporated down and analyzed through (+)ESI-MS, which showed mainly a peak for the target compound (VI) at 748.8 m/z.

III.4.3. Suitability experiments. These were performed as previously described for the large volume experiments, but using the Di probe and thin films of either Hp-aza-DEC^+I^- or Me-aza-DEC^+I^-, using a volume of the salts solutions that rendered films with a ν(CH) band intensity of ca. 0.6. The stability of the films in water was tested by comparing the dry film bands before and after an 8h-equilibration with water had taken place. The capability of the dry film to detect DDS^- from an aqueous solution (dd-water or SS) was determined by whether a film showed a ν(SO) band growing with time, as exchange took place. The capability of the dry film to quantify DDS^- from SS was determined by whether a calibration curve with a linear portion useful for quantification could be built.

IV. Conclusions

The results presented here confirm the abilities of the ATR-FTIR spectroscopy technique in the detection and quantification of pollutants using DEC^+ salts, using traditional parameters like a 100-mL sample volume, films made with 60 nmol of extractant, and detection of a single analyte per experiment, using the time-dependent exchange method. The author also:

(i) successfully achieved quantification of perfluoro-*n*-octanesulfonate in a smaller volume of sample (1 mL), at concentrations as low as 10 μM, using a $DEC^+ClO_4^-$ film; anion detection, specifically perrhenate, using different film thicknesses (made with 60 and 6 nmol of extracting compound) and multiple-anion detection using different film thicknesses (perrhenate and perchlorate were detected in a mixture using $DEC^+ClO_4^-$ films made both with 60 and 6 nmol of material) with comparable results;

(ii) investigated ATR-FTIR spectroscopy technique capabilities to detect and quantify two new analytes: the quantification of free cyanide using a Ni complex was

carried on successfully (the results obtained were comparable to those obtained by Johnson et al. using the WAD method); the detection of dodecylsulfate, in aqueous biological samples containing many other species, was possible using the time-dependent exchange method and a $DEC^{+}NO_3^{-}$ film (quantification was not possible given the high instability of this ferrocenium salt in the media);

(iii) successfully synthesized a new salt, Me-Aza-$DEC^{+}I^{-}$, to be used for the quantification of free dodecylsulfate using the ATR-FTIR spectroscopy thechnique and the time-dependent exchange method.

V. References

(1) Hebert, G. N.; Odom, M. A.; Bowman, S. C.; Strauss, S. H. *Analytical Chemistry* **2004**, *76*, 781-787.

(2) Hebert, G. N.; Odom, M. A.; Craig, P. S.; Dick, D. L.; Strauss, S. H. *J. Environ. Monitoring* **2002**, *4*, 90-95.

(3) Hebert, G. N. Ph.D. dissertation, Colorado State University, 2004.

(4) Gansle, K. M. R. Ph.D. Dissertation, Colorado State University, Fort Collins, CO, 1998.

(5) Pendin, A. A.; Zakhar'evskii; Leont'evskaya, P. K. *Kinetics and Catalysis* **1966**, *7*, 922-925.

(6) Pendin, A. A.; Leont'evskaya, P. K. *Kinetics and Catalysis* **1976**, *17*, 303–306.

(7) Pendin, A. A.; Leont'evskaya, P. K.; Bundina, T. K. *Kinetics and Catalysis* **1977**, *18*, 1087–1090.

(8) Prins, R.; Korswagen, A. R.; Kortbeek, A. G. T. G. *Journal of Organometalic Chemistry* **1972**, *39*, 335-344.

(9) Kosak, E. D. M.S. Thesis, Colorado State University, Fort Collins, CO, 2003.

(10) Strauss, S. H.; Odom, M. A.; Herbert, G. N.; Clapsaddle, B. J. *Journal of the American Water Works Association* **2002**, *94*, 109-115.

(11) Moyer, B. A.; Bonnesen, P. V. *Supramolecular Chemistry of Anions*; VCH Publishers: New York, 1997.

(12) Korossis, S. A.; Booth, C.; Wilcox, H. E.; Watterson, K. G.; Kearney, J. N.; Fisher, J. *J Heart Valve Dis* **2002**, *11*, 463-471.

(13) Kim, W. G.; Park, J. K.; Lee, W. Y. *Int J Artific Organs* **2002**, *25*, 791-797.

(14) Gonçalves, A.; Griffiths, L. G.; Anthony, R. V.; Orton, E. C. *J Heart Valve Dis* **2005**, *14*, 212-217.

(15) Pfeffer, H. A.; Wolfe, G. E.; (FMC Corp., USA). Application: CA CA, 1992, pp 19.

(16) Ushio, R.; Kikuta, N.; (Sumitomo Metal Mining Co., Ltd., Japan). Application: JP JP, 2002, pp 7 pp.

(17) EPA, March 2009.

(18) Soto-Blanco, B.; Marioka, P. C.; Gorniak, S. L. *Ecotoxicol. Environ. Saf. FIELD Full Journal Title:Ecotoxicology and Environmental Safety* **2002**, *53*, 37-41.

(19) Soto-Blanco, B.; Stegelmeier, B. L.; Pfister, J. A.; Gardner, D. R.; Panter, K. E. *J. Appl. Toxicol. FIELD Full Journal Title:Journal of Applied Toxicology* **2008**, *28*, 356-363.

(20) EPA, March 2009.

(21) Barnes, D. E.; Wright, P. J.; Graham, S. M.; Jones-Watson, E. A. *Geostand. Newsl. FIELD Full Journal Title:Geostandards Newsletter* **2000**, *24*, 183-195.

(22) EPA, March 2009.

(23) http://www.oico.com/default.aspx?id=product&productid=94 **2009**.

(24) Urbansky, E. T. *Bioremediation J.* **1998**, *2*, 81–95.

(25) Urbansky, E. T.; Schock, M. R. *Journal of Environmental Management* **1999**, *56*, 79-95.

(26) Rickman, J. E.: LOS ALAMOS, NM, 2003.

(27) Kirk, A. B.; Smith, E. E.; Tian, K.; Anderson, T. A.; Dasgupta, P. K. *Environmental Science and Technology* **2003**, *37*, 4979-4981.

(28) Sanchez, C. A.; Crump, K. S.; Krieger, R. I.; Khandaker, N. R.; Gibbs, J. P. *Environmental Science and Technology* **2005**, *39*, 9391-9397.

(29) Krynitsky, A. J.; Niemann, R. A.; Nortrup, D. A. *Analytical Chemistry* **2004**, *76*, 5518-5522.

(30) Dyke, J. V.; Kirk, A. B.; Kalyani Martinelango, P.; Dasgupta, P. K. *Analytica Chimica Acta* **2006**, *567*, 73-78.

(31) Stetson, S. J.; Wanty, R. B.; Helsel, D. R.; Kalkhoff, S. J.; Macalady, D. L. *Analytica Chimica Acta* **2006**, *567*, 108-113.

(32) U.S. EPA, Office of Research and Development, National Center for Environmental Assessment, U.S. Government Printing Office: Washington, DC, 2002.

(33) Hogue, C. *Chem. Eng. News* **2003**, *81*, 37−46.

(34) Sanchez, C. A.; Barraj, L. M.; Blount, B. C.; Scrafford, C. G.; Valentin-Blasini, L.; Smith, K. M.; Krieger, R. I. *Journal of Exposure Science & Environmental Epidemiology* **2009**, *19*, 359-368.

(35) Sanchez, C. A.; Blount, B. C.; Valentin-Blasini, L.; Krieger, R. I. *Bulletin of Environmental Contamination and Toxicology* **2007**, *79*, 655-659.

(36) Clark, J. J. J. In *Perchlorate in the Environment*; Urbansky, E. T., Ed.; Kluwer/Plenum: New York, 2000, pp 15−29.

(37) Christen, K. *Environ. Sci. Technol.* **2000**, *34*, 374A−375A.

(38) Kirk, A. B. *Analytica Chimica Acta* **2006**, *567*, 4-12.

(39) Ericksen, G. E.; US Department of the Interior: Washington DC, 1981.

(40) Collette, T. W.; Williams, T. L.; Urbansky, E. T.; Magnuson, M. L.; Hebert, G. N.; Strauss, S. H. *Analyst* **2003**, *128*, 88-97.

(41) Urbansky, E. T.; Brown, S. K.; Magnuson, M. L.; Kelty, C. A. *Environ. Pollut.* **2001**, *112*, 299−302.

(42) Foubister, V. *Analytical Chemistry* **2006**, *78*, 7914-7915.

(43) *Fed. Regist.* **1998**, *63*, 10273−10287.

(44) *Fed. Regist.* **1999**, *64*, 50555−50620.

(45) NationalResearchCouncil; National Academies Press
Washington, D. C., 2005.

(46) EPA, 2009; Vol. 2009.

(47) EPA, 2005; Vol. 2009.

(48) Darab, J. G.; Smith, P. A. *Chem. Mater.* **1996**, *8*, 1004-1021.

(49) EPA, 1998; Vol. 63.

(50) EPA: Washington, D.C., 2004; Vol. 2009.

(51) Stewart, T. L.; Frey, J. A.; Geiser, D. W.; Manke, K. L. In *Science and Technology for Disposal of RadioactiVe Tank Wastes*

First ed.; Schulz, W. W., Lombardo, N. J., Eds.; Springer: New York, 1998, pp 3.

(52) *Fed. Regist.* **2002**, *67*, 11008−11030.

(53) Howell, R. D.; Tucker, E. E. *Am. Environ. Lab* **1996**, *12*, 10−11.

(54) Schlummer, M.; Gruber, L.; Schmitt, A.; Lange, F. T. *Organohalogen Compounds* **2008**, *70*, 722-725.

(55) Darwin, R. L.; Ottman, R. E.; Norman, E. C.; Gott, J. E.; Hanauska, C. P. *Natl. Fire Protect. Assoc.* **1995**, 67−73.

(56) Chan, D. B.; Chian, E. S. K. *Environ. Prog.* **1986**, *5*, 104−109.

(57) Moody, C. A.; Hebert, G. N.; Strauss, S. H.; Field, J. A. *J. Environ. Monit.* **2003**, *5*, 341−345.

(58) Kissa, E. *Fluorinated Surfactants: Synthesis, Properties, and Applications*; Marcel Dekker: New York, 1994.

(59) Erten-Unal, M.; Schafran, G. C.; Paranjape, S.; Williams, F.; Cotnoir, D.; Kirk, D. *Proceedings of the National Conference on Environmental Engineering* **1998**, *98*, 494−499.

(60) Lein, N. P. H.; Fujii, S.; Tanaka, S.; Nozoe, M.; Tanaka, H. *Desalination* **2008**, *226*, 338-347.

(61) Murakami, M.; Kuroda, K.; Sato, N.; Fukushi, T.; Takizawa, S.; Takada, H. *Environmental Science & Technology* **2009**, *43*, 3480-3486.

(62) Seacat, A. M.; Thomford, P. J.; Hansen, K. J.; Olsen, G. W.; Case, M. T.; Butenhoff, J. L. *Toxicol. Sci.* **2002**, *68*, 249−264.

(63) Case, M. T.; York, R. G.; Christian, M. S. *Int. J. Toxicol.* **2001**, *20*, 101−109.

(64) Curran, I.; Hierlihy, S. L.; Liston, V.; Pantazopoulos, P.; Nunnikhoven, A.; Tittlemier, S.; Barker, M.; Trick, K.; Bondy, G. *Journal of Toxicology and Environmental Health Part A: Current Issues* **2008**, *71*, 1526-1541.

(65) Boudreau, T. M.; Sibley, P. K.; Mabury, S. A.; Muir, D. G. C.; Solomon, K. R. *Arch. Environ. Contam. Toxicol.* **2003**, *44*, 307–313.

(66) Sanderson, H.; Boudreau, T. M.; Mabury, S. A.; Cheong, W.-J.; Solomon, K. R. *Environ. Toxicol. Chem.* **2002**, *21*, 1490–1496.

(67) Kannan, K.; Corsolini, S.; Falandysz, J.; Oehme, G.; Focardi, S.; Giesy, J. P. *Environ. Sci. Technol.* **2002**, *36*, 3210–3216.

(68) Kannan, K.; Tao, L.; Sinclair, E.; Pastva, S. D.; Jude, D. J.; Giesy, J. P. *Archives of Environmental Contamination and Toxicology* **2005**, *48*, 559-566.

(69) Corsolini, S.; Kannan, K. *Organohalogen Compounds* **2004**, *66*, 4029-4035.

(70) Sinclair, E.; Mayack, D. T.; Roblee, K.; Yamashita, N.; Kannan, K. *Archives of Environmental Contamination and Toxicology* **2006**, *50*, 398-410.

(71) Taniyasu, S.; Kannan, K.; Horii, Y.; Hanari, N.; Yamashita, N. *Environ. Sci. Technol.* **2003**, *37*, 2634–2639.

(72) Yeung, L. W. Y.; Yamashita, N.; Taniyasu, S.; Lam, P. K. S.; Sinha, R. K.; Borole, D. V.; Kannan, K. *Chemosphere* **2009**, *76*, 55-62.

(73) Tao, L.; Kannan, K.; Kajiwara, N.; Costa, M. M.; Fillmann, G.; Takahashi, S.; Tanabe, S. *Environmental Science & Technology* **2006**, *40*, 7642-7648.

(74) Giesy, J. P.; Kannan, K. *Environ. Sci. Technol.* **2001**, *35*, 1339–1342.

(75) Kannan, K.; Yun, S. H.; Evans, T. J. *Environmental Science and Technology* **2005**, *39*, 9057-9063.

(76) Kannan, K.; Perrotta, E.; Thomas, N. J. *Environmental Science & Technology* **2006**, *40*, 4943-4948.

(77) Shaw, S. D.; Berger, M. L.; Brenner, D.; Kannan, K. *Organohalogen Compounds* **2006**, *68*, 2042-2046.

(78) Yoo, H.; Kannan, K.; Kim, S. K.; Lee, K. T.; Newsted, J. L.; Giesy, J. P. *Environmental Science & Technology* **2008**, *42*, 5821-5827.

(79) Schiavone, A.; Corsolini, S.; Kannan, K.; Tao, L.; Trivelpiece, W.; Torres, D.; Focardi, S. *Science of the Total Environment* **2009**, *407*, 3899-3904.

(80) Hart, K.; Gill, V. A.; Kannan, K. *Archives of Environmental Contamination and Toxicology* **2009**, *56*, 607-614.

(81) Brown, D.; Mayer, C. E. In *The Washington Post*: Washington DC, 2000, pp A1.

(82) Tullo, A. *Chem. Eng. News* **2000**, *May 22*, 9–10.

(83) Maizel, J. V., Jr In *Fundamental Techniques in Virology*; Habel, K., and Salzman, N. P., Ed.; Academic Press: New York, 1969, pp 334.

(84) Wilcox, H. E.; Korossis, S. A.; Booth, C.; Watterson, K. G.; Kearney, J. N.; Fisher, J.; Ingham, E. *J Heart Valve Dis* **2005**, *14*, 228-237.

(85) Rieder, E.; Kasimir, M. T.; Silberhumer, G.; Seebacher, G.; Wolner, E.; Simin, P.; Weigel, G. *J Thoracic Cardiovasc Surg* **2004**, *127*, 399-405.

(86) Chambliss, C. K.; Odom, M. A.; Morales, C. M. L.; Martin, C. R.; Strauss, S. H. *Analytical Chemistry* **1998**, *70*, 757-765.

(87) Hebert, G. N.; Strauss, S. H.; Colorado State University: Fort Collins, 2001.

(88) Fisher, F. B.; Brown, J. S. *Anal. Chem.* **1952**, *24*, 1440-1444.

(89) Moyer, B. A.; Bonnesen, P. V. In *Supramolecular Chemistry of Anions*; Bianchi, A., Bowman-James, K., Garcia Espana, E., Eds.; VCH Publishers: New York, 1997, pp 1–44.

(90) Shriver, D. F.; Drezdzon, M. A. *The Manipulation of Air-Sensitive Compounds, 2nd Ed.*; Wiley-Interscience: New York, 1986.

(91) Rebiere, F. *Tetrahedron Letters* **1990**, *31*, 3121-3124.

(92) Bildstein, B. *Organometallics* **1999**, *18*, 4325-4336.

(93) Szardenings, A. K. *J. Org. Chem.* **1996**, *61*, 6720-6722.

Chapter 4

Using ATR-FTIR Spectroscopy to Aid Heart-Valve Research

I. Introduction

I.1. Tissue engineering. One of the aims of state-of-the-art research in the field of tissue engineering is to develop a heart valve implant that would resolve the issues of thrombosis and durability associated with currently available prostheses. Among the materials presently being investigated as scaffolds for a tissue-engineered heart valve are synthetic biodegradable materials,[1-5] collagen gels,[6] and unfixed xenogeneic tissues[7-10] (tissues from a different species). Scaffolds constructed of the latter present certain theoretical advantages, such as appropriate mechanical properties, provision of a suitable environment for cell differentiation and orientation, and the ability to be implanted immediately in the patient without a need for extended in vitro processes. A significant disadvantage of unfixed xenogeneic tissue scaffolds is that they inherently produce an immune response. For this reason, removal of antigenic proteins that are presumed to be primarily associated with the cellular component of the tissue, by a process that has come to be known as "decellularization," is needed. An ideal decellularization treatment for xenogeneic bioscaffolds should remove non-matrix xenogeneic antigens, maintain biomechanical properties of the tissue, and be compatible with in vitro or in vivo recellularization by autogenous cells.

Recent clinical experience with decellularized heart valve xenografts (a graft of tissue taken from a donor of one species and grafted into a recipient of another species) has confirmed the critical importance of exhaustive removal of antigenic proteins.[11]

Based on light microscopy, transmission electron microscopy, and immunohistochemistry and western blot analysis of known antigens, sodium dodecylsulfate (SDS) has consistently emerged as a detergent used in promising decellularization/antigen-clearing treatments.[12-16] However, questions have been raised about the possible cytotoxicity of SDS-treated xenogeneic tissues. Such cytotoxicity could be caused by free SDS leaching from treated tissues or residual bound SDS within treated tissues, or both. Rieder et al. have reported significant toxicity on cultured human vascular cells exposed to media used to store SDS-treated porcine aortic conduits.[17] On the other hand, Wilcox et al. were unable to demonstrate any significant cytotoxic effect associated with media that had contained SDS-treated porcine aortic conduits.[18] Similarly conflicting results were reported with regard to in vitro recellurization of SDS-treated tissues (i.e., cell attachment and migration).[13,17-19]

I.2. The analytical Problem. Christopher Orton, D.V.M., a clinical researcher at the Veterinary Teaching Hospital (VTH) at Colorado State University (CSU) in Fort Collins, CO, in his ongoing studies of heart-valve scaffolds, began working on a project to (i) confirm the toxicity of the detergent anion dodecylsulfate (DDS^-) to cells and (ii) study the extent of leaching of DDS^- from SDS-treated tissues. The latter part of this project, which is the subject of this chapter, involved developing methods to measure (i) the amount of DDS^- leached from the tissue by soaking it in an appropriate "soaking solution" (SS) and (ii) the amount of DDS^- remaining in the tissue after washing had been performed.

The Strauss Group at CSU has developed an analytical method to quantify polyatomic anions (A^-) in aqueous samples using attenuated-total-reflectance Fourier transform infrared (ATR-FTIR) spectroscopy.[20,21] The concentration of A^- is determined by measuring its rate of ion exchange into a thin film of a selective, water-insoluble ion-exchange salt that is deposited on an ATR crystal. As A^- undergoes ion exchange with the sacrificial anion originally in the thin film (e.g., chloride or nitrate), the rate of anion

exhange is determined by monitoring the absorbance of one of more IR bands of A^- in the thin film over time (usually about 10 minutes) and a linear calibration curve of d*A*/d*t* vs. concentration is constructed (see Chapter 3 for more details).[20,22] Among the anions studied, perfluorooctanesulfonate ($PFOS^-$) was detected in sub-ppm concentrations in aqueous samples.[23] Given the structural similarities of the detergent anions $PFOS^-$ and DDS^-, the author agreed to suitably modify the group's ATR-FTIR methodology to determine the amount of DDS^- in SDS-treated tissue samples from Orton's lab. As part of this study, the author of this dissertation also (i) advised Dr. Orton and his co-worker Shiori Arai, D.V.M., about the proper procedures to reproducibly prepare complex aqueous solutions of biochemical reagents and (ii) assisted Dr. Arai in the preparation of many of the SDS-treated and subsequently soaked tissue samples used in this investigation.

At the completion of this study, which was published in the *Journal of Heart Valve Disease*,[19] several possible avenues for future work became apparent. As discussed below, it was discovered that measuring the amount of DDS^- remaining in tissue samples after exhaustive soaking could not be accomplished using the at-the-moment current ATR-FTIR method. The feasibility of a suitable alternative quantification methodology was investigated (but not applied to the problem; that would be a separate project for another researcher in the future). This feasibility study consisted of (i) a theoretical analysis of beta-scintillation-counting (BSC) statistics to demonstrate the potential efficacy of BSC using tracer amounts of [^{35}S]SDS to detect DDS^- in solution *and* DDS^- that is "irreversibly" bound to tissue samples and (ii) an experimental study to determine if small amounts of SDS can be made from commercially-available dilute solutions of [^{35}S]sulfuric acid.

II. Results and Discussion.

II.1. SDS quantification using ATR-FTIR. The general protocol used by Orton et al. in decellularization experiments consists of cutting pieces of tissue samples (e.g., bovine pericardium), allowing them to soak for a period of time in a solution containing SDS and designed to maintain sterile conditions (SS), and then submitting the tissues to a series of washes. The author designed a soaking regime, described in Table 4.1, which included preparing five groups of tissue samples (10 pieces/group), treating them with SS containing various concentrations of SDS (0.1-1%) for 24 hours and submitting them to four subsequent 24-hour washes with fresh SS each. The details of this soaking regime are described in the experimental section III.3.2.

Chapter 3 illustrates how ATR-FTIR spectroscopy using ATR crystals coated with thin films of organometallic ion-exchange compounds can be used as a reliable, precise, and sensitive method to determine the concentrations of polyatomic anions at sub-ppm to ppb levels in aqueous samples. This chapter discusses the application of this technique to a biomedical project, being the aim to prepare xenogeneic "living" heart valve replacements. The goal was to analyze samples of aqueous solutions in which pieces of bovine pericardium had been soaked *after* they had been treated with aqueous solutions containing SDS. It was first determined that DDS^- can be quantified *in dd-H_2O* down to at least 0.2 ppb with our standard ATR-FTIR method using thin films of $DEC^+NO_3^-$, as shown in Chapter 3. However, it was quickly discovered that thin films of $DEC^+NO_3^-$ are not stable in contact with the complex aqueous media in which the SDS-treated tissue samples had been soaked, which contained DDS^- and a mixture of components aimed to preserve the physiological samples during treatments and assure sterile conditions throughout, as shown in Table 4.2. Therefore, several variations of the method described in Chapter 3 had to be developed for this project, including the synthesis of a new organometallic ion-exchange compound more stable with respect to nucleophilic degradation than $DEC^+NO_3^-$. Finally, since even the improved ATR-FTIR methods could

Table 4.1. Description from soaking regime applied to SDS-treated tissue samples.

[SDS] during treatment	first 24 hour wash	second 24 hour wash	third 24 hour wash	fourth 24 hour wash
0.01 %	24 h 0.01%	48 h 0.01%	72 h 0.01%	96 h 0.01%
0.05 %	24 h 0.05%	48 h 0.05%	72 h 0.05%	96 h 0.05%
0.1 %	24 h 0.1%	48 h 0.1%	72 h 0.1%	96 h 0.1%
0.5 %	24 h 0.5%	48 h 0.5%	72 h 0.5%	96 h 0.5%
1 %	24 h 1%	48 h 1%	72 h 1%	96 h 1%

Table 4.2. Soaking solution composition and components concentration.

component	concentration
phosphate	10.4 mM
sodium chloride	1193.9 mM
potasium chloride	2.8 mM
aprotinin	9.2×10^{-2} % v/v
ethylenediaminetetraacetic acid	0.1 % w/v
trizma hydrochloride buffer	1050 mM
penicillin G	1×10^{4} U/mL
streptomycin sulfate	10 mg/mL
amphotericin B	25 mg/mL

To prepare this solution, a 1 L PBS solution was prepared in dd-water, and then used to dissolve/dilute the rest of the components to a final volume of 250 mL. This final solution was used to soak tissue samples in a precise soaking regime, as described in the experimental section.

not be used to determine how much DDS^- remained in the tissue samples after exhaustive soaking, the efficacy of an entirely different method that might be applied in a future study was investigated.

Two new approaches tested in order to quantify DDS^- (and thereby study its leaching from the tissues) in SS: 1) a new methodology based on liquid-liquid exchange was developed, which does not require a prolonged contact between the SS and the extractant and 2) a new, more stable extractant was synthesized, which formed thin-films that could withstand prolonged contact with SS.

Furthermore, whether DDS^- leaches out of the tissue during the soaking steps as a free anion or complexed to proteins could affect the ability to accurately quantify it using this method, since the method requires the anion to be in its free form in order for the ion exchange to take place: this way, it is able to penetrate in between the layers of cations.

II.1.1. Equilibrium liquid-liquid Exchange Method: Using $DEC^+NO_3^-$ to detect SDS in Soaking Solution (SS). A novel method was developed as an alternative to the time-dependant exchange experiments. In this method, an aliquot of a CH_2Cl_2 solution containing $DEC^+NO_3^-$ was placed in contact with a portion of SS containing a known concentration of Na^+DDS^-. Vigorous mixing was applied for 5 minutes in order to facilitate anion exchange from one phase to the other, and next the organic phase was separated and used to make a thin film on the ATR crystal. The absorbance of the main ν(SO) IR band at 1254 cm^{-1} was correlated to the concentration of SDS.

The feasibility of this method to accurately quantify SDS in a SS sample of "unknown" concentration was confirmed by: i) construction of a linear d*A*/d*t* calibration curve and ii) use of this calibration curve in a 'blind test".

i. It was confirmed that, providing there is a molar excess of NO_3^- compared to DDS^-, differences in the [SDS]:[$DEC^+NO_3^-$] ratio does not interfere with the accurate determination of the DDS^- concentration. Therefore, the DDS^- calibration curve (linear from 24 μM to 500 μM; R = 0.99768; see description under III.3.3.a in the experimental

section) was constructed by combining the d*A*/d*t* values from different experiments with a variety of [SDS]:[$DEC^+NO_3^-$] ratios ([$DEC^+NO_3^-$]>[SDS] for all cases).

ii. In the "blind test", two "SDS in SS/$DEC^+NO_3^-$ in CH_2Cl_2" mixtures were prepared by a member of the Strauss Research Group, and labeled "200-400 μM SDS". Subsequently, these samples were analyzed (see description under III.3.3.c in the experimental section), showing an average SDS concentration of 305 μM (12% RSD for 4 repetitions). The real concentration of SDS in the sample, as reported to the author by the group member who prepared the solutions after the analysis was finished, was 300 μM, which demonstrates that it is possible to accurately quantify SDS in SS using $DEC^+NO_3^-$ and this method.

The absorbance values obtained for the ν(SO) bands of DDS^- using this equilibrium liquid-liquid exchange method were substantially smaller compared to those obtained using the time-dependant exchange method, as shown in Figure 4.1, where it can be observed that two samples with SDS concentrations an order of magnitude different show ν(SO) bands of comparable intensity. In order to reasonably evaluate the difference in absorbance signal obtained with these two methods, the peak absorbance for the spectrum acquired with the equilibrium liquid-liquid exchange method (signal: average of 1024 scans; collection time: ca. 12 min) was compared to the peak absorbance for one spectrum acquired with the time-dependant exchange method after ca. 12 min of exchange had elapsed (signal: average of 128 scans). Although the use of 1024 scans to generate each spectrum in the equilibrium liquid-liquid exchange method is not sufficient to provide a sensitivity comparable to that of the time-dependant exchange method, the SNR>>3 for the smaller [SDS] detected (24 μM).

The equilibrium liquid-liquid exchange method presents an alternative to the time-dependant exchange method described in Chapter 3. Among the advantages of using this method it can be pointed out that no monitoring of the thin film is necessary while

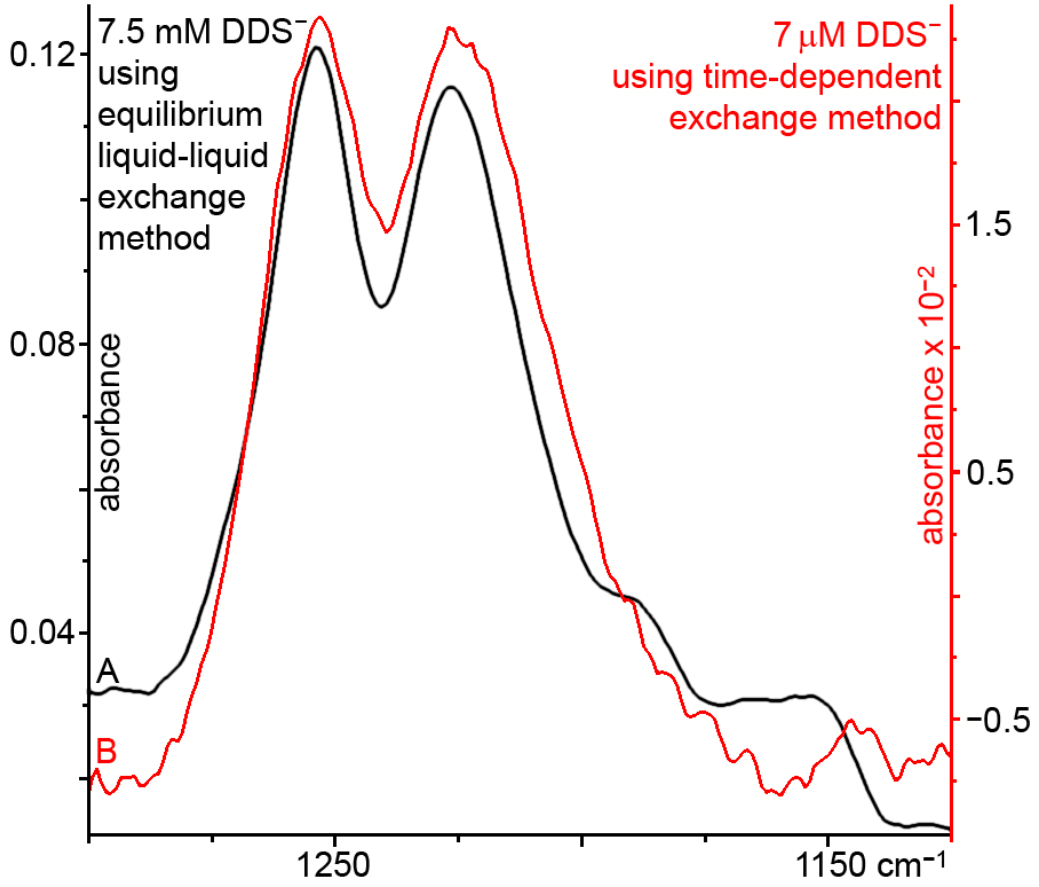

Figure 4.1. ATR-FTIR spectra of DDS^-, obtained using two different methods. **A.** *equilibrium liquid-liquid exchange:* a 24 μM solution of SDS in SS is allowed to exchange with a CH_2Cl_2 solution containing excess $DEC^+NO_3^-$, and a thin film is made with the organic phase (1024 scans, data collected for ca. 12 min). **B.** *time-dependent exchange:* a $DEC^+NO_3^-$ thin film is placed in contact with a 2 μM solution of SDS in SS and data is collected every two minutes, monitoring the exchange (spectra shown collected after ca. 12 min of exchange, 128 scans).

the ion exchange takes place; alternatively, the exchange occurs earlier during the mixing step. Therefore, the contact between the SS and $DEC^+NO_3^-$ takes place for only a short period of time (5 min), compared to the longer contact time (>25 min) required for quantification in the time-dependant exchange method. Furthermore, this method does not involve contacting a thin $DEC^+NO_3^-$ film with the SS, but rather an aliquot of equal volume of organic solution containing $DEC^+NO_3^-$. Both these features were designed to overcome the stability issues of thin films of this ferrocenium salt in the presence of SS. Finally, the use of the equilibrium liquid-liquid exchange method does not necessitate the ATR-FTIR crystal be in contact with an aqueous solution; which means that, potentially, the organic phase separated from the SS after the exchange could be used to make a thin film on an FTIR plate (e.g., NaCl), to be monitored and analyzed using traditional transmission-mode FTIR spectroscopy, instead of requiring the use of the ATR-FTIR attachment.

The equilibrium liquid-liquid exchange method was used to study in more detail the SS after SDS-treated tissue had been soaked in it for 24 hours. As discussed below, the author found that SDS continues to leech from treated tissues, even after several days of soaking in fresh SS. Considering SDS has a high bound affinity for proteins, it is unlikely that all DDS^- diffusing into the surrounding media would leech out of the tissue in its free form. Evidence of residual tissue SDS has been found in extracts of collagenase-digested SDS-treated porcine anterior cruciate ligament.[20] Moreover, the SS contained several species (see Table 4.2) that could potentially complex the detergent and form species too big to be extracted from the tissue matrix. The time-dependant exchange experiments require the analyte to penetrate in between the layers of extractant in order to exchange with the sacrificial anion. Free DDS^- had been detected with this method, but it was unclear whether other forms of SDS were present in the SS and not being detected.

In order to investigate this issue, several "before and after" experiments were performed. In these experiments, the initial concentration of free DDS^- present in a

sample was determined using the equilibrium liquid-liquid exchange method, as previously described. Subsequently, the aqueous sample was submitted to one of the three following treatments: use of other detergents which could potentially take the place of DDS^- in the complex (*replacement*), variation of the temperature which could affect the secondary structure of the proteins (*denaturing*) or variation of the media pH (*saponification*). These experiments and their results are summarized in Table 4.3.

II.1.1.a. Replacement Experiments (RPCM). In these experiments one of the aqueous samples that had been in contact with portions of tissue as part of the soaking regime (see experimental section E) were used as the media. The "48 h 0.1% SDS" sample was the SS sample used for the second soak of tissue pieces that had been treated with a 0.1% SDS solution (see Table 4.1). A fresh SS sample was also used for comparison. Two detergents, triton x-100 and hexadecyltrimethylammonium hydroxide (CTOH), were added to SS samples (both fresh and from the soaking regime), in separate experiments, before the extraction with an organic solution of $DEC^+NO_3^-$ took place. Triton x-100 ($C_{14}H_{22}O(C_2H_4O)_n$) is a nonionic surfactant containing a hydrophilic polyethylene oxide group (on average n = 9.5) and a hydrocarbon hydrophobic group. CTOH is a cationic detergent used as an antiseptic, chosen over the bromide salt because of the effects of nucleophiles in $DEC^+NO_3^-$ described in Chapter 3. The samples were analyzed by ATR-FTIR spectroscopy and (−)ESI-MS, before and after addition of the competing detergents.

None of these detergents helped in the study of the nature of the DDS^- anion once it leaches out of the tissue sample. In the case of Triton x-100, a series of previously not observed bands were present in the ν(SO) region of the ATR spectra of samples that had been treated with the detergent. These bands could be due to a slight solubility of the detergent in the organic phase. The presence and intensity of the bands made the detection, and hence the quantification, of DDS^- unsuccessful. In the case of CTOH,

Table 4.3. Treatments applied to SS samples to further study the SDS-protein interaction

treatment	description	SS sample[c]	$[DDS^-]_b$, μM	$[DDS^-]_a$, μM
RPCM	14.6 mg Triton-100	48 h 0.1%	-	-
RPCM	30 μL CTOH	Fresh	-	-
RPCM	30 μL CTOH	48 h 0.5%	-	-
DNT	50 °C	48 h 0.5%	440±29	414±29
DNT	70 °C	48 h 0.5%	440±29	418±30
DNT	85 °C	48 h 0.5%	440±29	428±11
SPN	**NaOH**	**24 h 0.05%**	**318±13**	**356±20**
SPN	**NaOH + HCl**	**24 h 0.05%**	**318±13**	**350±17**
SPN	NaOH	48 h 0.1%	269±12	279±11
SPN	NaOH	96 h 1%	290±22	272±9
SPN	NaOH + HCl	96 h 1%	290±22	284±16

$[DDS^-]_b$ = average concentration of free DDS^- before treatment. $[DDS^-]_a$ = average concentration of free DDS^- after treatment. [c] Refer to Table 4.1 for details on these samples. The equilibrium liquid-liquid exchange method was used. For the replacement experiments (RPCM), detergents were added to the aqueous phase before exchange occurred. For the denaturing experiments (DNT), temperatures were maintained for 5 minutes. For the saponification experiments (SPN), the pH in the final samples was ca. 11 for the samples in which NaOH alone was added, and ca. 7 for those in which neutralization with HCl was performed. All values are averages of 3 or more measurements.

even when DDS^- could be detected, the ν(SO) bands in the ATR spectra of the thin films made from samples after detergent addition showed different shapes and appeared at different wavenumbers as those in the samples from before. This rendered quantification impossible, and suggested that DDS^- was being extracted from the aqueous phase into the organic one (confirmed by (−)ESI-MS) not as free DDS^-, but as a complex of the anion. It is probable that the detergent cation was interacting with DDS^- and creating a complex species with it, which showed different ν(SO) bands in the IR than free DDS^-.

II.1.1.b. Denaturing experiments (TDNT). A SS sample that had been in contact with portions of tissue as part of the soaking regime (see experimental section E) was used as the media: the "48 h 0.05% SDS" sample, used for the first soak of tissue pieces that had been treated with 0.05% SDS (see Table 4.1). An aliquot of the sample was heated in a water bath to a target temperature: either 50 °C, 70 °C or 85°C. The temperature was maintained for 5 minutes. Free DDS^- present in the sample was extracted with an organic solution of $DEC^+NO_3^-$ and analyzed by ATR-FTIR spectroscopy according to the equilibrium liquid-liquid exchange method. The results were compared to the ones obtained for another aliquot extracted before the temperature treatment.

As it can be seen in Table 4.3, none of these treatments showed a statistically different concentration of DDS^- in the SS samples before and after the temperature raise, suggesting that either no DDS^- complex was present in this sample, or the temperature raise applied as part of this work does not exert an effect in freeing the anion from such complexes.

II.1.1.c. Saponification Experiments (SPN). A test was first carried on to confirm that the presence of base in SS does not affect the determination of free DDS^-: the concentration of DDS^- in a sample of SS was determined before and after addition of concentrated NaOH, and the results compared. No significant change in concentration was observed. Then, for the saponification experiments themselves, three aqueous

samples that had been in contact with portions of tissue as part of the soaking regime (see experimental section E) were used as the media. The "24 h 0.05% SDS" sample was the SS sample used for the first soak of tissue pieces that had been treated with 0.05% SDS (see Table 4.1). Similarly, the "48 h 0.1% SDS" and "96 h 1% SDS" samples were the SS sample used for the second and fourth soaks, respectively, of tissue pieces that had been treated with 0.1% and 1% SDS, respectively. Two aliquots of each samples were treated with concentrated (4 M) aqueous NaOH, and subsequently one of the aliquots of each sample was extracted with an organic solution of $DEC^{+}NO_3^{-}$ and analyzed by ATR-FTIR spectroscopy using the equilibrium liquid-liquid exchange method, while the other was neutralized with HCl before the extraction took place (except for the "48 h 0.1% SDS", which was not submitted to neutralization). Both basic and neutralized aliquots were compared with the corresponding untreated sample from the soaking regime, as a control.

The results of these experiments are summarized in Table 4.3. It can be seen that both the "48 h 0.1% SDS" and the "96 h 1% SDS" experiments do not show a statistically different concentration of DDS^{-} before and after the treatment. This is also true for the "96 h 1% SDS" aliquot that was neutralized after treatment. The experiments performed with the "24 h 0.05% SDS" sample show, however, that there is a significant difference between the [DDS^{-}] measured before and that measured after the NaOH treatment. What these results indicate is (i) that even when there is no evidence of DDS^{-} complexes being present in SS samples used in the soaking regime after the first 24 hours of washing, there is clear evidence of these complexes in samples from the initial 24 hours, even for those that had initially been treated with SDS concentrations as low as 0.05% and (ii) that saponification is a useful method to decomplexate DDS^{-} from other species in SS samples.

Summarizing, no significant difference in the concentration of free DDS^{-} before and after treatment was observed for any of the samples, with any of the treatments

applied, except for the 24 h 0.01% SDS sample after saponification treatment was applied.

II.1.2. A Stable Extractant for Time-Dependant Exchange Method using Me-Aza-DEC$^+$I$^-$. The second approach explored as part of this project was the use of a new compound for thin films as an ion-exchange extractant to *quantify* DDS$^-$: Me-aza-DEC$^+$I$^-$. The synthesis of this salt has been described in detail in Chapter 3. It contains the $(Fc'NM_3)^+$ cation, which maintains the Fe atom in its reduced form and places the positive charge on a N atom, in a different part of the molecule instead, which provides enhanced stability to the molecule due to the superior stability of Fe(II) vs. Fe(III).

II.1.2.a. SDS quantification using Me-Aza-DEC$^+$I$^-$. The results from the SDS quantification are shown in Figure 4.2. It was found that SDS leaching from bovine pericardium depends on the %SDS treatment and diminishes with time. In reference to the question on whether SDS leeches from treated tissue, SDS was present in detectable amounts in the soaking solution of SDS-treated bovine pericardium. The concentration of SDS in soaking solutions was dependent on the initial treatment concentration of SDS and diminished with subsequent 24 h washes. SDS was not detected in the PBS-only control treatment group. Total amounts of SDS that washed out of treated bovine pericardium over 96 h were 51 ± 5 mg/g for 1.0% SDS treated tissue, 26 ± 2 mg/g for 0.5% treated tissue, 16 ± 1 mg/g for 0.1% treated tissue, 11 ± 2 mg/g for 0.05% treated tissue, and 2.1 ± 0.1 mg/g for 0.01% SDS treated tissue. This confirms that free SDS does leach out of SDS-treated bovine pericardium at concentrations that are potentially cytotoxic, as described next, even after the tissues have been soaked in subsequent fresh aliquots of SS for over 96 hours, and depending on the initial treatment.

Dr. Arai, at the Orton Research Group, found in an independent study what concentrations of SDS are cytotoxic to ovine vascular myofibroblasts. In this study, 1×10^5 cells were cultured in DME media at 37º C for 24 hours and subsequently SDS

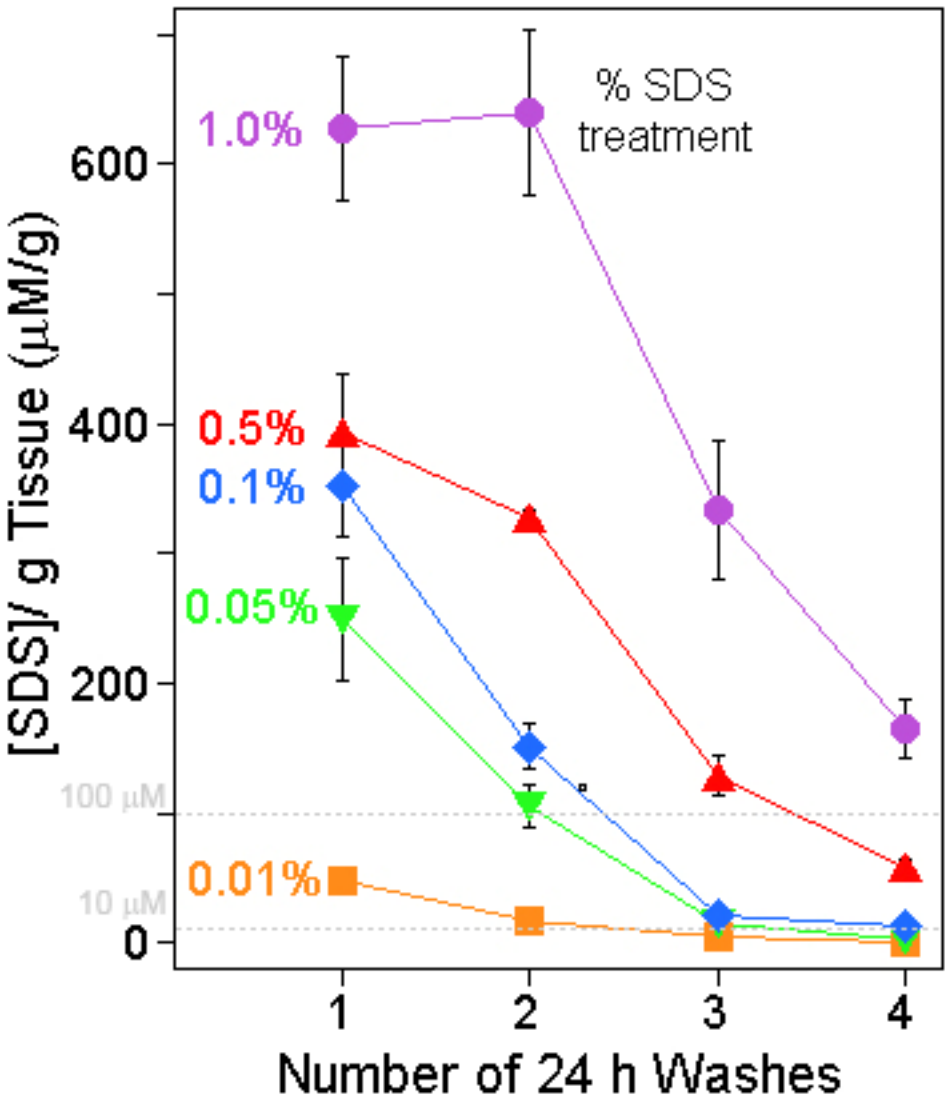

Figure 4.2. Concentration of SDS per g of tissue that leaches out of SDS-treated bovine pericardium tissue samples with successive 24-hour washes. The dotted lines show the two potentially cyotoxic SDS concentrations according to "total cell/well" (10 µM) and "live cell %" (100 µM) count methods. The errors shown for the [SDS] values are ±1σ.

solutions in concentrations ranging from 10 to 1000 μM were added. After 48 hours of incubation, two different counting methods were used: "total cells/well" were determined and a "live cell %" assay based on trypan blue exclusion was performed (n=5).[19] These experiments showed cell count significantly decreased at SDS concentration as low as 10 μM according to the "total cell/well" counting method, while 100 μM was the cytotoxic concentration, significantly decreasing the cell count according to the "live cell %" counting method.

Although other SDS-treated xenogeneic tissues, such as porcine aortic valve or conduit, were not specifically studied here, it is reasonable to assume that the same phenomena would occur in such cases. These results offer then an explanation for the findings of Rieder et al.[17] that media used to store SDS-treated porcine aortic valves can be toxic to cultured vascular cells. This research group reported complete inhibition of in vitro re-seeding on 0.1% SDS-treated porcine aortic leaflet or conduit with human endothelial cells. Furthermore, our results also demonstrate that leaching of free SDS into media diminishes considerably over a 96 hour period. Several factors were identified that are likely to be influencing the concentration of free SDS in soaking or storage media including the initial treatment concentration of SDS, the ratio of tissue weight to soaking solution volume, and the duration and number of wash changes. Thus, it is possible that as long as SDS-treated tissues are washed with sufficient volumes and number of washes over time, free SDS concentrations may fall below concentrations that are overtly toxic to cultured cells. As such, the present results are also consistent with the results of Wilcox et al.[18] and Knight et al.[21], who have demonstrated in vitro recellularization (attachment and migration) of 0.1% SDS-treated porcine aortic valve conduit by porcine myofibroblasts and human mesenchymal progenitor cells, respectively. Our results also explain those presented by Kim et al.[13], which show in vitro re-seeding of 0.5% SDS-treated pulmonary valve leaflets with caprine endothelial cells. Differences in the decellularization protocols such as protease inhibition, treatment with trypsin, and/or duration, volume, and

temperature of the soaking protocol could partially account for differences in results between centers. It is then reasonable to say that SDS-treated porcine valves or conduits might not demonstrate a clear cytotoxic effect on cultured vascular cells if treated tissues are washed with sufficient volumes and numbers of washes over a sufficient period of time.

II.2. Quantification of Total SDS. It has been pointed out that the ATR-FTIR methodology used to analyze the bathing media of treated tissues only measures free DDS^-. SDS bound to soluble proteins within the media cannot be detected this way. It is possible that additional SDS leeches from treated tissues in the form of soluble protein-bound SDS. Furthermore, these results do not address the issue of residual SDS retained within treated tissues. SDS residues bound to retained soluble or matrix proteins within the tissue might well exert a toxic effect on repopulating cells that could inhibit or impair in vivo or in vitro recellularization. It is clear from the discussion presented so far that a method that allows for the determination of Total SDS is necessary. This would include free SDS and SDS complexed with other species, like proteins both soluble (these complexes would be leeching into the SS) and insoluble or structural (these complexes would remain in the tissue samples).

An alternative that would allow for the quantification of Total SDS in tissue samples after treatment with the detergent, is liquid scintillation counting (LSC). Considering that ^{35}S is a beta emitter, LSC can be used to quantify [^{35}S]SDS in a homogenous sample in a simple and straightforward manner. In this technique, the sample is mixed with a "scintillation cocktail" containing an aromatic solvent and other additives. Beta particles emitted from the radionuclide interact with solvent molecules, which transfer energy to the additives. The excited-state additive molecules emit photons when they relax to the ground state, which are detected by the instrument. For this to be applicable to our problem, bovine pericardium samples similar to those used in the procedures described before would have to be submitted to the decellularization

treatment using [^{35}S]SDS instead of SDS. Then they would have to undergo a soaking regime, a homogenization protocol and an analysis through LSC.

This approach is not as straightforward, cost effective or simple as it sounds, considering that [^{35}S]SDS is only commercially available from custom synthesis, which makes it expensive and not readily available. Therefore, it was reasonable to attempt to synthesize this compound ourselves.

II.2.1. Evaluation of SDS Synthesis. In reference to the synthesis of SDS, the literature contains mostly procedures concerned with gaseous starting materials or reagents. The author wanted to avoid the use of reactants in such state, considering the potential problems with manipulating radioactive gases. An alternative synthesis, based on the preparation of sulphonic acids by reacting alcohols and sulfuric acid, was designed. The general synthetic route is shown next:

$$C_{12}H_{25}OH\ (l) + H_2SO_4\ (l) \rightarrow\ C_{12}H_{25}SO_3OH\ (l) + H_2O\ (l) \qquad (4.1)$$

$$C_{12}H_{25}SO_3OH\ (l) + Na^+OH^-\ (l) \rightarrow Na^+C_{12}H_{25}SO_4^-\ (s) \qquad (4.2)$$

The radioactively labeled acid $H_2{}^{35}SO_4$ is commercially available ($290 for 2 mCi), and a synthesis from this starting material would avoid the need to purchase customly synthesized [^{35}S]SDS ($15,500 for 2 mCi).

The 2 mCi of $H_2{}^{35}SO_4$ that would be purchased for the synthesis of [^{35}S]SDS (this is the smallest amount of sample that is commercially available) is equivalent to 4.4×10^9 counts/min (CPM), which assuming 100% efficiency (it is 95% in practice), is equivalent to 4.4×10^9 disintegrations/minute (DPM; considering that 1 mCi equals 2.2×10^9 DPM). After consulting with James Oldenburg, a radiation control technician at the Radiation Control Office at CSU, it became apparent that BSC would allow us to detect 400 DPM

with 10% accuracy. This means that the received 4.4×10^9 DPM could be diluted by a factor of 1×10^7.

When purchasing 2 mCi of $H_2{}^{35}SO_4$ for the synthesis, these would be supplied as 2 mL of solution. If the $H_2{}^{35}SO_4$ in these 2 mL was converted to [^{35}S]SDS, the resulting reaction product could be diluted a factor of 1×10^7 and provide 20,000 L of radioactive solution, if the synthesis had 100% conversion. Each 20 mL of this solution would have 4000 DPM, which means 1,000,000 20-mL BSC samples could be prepared, and each would give a signal 10 times above the limit of detection (LOD). It is not a real problem that the concentration of SDS in solution will be too low to eliminate antigens in tissue treatments (concentrations used in the non-radioactive experiments presented here were 0.01-1%; see section II.1.), as any desired amount of non-radioactive SDS can be added to the solutions before treating tissue samples with them, and this would enhance the amount of SDS available to eliminate antigenic proteins, without affecting the radioactivity of the solution.

Our goal was to prove that SDS could be synthesized using starting materials that were commercially available in their radioactively labeled form (in order to show it is possible to eventually synthesize [^{35}S]SDS in our own laboratories), but test the yield and purity of this route using non-radioactive starting materials first. The route designed (equations 4.1 and 4.2) was pursued as described in the experimental section.

The objective was achieved, as shown in Figures 4.3 and 4.4. Figure 4.3 shows the (−)ESI-MS spectrum of the reaction crude. The peak at 265 m/z corresponds to DDS^-, and the subsequent peaks (553, 841, 1129 and 1417 m/z) are due to clusters formed by whole SDS (Na^+DDS^-) units (1, 2, 3 and 4 units, respectively) combined with another DDS^- anion. The formation of clusters was expected and confirmatory of the presence of SDS, as shown in the spectrum of the commercial sample (Figure 4.3, insert). In order to check the purity of the sample, a ^{1}H-NMR spectrum was obtained and it is

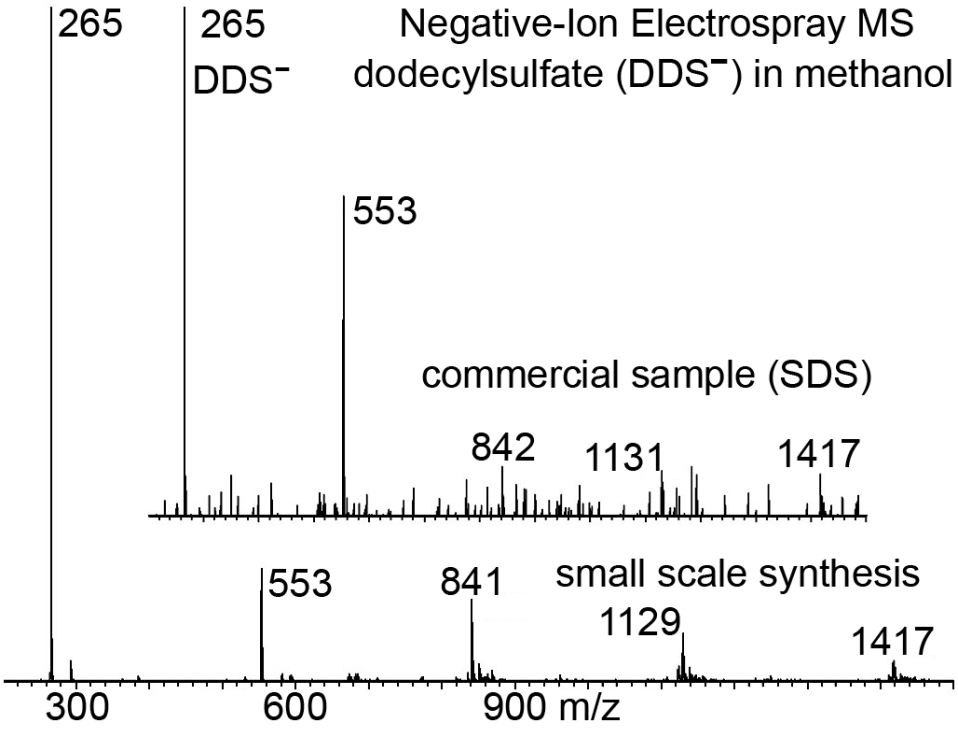

Figure 4.3. (−)ESI-MS Spectrum of reaction mixture containing synthesized DDS^- from a small scale synthesis. *Insert:* (−)ESI-MS spectrum of an SDS commercial sample.

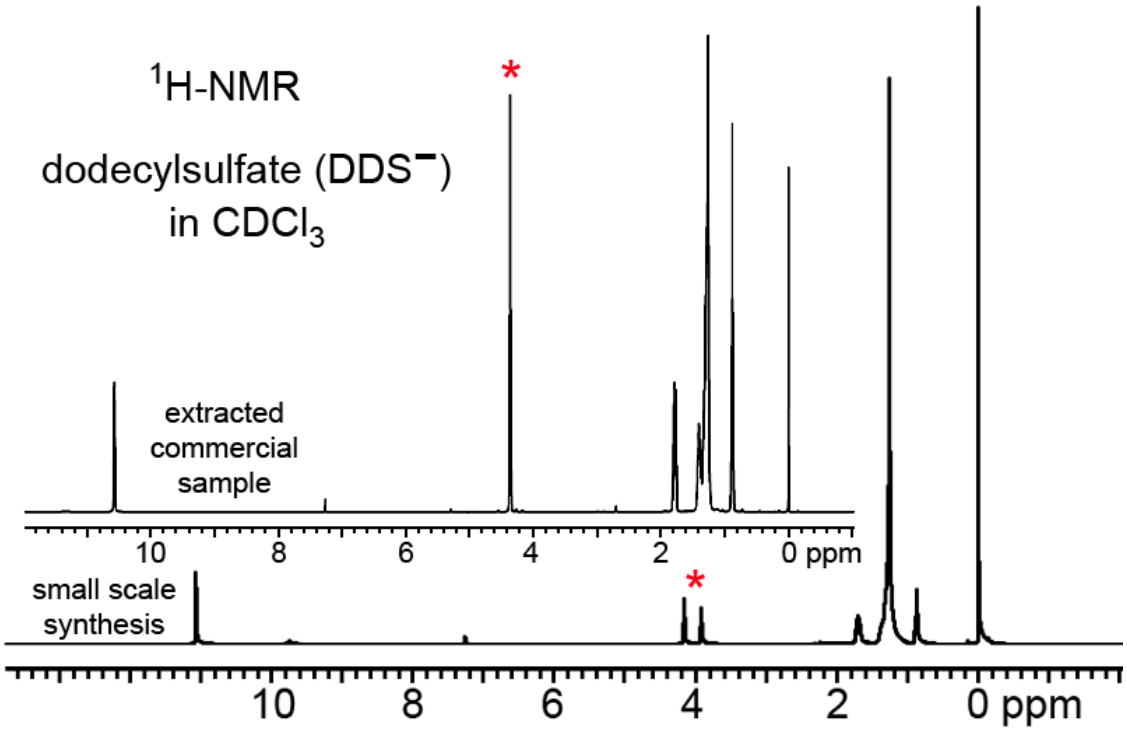

Figure 4.4. ^{1}H-NMR spectrum of reaction mixture containing synthesized DDS^- from a small scale synthesis. *Insert:* ^{1}H-NMR spectrum of an SDS commercial sample.

shown on figure 4.4. When comparing the spectrum obtained for the reaction crude (main figure) with the one for the commercial sample (insert) the main difference is observed at around 4 ppm: the spectrum for the synthesis shows the two sets of triplets (integrated area is 0.91 for the peak at 3.9 ppm and 1.03 for the one at 4.2 ppm), while the commercial sample shows only one ($\int$ = 1.96 at 4.4 ppm). These results point out to the presence of two different molecules with sulphonic acid substituent in them, which would indicate that the starting material is still present in the reaction mixture and the conversion stops at approximately 50%. These results are not surprising: According to equation 4.1, after an equimolar mixture of sulfuric acid and dodecanol has reacted, the result is an equimolar mixture of sulfuric acid, dodecanol, water and the sulphonic acid. This means that at this point, the starting materials have undertaken a two-fold dilution. Different strategies were tested in order to eliminate the water from this mixture, including change in reaction temperature, reaction time or addition of benzene to create an azeotrope. The reaction could not be pushed forward.

Although SDS could not be obtained as a pure reaction product, its synthesis was successful. Separation strategies would be necessary to isolate the detergent from the unreacted starting materials. Even if only 1% conversion is achieved from this synthesis, and the product [^{35}S]SDS is isolated and purified, that means that instead of 20,000 L of radioactive solution, 200 L could be prepared. This would still allow the preparation of 10,000 samples, of 20 mL each, which could be analyzed by BSC. If this solution were to be used for a soaking regime, which requires 100 mL to treat 10 pieces of tissue/experiment, this would still allow for the completion of 2,000 experiments.

It can be easily seen from the discussion presented here that the synthesis, although not very effective from a synthetic point of view, represents a viable alternative that would allow that experiments be carried on with radioactive [^{35}S]SDS without having to spend an exorbitant amount of money for a custom synthesis.

III. Experimental Section

III.1. Reagents, Solvents, and Solutions. All reagents and solvents were ACS grade or better unless stated otherwise. All solutions used were prepared in Class A volumetric glassware. The distilled deionized water (dd-H_2O) used for solution preparation had an initial resistivity of 18 MΩ cm. Syntheses which involved air-sensitive compounds were carried out under a purifieddinitrogen atmosphere using standard Schlenk techniques.[22] In all cases, stirring and heating were done using a magnetic stirrer and a hot plate.

III.1.1. Tissue Decellularization and SDS Quantification in Biological Samples. Sterile containers and instruments were used throughout the experiments that involved tissue samples and solutions that were in contact with them. The following reagents/solvents were used as received (common name/abbreviation; formula; and vendor are indicated in parenthesis): dichloromethane (Fisher Scientific), 10 mM phosphate buffered saline/PBS, a solid that when dissolved in 1 L of water will render a solution containing 10 mM phosphate, 138 mM NaCl, and 2.7 mM KCl (Sigma-Aldrich), bovine lung aprotinin/BLA ($C_{284}H_{432}N_{84}O_{79}S_7$; Sigma-Aldrich), Trizma hydrochloride buffer/Triz (Sigma-Aldrich), ethylenediaminetetraacetic acid/H_4EDTA (Sigma-Aldrich), and antibiotic-antimycotic stabilized/AAS, an aqueous suspension of antibiotics/antimycotics consisting of 10,000 units/mL penicillin G, 10 mg/mL streptomycin sulfate, 25 μg/mL amphotericin B (Sigma-Aldrich), and sodium hydroxide (Fisher Scientific). The detergents hexadecyltrimethylammonium hydroxide/CTOH (25% in MeOH; $(C_{16}H_{33})N(CH_3)_3OH$; Acros), and Triton x-100 ($C_{14}H_{22}O(C_2H_4O)_n$; Anatrace) were obtained from the Henry Research Group and the Levinger Research Group, respectively. The polyalkylated ferrocenium salts 1,1',3,3'-tetrakis-(2-methyl-2-nonyl)ferrocenium nitrate/chloride ($DEC^+NO_3^-$/DEC^+Cl^-) were synthesized according to literature methods[23,24] by other members of the Strauss Research Group. The salt aza-DEC^+I^- was synthesized as described in Chapter 3 by the author in collaboration with Igor V. Kuvychko.

III.1.2. Synthesis of SDS. Concentrated Sulfuric acid (98%; Mallinckrodt AR), 1-dodecanol (Eastman Organic Chemicals), and sodium hydroxide (Fisher Scientific) were used as received. Benzene (Fisher Scientific) was purified according to literature procedures.[25]

III.2. Instrumentation. Distilled, dionized water (dd-H_2O) was purified using the Barnstead NANOpure system, Thermo Scientific (Dubuque, IA); the pH was measured using an Orion meter (Boston, MA) with a Corning pH electrode (Corning, NY); the shaker bath used was a Lab line 3545 (location); electrospray ionization mass spectra (ESI-MS).was recorded using a 2000 Finnigan LCQ-DUO mass-spectrometer (MeOH as carrier solvent, 0.3 mL/min flow rate); nuclear magnetic resonance of protons (^{1}H-NMR) data was obtained using either a Bruker Inova-300 or Inova-400 instrument (25 °C, TMS internal standard); IR spectra were recorded using the ATR-FTIR spectrometer described in Chapter 3 (ReactIR-1000, Mettler-Toledo, Columbus, OH) that was equipped with a diamond (DiComp) ATR probe (Mettler-Toledo, Columbus, OH) and a liquid-nitrogen-cooled mercury cadmium telluride (MCT) detector. The spectral window was 4000 to 650 cm^{-1} with a nominal spectral resolution of 8 cm^{-1}. The electronic gain was 2 (DiComp probe). Happ-Ganzel apodization was used with no post-run spectral smoothing. The DiComp® probe consisted of a 18-bounce diamond ATR crystal mated to a ZnSe optical focusing element and housed in a 1.3 cm thick × 7.6 cm diameter stainless-steel DuraDisk™ (Mettler-Toledo, Columbus, OH). The wetted surface of the diamond ATR crystal was a circular area 0.9 cm in diameter (see Chapter 1 for more details).

III.3. SDS Quantification using ATR-FTIR Spectroscopy and $FeCp_2'^+X^-$ Films.

III.3.1. Soaking Solution Preparation. One package of PBS was added to 1 L flask and dissolved in 1 L dd-H_2O. BLA (0.23 mL), Triz (10 mL), H_4EDTA (0.25 mg), AAS (25 μL) and PBS solution were mixed to a final total volume of 250 mL. Sonication

was used to aid dissolution of all solids. The solution was filtered using a 0.2 μm size filter and stored in a refrigerator when not in use.

III.3.2. Tissue Decellularization and Soaking Regime. Bovine pericardium was obtained postmortem, cleaned of adipose tissue, washed with sterile PBS solution, cut into 1 cm^2 squares, and stored at −70 °C until used. Bovine pericardium tissue squares were thawed and weighed just prior to undergoing decellularization. Tissues were treated to cause hypotonic lysis of cells with Tris-buffered water under gentle agitation at room temp for 4 h. Tissue squares were then divided into 6 groups and treated with PBS only (control group) or one of five concentrations (w/v) of SDS in PBS: 0.01%, 0.05%, 0.1%, 0.5%, 1.0% (n = 10 tissue squares per concentration) under gentle agitation at room temp for 24 h. The SDS solutions were prepared with reagent-grade SDS (SigmaUltra, Sigma-Aldrich). Finally, each group of SDS-treated bovine pericardium was washed with 4 consecutive washes of 100 mL PBS under gentile agitation at room temp for 24 h each wash. The PBS soaking solution was changed each 24 h and collected for subsequent SDS analysis. Tissues were rinsed with 3 ml of PBS between each wash to prevent transfer of any free SDS. Total wash time for each tissue was 96 h.

III.3.3. ATR-FTIR Measurements: Equilibrium Liquid-Liquid Exchange Method. An aliquot of a solution of SDS in SS was placed in a 20mL vial and placed in contact with a CH_2Cl_2 solution of $DEC^+NO_3^-$. In general, equal volumes of the organic and the aqueous phase were used. The vial was manually shaked for 5 min and allowed to settle on the counter for 2 min. Once the phases had separated, the organic (bottom) phase was extracted using a glass pipette and placed in a clean vial. A 20 μL aliquot of this CH_2Cl_2 phase was placed on the ATR Di probe. In this case, the absorbances were <0.05. Evaporation of the solvent was allowed, and a sample spectrum was taken. Each spectrum was produced by averaging 1024 scans.

III.3.3.a. Calibration Curve Experiments. A single absorbance measurement was obtained from each film, and an average of three or more absorbances measured for

the ν(SO) band at 1254 cm^{-1} from different films was plotted vs [SDS] to obtain each datapoint. All experiments used to construct the calibration curve had an excess of NO_3^- (2-5 times higher than the [DDS^-]), although the DDS^-:NO_3^- ratio varied.

III.3.3.b. Real Samples Experiments. The procedure was the same as for the calibration curve datapoints, except that three vials with three different amounts of $DEC^+NO_3^-$ were used. If the average absorbance for all three experiments was the same (within experimental error of 5%), the calibration curve was used to find the concentration of DDS^- in the unknown sample. If the absorbances were different by more than 5%, it was assumed that there was not enough NO_3^- to extract all the DDS^-. In those cases, a new vial was prepared containing a 1.5-2.5 excess NO_3^- compared to the more concentrated one of the original three vials. The absorbance was recorded again, and this procedure was repeated until the absorbance stopped changing, signifying that an excess NO_3^- had been achieved.

III.3.3.c. Blind Test Experiments. A member of the Strauss Group prepared two two-phased samples that were to undergo liquid-liquid ion exchange: One of the samples contained in the organic phase a [SDS] somewhere between 200 and 400 μM, and 800 μM [$DEC^+NO_3^-$] in the aqueous phase. The other mixture contained in the organic phase the same amount of SDS as the first one, while the aqueous phase had twice as much $DEC^+NO_3^-$ as the organic phase had SDS. The samples were analyzed by the author as described above without knowing the real [SDS] in these mixtures. The calibration curve was used to determine the [SDS] and the value obtained was compared with the real value, revealed to the author once the analysis was finished.

III.3.3.d. Before and After Experiments. In all these experiments, which included the RPCM, TDNT and SPN experiments, the procedure was as follows: an aliquot of a SS sample (either a sample from the soaking regime (see Table 4.1) or a fresh SS sample) was analyzed using the equilibrium liquid-liquid exchange method and the ATR-FTIR spectrometer, as described for the real samples. Subsequently, one of the

three treatments was applied to another aliquot of the sample. Fort the RPCM experiments, another detergent was added to the vial containing the SS aliquot, which was mixed manually for 5 minutes. In the TDNT experiments, the vial containing the SS aliquot was placed in a water bath and heated on a hot plate until the target temperature (50, 70 or 85 °C) was achieved. The solution was kept at this temperature for 5 minutes. In the SPN experiments, 30 µL of a 4 M NaOH solution were added to the SS aliquot, and the vial was mixed for 5 minutes. In the case of neutralized SPN experiments, small amounts of HCl were added to the vial after this, until the pH of the samples was neutral. Next, the $DEC^+NO_3^-$ organic solution was added and the sample was analyzed as described for the real samples.

III.3.4. ATR-FTIR Measurements: Time-Dependant Exchange Method. The SDS determination were performed in 100 mL of aqueous, homogenous SS, using ATR-FTIR and a Di crystal modified with a thin film. The films were made by dissolving the salt of interest in dichloromethane. An aliquot (20 µL for DEC^+X^- and 50 µL for $NMe_3R^+I^-$) of a 3.0 mM dichloromethane solution (i.e. 60 nmol and 150 nmol of the salts, respectively) was deposited on the ATR crystal using a pipetor. The volumes were chosen so that they would produce a film for which the absorbance of the main ν(CH) band would be between 0.8 and 0.9. Evaporation of the solvent was allowed, and a background spectrum was taken. Each spectrum was produced by averaging 128 scans. The film coated probe was then placed in contact with 100 mL of SS with stirring (*ca.* 60 rpm), and equilibration was allowed for 15 min. After completion of the equilibration another background spectrum was recorded. The DDS^- determination was performed differently at this point, depending on whether the sample was a standard solution to obtain a calibration curve datapoint or a real sample.

III.3.4.a. Calibration Curve Experiments. In these experiments, a volume of SS containing SDS was added to the SS used for the equilibration (having previously removed the same volume of SS to maintain the same final volume), so that the final

concentration was the desired one. Spectra were collected for a pre-determined amount of time. For each spectrum, the initial d*A*/d*t* value at 1221 cm^{-1} (one of the ν(SO) bands of DDS^-) was determined as explained next, and a calibration curve was constructed by graphing this value for each spectrum vs the concentration of SDS. For the determination of d*A*/d*t* in the DEC^+-salt experiments, the first 10-15 minutes of an exchange reaction were used to calculate d*A*/d*t*. For the determination of d*A*/d*t* in the Me-aza-DEC^+I^- experiments, the data was chosen using two different criteria: for concentrations below 10 μM the d*A*/d*t* values were calculated using data from the first 15 minutes of the exchange (most linear portion for this data); while for concentrations above 10 μM the d*A*/d*t* values were calculated using the data that better adjusted to a straight line, which was (in most cases) less than 15 min. A new thin-film coating of the ion-exchange extractant was used for each analysis, and all analyses were performed in triplicate and averaged to produce one datapoint in the calibration curve.

III.3.4.b. Real Samples Experiments. These samples were analyzed using aza-DEC^+I^- only. The experiments were carried out in the same manner as stated above, except that a portion from one of the washes from the "tissue soaking regime" was added to the SS used for the equilibration for each experiment. The volume was chosen so that the SDS concentration of the new diluted media would be in the lower part of the calibration curve (<10 μM), which was the most precise portion of the curve.

Final washout SDS concentrations were reported as μM/g of tissue/100 ml of SS. Total amounts of SDS washed out from treated bovine pericardium over 96 h were calculated and reported as mg/g of tissue.

III.4. Quantification of Total SDS.

III.4.1. ***Evaluation of SDS Synthesis.*** For this synthesis, 1 g of sulfuric acid was placed in a vial with 10 μL of dd-H_2O. An excess of 1.9 g of 1-dodecanol at 50 °C were added and the mixture was placed in a water bath under vigorous stirring at *ca.* 55 °C. Within the first 15 minutes of mixing, a caramel colored gel forms, which becomes

harder when temperature decreases. After 30 min, a portion of the reaction crude was placed in a vial with CD_3Cl and set to shake for 1 h and analyzed by ESI-MS and ^{1}H-NMR. The reaction was allowed to continue for a total of 24 h, and another aliquot was treated like described above and analyzed again by ESI-MS and ^{1}H-NMR. A 0.223 g portion of the crude was placed in a vial. A 3.4 mL aliquot of a 4 M solution of NaOH in dd-H_2O was added, and the vial was set to stir at room temperature. Within 5 minutes, a white solid appeared dispersed in the emulsion. A portion of this solid was placed in a vial with CD_3Cl and set to shake for 1 h, dried in a vacuum line and analyzed by ESI-MS and ^{1}H-NMR.

IV. Conclusions

The results presented here demonstrate a novel application of ATR-FTIR spectroscopy in heart-valve research. It became clear early in this endevour that understanding the process of SDS washout was a key part in allowing scientist to create protocols for preparing biological scaffolds free of cytotoxicity. The author also:

(i) developed a new method to detect and quantify free SDS in biological samples using $DEC^+NO_3^-$: the equilibrium liquid-liquid exchange method (this method eliminated instability issues using this ferrocenium salt and opened doors for conventional FTIR quantification of species using this kind of extractants);

(ii) helped shine light in the question of whether SDS leaches out of SDS-treated tissues after a soaking regime has been implemented, discovering that not only does SDS leach from bovine pericardium but in what concentrations (depending on the initial treatment, in concentrations that are potentially cytotoxic) and in what form (both free and as complex of other species at initial stages of the soaking regime);

(iii) evaluated the synthesis of [^{35}S]SDS by successfully synthesizing SDS in the Strauss Research Group laboratories, using standard starting materials, one of which (H_2SO_4) can be obtained in its radioactively labeled form (being the objective before this

synthesis to eventually quantify [^{35}S]SDS directly in [^{35}S]SDS-treated tissue samples after soaking regime).

V. References

(1) Hoerstrup, S. P.; Kadner, A.; Melnitchouk, S.; Trojan, A.; Eid, K.; Tracy, J.; Sodian, R.; Visjager, J. F.; Kolb, S. A.; Grunenfelder, J.; Zund, G.; Turina, M. *Circulation* **2002**, *106*, I143-150.

(2) Hoerstrup, S. P.; Sodian, R.; Daebritz, S.; Wang, J.; Bacha, E. A.; Martin, D. P.; Moran, A. M.; Guleserian, K. J.; Sperling, J. S.; Kaushal, S.; Vacanti, J., P.; Schoen, F. J.; Mayer, J. E. J. *Circulation* **2000**, *102*, III44-49.

(3) Shinoka, T.; Breuer, C. K.; Tanel, R. E.; Zund, G.; Miura, T.; Ma, P. X.; Langer, R.; Vacanti, J. P.; Mayer, J. E. J. *The Annals of thoracic surgery* **1995**, *60*, S513-516.

(4) Shinoka, T.; Shum-Tim, D.; Ma, P. X.; Tanel, R. E.; Langer, R.; Vacanti, J. P.; Mayer, J. E. J. *Circulation* **1997**, *96*, II-102-107.

(5) Sodian, R.; Hoerstrup, S. P.; Sperling, J. S.; Daebritz, S.; Martin, D. P.; Moran, A. M.; Kim, B. S.; Schoen, F. J.; Vacanti, J., P.; Mayer, J. E. J. *Circulation* **2000**, *102*, III22-29.

(6) Tower, T. T.; Neidert, M. R.; Tranquillo, R. T. *Ann Biomed Eng* **2002**, *30*, 1221-1233.

(7) Badylak, S. F. *Transplant Immunology* **2004**, *12*, 367-377.

(8) Cebotari, S.; Mertsching, H.; Kallenbach, K.; Kostin, S.; Repin, O.; Batrinac, A.; Kleczka, C.; Ciubotaru, A.; Harerich, A. *Circulation* **2002**, *106* I-63-I-68.

(9) Schmidt, C. E.; Baier, J. M. *Biomaterials* **2000**, *21*, 2215-2231.

(10) Steinhoff, G.; Stock, U.; Karim, N.; Mertsching, H.; Timke, A.; Meliss, R. R.; Pethig, K.; Haverich, A.; Bader, A. *Circulation* **2000**, *102*, III-50 - 55.

(11) Simon, P.; Kasimir, M. T.; Seebacher, G.; Weigel, G.; Ulrich, R.; Salzer-Muhar, U.; Rieder, E.; Wolmer, E. *Eur J Cardiothoracic Surg* **2003**, *23*, 1002-1006.

(12) Korossis, S. A.; Booth, C.; Wilcox, H. E.; Watterson, K. G.; Kearney, J. N.; Fisher, J. *J Heart Valve Dis* **2002**, *11*, 463-471.

(13) Kim, W. G.; Park, J. K.; Lee, W. Y. *Int J Artific Organs* **2002**, *25*, 791-797.

(14) Gonçalves, A.; Griffiths, L. G.; Anthony, R. V.; Orton, E. C. *J Heart Valve Dis* **2005**, *14*, 212-217.

(15) Courtman, D. W.; Perira, C. A.; Kashef, V.; McComb, D.; Lee, J. M.; Wilson, G. J. *J Biomed Mater Res* **1994**, *28*, 655-666.

(16) Booth, C.; Korossis, S. A.; Wilcox, H. E.; Watterson, K. G.; Kearney, J. N.; Fisher, J. *J Heart Valve Dis* **2002**, *11*, 457-462.

(17) Rieder, E.; Kasimir, M. T.; Silberhumer, G.; Seebacher, G.; Wolner, E.; Simin, P.; Weigel, G. *J Thoracic Cardiovasc Surg* **2004**, *127*, 399-405.

(18) Wilcox, H. E.; Korossis, S. A.; Booth, C.; Watterson, K. G.; Kearney, J. N.; Fisher, J.; Ingham, E. *J Heart Valve Dis* **2005**, *14*, 228-237.

(19) Caamaño, S.; Arai, S.; Strauss, S. H.; Orton, E. C. *Journal of Heart Valve Disease* **2009**, *18*, 105-0000.

(20) Gratzer, P. F.; Harrison, R. D.; Woods, T. *Tissue Eng* **2006**, *12*, 2975-2983.

(21) Knight, R. L.; Booth, C.; Wilcox, H. E.; Fisher, J.; Ingham, E. *J Heart Valve Dis* **2005**, *14*, 806-813.

(22) Shriver, D. F.; Drezdzon, M. A. *The Manipulation of Air-Sensitive Compounds, 2nd Ed.*; Wiley-Interscience: New York, 1986.

(23) Clapsaddle, B. J.; Clark, J. F.; Clark, D. L.; Gansle, K. M.; Gash, A. E.; Chambliss, C. K.; Odom, M. A.; Miller, S. M.; Anderson, O. P.; Hughes, R. P.; Strauss, S. H. *Inorg. Chem.* **unpublished work**.

(24) Clark, J. F.; Clark, D. L.; Whitener, G. D.; Schroeder, N. C.; Strauss, S. H. *Environ. Sci. Technol.* **1996**, *30*, 3124-3127.

(25) Armarego, W. L. F. *Purification of Laboratory Chemicals*, 4th ed.; Butterworth-Heinemann, 1997.